Aus dem LIFE-Zentrum Klinikum Großhadern und der Urologischen Klinik und Poliklinik der Ludwig-Maximilians-Universität München

Dissertation
zum Erwerb des Doctor of Philosophy (Ph.D.)
an der Medizinischen Fakultät der
Ludwig-Maximilians-Universität zu München

The influence of phytochemicals on cancer stem cells in prostate cancer

vorgelegt von:

Lili Wang

aus:

Siping/Jilin, China

Jahr:

2021

Mit Genehmigung der Medizinischen Fakultät der
Ludwig-Maximilians-Universität zu München

First evaluator (1. TAC member): Priv. Doz. Dr. Heike Pohla
Second evaluator (2. TAC member)*:* Prof. Dr. Alexander Buchner
Third evaluator (3. TAC member): Prof. Dr. Elfriede Nössner

Dean: **Prof. Dr. med. Thomas Gudermann**

date of the defense:

15.11.2021

Contents

Abstract:

Background: Cancer stem cells are a small subpopulation of cancer cells, characterized by self-renewal, maintaining stemness properties, and are importantly responsible for developing therapeutic resistance in the field of chemotherapy and radiotherapy. Therefore, targeting cancer stem cells would be a new treatment strategy for therapy-resistant cancer patients. Recently, the phytochemicals shikonin and berbamine have been caught the attention for their cytotoxic effects on cancer cells. The aim of this thesis is to investigate whether these two phytochemicals shikonin and berbamine have an anti-cancer effect on prostate cancer stem cells and cabazitaxel-resistant prostate cancer cells.

Methods: To generate prostate cancer stem cells, the sphere formation assay was conducted. Also, to evaluate the anti-cancer effect of shikonin and berbamine, several techniques were performed including CellTiter-Blue cell viability assay, CellTiter 96 AQueous One Solution cell proliferation assay, apoptosis assay, scratch wound healing assay, and cell invasion assay. The prostate cancer stem cell markers were detected and assessed by flow cytometry and qRT-PCR. A cabazitaxel-resistant prostate cancer cell line was generated by gradually increasing the concentration of cabazitaxel over at least eight months. Furthermore, the cytotoxic mechanism of shikonin was analyzed by staining for reactive oxygen species and mitochondrial membrane potential. A small RNA-sequencing technique was used to select differentially expressed microRNAs which berbamine regulated. Small interfering RNAs, mimics, and inhibitors were used to investigate the downstream pathways of berbamine.

Results: Both shikonin and berbamine inhibited the cell viability, proliferation, invasion, migration, and enhanced the apoptosis rate of prostate cancer stem cells. Also, shikonin and berbamine augmented the anti-cancer effect of cabazitaxel. Shikonin triggered apoptosis via ROS production and disrupted the mitochondrial membrane potential. Furthermore, shikonin suppressed the level of ALDH3A1 and ABCG2 in prostate cancer stem cells, which are two drug resistance markers. Decreasing the expression level of ABCG2 and ALDH3A1 reversed the drug resistance of cabazitaxel-resistant prostate cancer cells to cabazitaxel. Berbamine suppressed the expression of ABCG2, CXCR4, and ALDH1A1. Inhibiting the expression of ABCG2 and CXCR4 reversed cabazitaxel resistance. RNA-sequencing identified that berbamine enhanced the expression of let-7 family, miR-26a, and miR-26b. The individual miRCURY LNA miRNA PCR assay further verified that berbamine up-regulated let-7 family, miR-26a, and miR-26b. Ber-

bamine inhibited the expression of IGF2BP1 and silencing of CXCR4, and mimics of the let-7 family also downregulated the expression of IGF2BP1. In addition, berbamine inhibited p-STAT3 and silencing of ABCG2 and mimics of miR-26b also downregulated the expression of p-STAT3.

Conclusion: Shikonin enhances the anti-cancer effect of cabazitaxel in prostate cancer stem cells and reverses the cabazitaxel resistance by inhibiting ALDH3A1 and ABCG2. Berbamine targets both prostate cancer cells and prostate cancer stem cells and reverses the cabazitaxel resistance through berbamine/CXCR4/let-7 family/IGF2BP1 axis and berbamine/ABCG2/miR-26b/p-STAT3 axis.

List of figures

List of tables

List of abbreviations

ABCG2	ATP-binding cassette G2
ACAS	Automated Cellular Analysis System
AGO1–4	Argonaut protein complex 1–4
ALDH	Aldehyde dehydrogenase
APC	Allophycocyanin
BSA	Bovine Serum Albumin
bFGF	Basic fibroblast growth factor
BTYNB	BTYNB IMP1 Inhibitor
caba-DU145	Cabazitaxel-resistant DU145 cell line
CPT	Cryptotanshinone
CRPC	Castration-resistant prostate cancer
CSCs	Cancer stem cells
CSC-EXO	CSCs derived exosomes
CXCR4	C-X-C Motif Chemokine Receptor 4
DCF	Dichlorofluorescein
DCFDA	2',7'-dichlorofluorescein diacetate
DEAB	N, N-diethylaminobenzaldehyde
DGCR8	DiGeorge critical region gene 8,
DKK	Dickkopf
EGF	Epidermal growth factor
EMT	Epithelial-mesenchymal transition

LIST OF ABBREVIATIONS

EZH2	Enhancer of Zeste 2
FCS	Fetal calf serum
FITC	Fluorescein isothiocyanate
GLI	Glioma-associated oncogene
GnRH	Gonadotropin-releasing hormone
GSK - 3β	glycogen synthase kinase
HDL	high-density lipoproteins
HMGA1	High mobility group protein HMG-I/HMG-Y
HMGA2	High mobility group protein HMGI-C
IC50	Half-maximal inhibitory concentration
IGF2BP1	Insulin-like growth factor 2 mRNA-binding protein 1
JAG1	Jagged1
JC-1	Tetraethylbenzimidazolylcarbocyanine iodide
LIN28B	Protein lin-28 homolog B
LNA	Locked nucleic acids
MDR	Multiple drug resistance
MEM	Minimum Essential Media
miRISC	miRNA-induced silencing
miRNAs	MicroRNAs
NAC	N-acetyl-L-cysteine
PBS	Phosphate-buffered saline
PCa	Prostate cancer

PCSCs	Prostate cancer stem cells
PE	Phycoerythrin
pre-miRNAs	precursor miRNAs
pri-miRNAs	primary miRNA transcripts
p-STAT3	Phospho-STAT3 (Tyr705)
PTCH	Patched 1
PTEN	Phosphatidylinositol 3,4,5-trisphosphate 3-phosphatase and dual-specificity protein phosphatase PTEN
qRT-PCR	Quantitative real-time polymerase chain reaction
RISC	RNA-induced silencing complex
ROS	Reactive oxygen species
SCD1	stearoyl desaturase 1
SEM	Standard error of the mean
siRNAs	small interfering RNAs
SMO	Smoothened
SNAI1	Snail family zinc finger 1
STARD13	StAR-related lipid transfer protein 13
STAT3	Signal transducer and activator of transcription 3
TRBP	transactivation response element RNA-binding protein
WIF1	WNT Inhibitory Factor 1
3'UTR	3'-untranslated region
7-AAD	7-aminoactinomycin D

1. Introduction

1.1 Objectives of the study

Prostate cancer (PCa) is the most frequent malignant disease and a leading cause of cancer death in the male population in the world in 2020. The incidence of prostate cancer ranks first among men in developed countries. A total of 1.4 million new cases and 375,000 PCa-related deaths were counted worldwide in 2020 [1]. Normally, PCa patients will be initially treated by prostatectomy, followed by treatment with Gonadotropin-releasing hormone (GnRH) analogs to repress the androgen receptor signaling pathway [2]. Unfortunately, with disease progression, patients develop resistance to GnRH analogs. Patients with castration-resistant prostate cancer (CRPC) were treated with chemotherapeutic drugs like docetaxel and cabazitaxel, or with other agents like abiraterone acetate and enzalutamide [3]. Nevertheless, most of the CRPC patients develop resistance to these drugs and nearly 60% of the patientsdeveloped metastases during the first five years [4]. Once CRPC patients obtain resistance to docetaxel, the second-line chemotherapeutic drug, cabazitaxel will be applied [5] and is still active in CRPC patients even after treatment with ten cycles of docetaxel [6]. Therefore, it is crucial and meaningful to find new agents to target prostate cancer stem cells and reverse the drug resistance of cabazitaxel.

The objective of this thesis was to identify novel phytochemicals from traditional herbs targeting prostate cancer stem cells, and to reverse the cabazitaxel-resistant state in prostate cancer. Various approaches were used for the selection of promising candidate phytochemicals, including viability, proliferation, migration, invasion, and apoptosis assays. Based on our preliminary research, we mainly focus on shikonin and berbamine, since there are almost no data available about the role of shikonin and berbamine in prostate cancer stem cells and reversal of cabazitaxel resistance. Also, potential mechanisms of shikonin and berbamine involved in targeting prostate cancer stem cells and reversing the cabazitaxel resistant state were investigated. Additionally, genes related to cancer stem cells were analyzed in this study. Details of cancer stem cells, and other investigated cancer stem cell markers, and shikonin and berbamine were provided in the following sections.

1.2 Cancer stem cells

Cancer stem cells (CSCs) are a small subpopulation of undifferentiated cancer cells, responsible for tumor progression, invasion, tumor spread, and therapeutic relapse. Those CSCs maintain self-renewal, stemness properties similar to other types of stem cells [7, 8]. Cancer relapse is the result of resistant CSCs existing in the primary tumor, and their abilities of sphere formation and self-renewal. Furthermore, those resistant CSCs can drive metastatic tumors through vessel spread ([9], **Figure 1**).

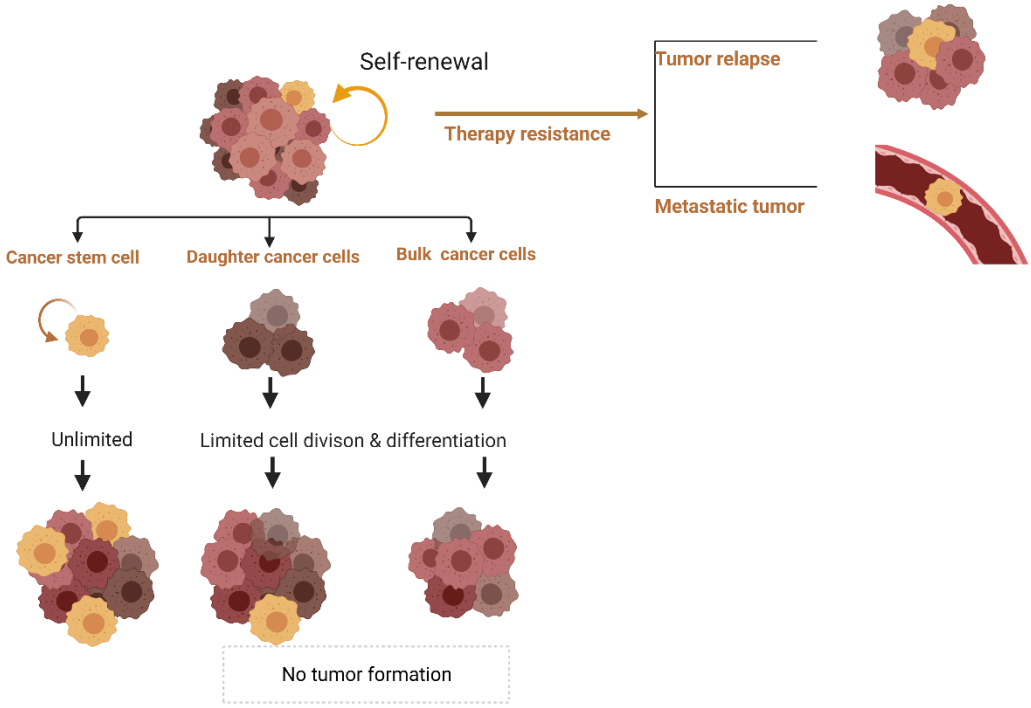

Figure 1. Cancer stem cells drive drug resistance and distant metastasis. Heterogeneous tumors contain CSCs, that support tumor cell proliferation due to their ability of self-renewal. Then, tumor recurrence and metastases will appear (Figure created with BioRender.com).

1.2.1 Concept of CSCs

For the concept of CSCs, it was initially detected in leukemia and myeloma. Among those cancer cells, just a small part of cancer cells hold the capacity of extensive proliferation [10]. Merely 1 in 10000 to 1 in 100 myeloma cells can form colonies in vitro using colony formation assay. When injected those leukemia cells back in vivo, only 1-4% of the cells could form spleen colonies [10]. Those cancer cells with the principal property of clonal tumor initiation ability and clonal long-term repopulation potential are called cancer stem cells. Different theories have shown that CSCs can be derived from normal stem cells induced by gene mutations or from tumor cells or dedifferentiated cells through abnormal genetic and epigenetic changes [11] (**Figure 2**).

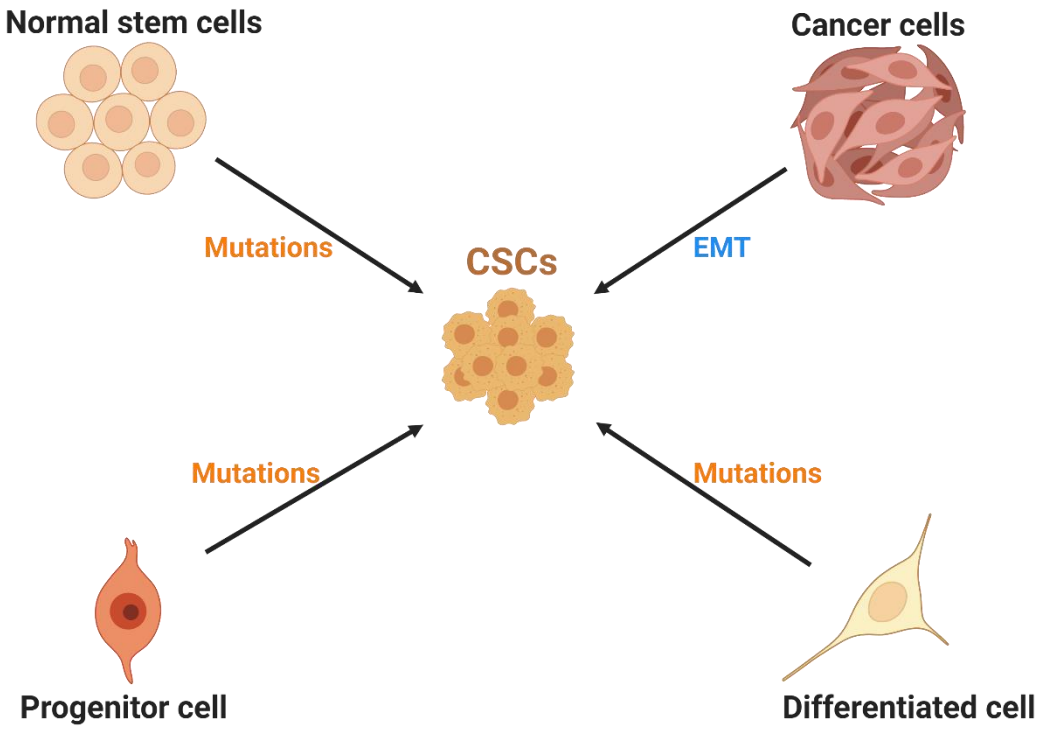

Figure 2. The origin of CSCs in tumor development. The CSCs can be derived from normal stem cells, progenitor cells, or differentiated cells through gene mutations. In addition, cancer cells can be transformed into CSCs through epithelial-mesenchymal transition (EMT) (Figure created with BioRender.com).

1.2.2 Mechanisms of CSCs related to drug resistance

So far, several mechanisms of therapy resistance of CSCs have been revealed, including cell cycle quiescence [12], overexpression of efflux pumps, like ABCG transporter proteins and detoxifying enzymes [13-16], or anti-apoptotic proteins, like Bcl-2, Bcl-X, and c-FLIP [13, 17, 18], forming a protective niche and repair DNA damage [13], boosting the activity of aldehyde dehydrogenase (ALDH) [19], activating the prosurvival signaling proteins such as NOTCH, Wnt/β-catenin, and NF-κB [19-21], enhancement in activities of PI3K/Akt/mTOR pathway and maternal embryonic leucine zipper kinase (MELK) [18, 22, 23]. The factors related to drug resistance in CSCs [11] are shown in **Figure 3.**

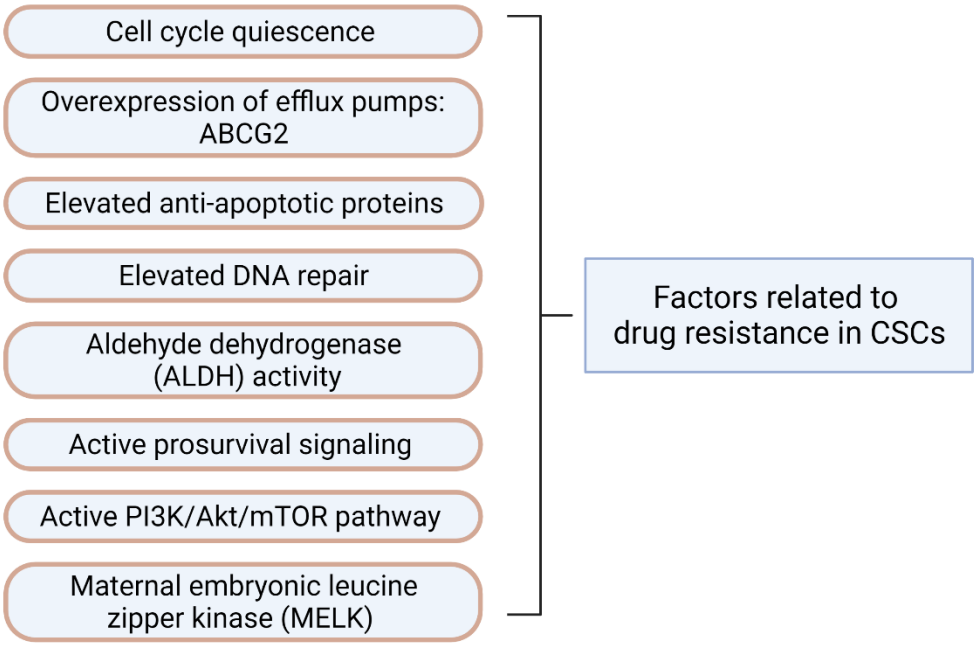

Figure 3. The factors contributing to drug resistance in CSCs. The factors, activation of cell cycle quiescence, cell prosurvival signaling pathways, PI3K/Akt/mTOR pathway, enhancement of efflux pumps, anti-apoptotic proteins, ALDH, MELK, and elevated DNA damage repair lead to CSC resistance (Created with BioRender.com).

1.2.3 Cancer stem cell markers correlate to drug resistance

There are several prostate cancer stem cell markers involved in drug resistance. First of all, ATP-binding cassette G2 (ABGC2) is highly expressed in prostate cancer stem cells (PCSCs). ABCG2 obtains the energy produced by ATP hydrolysis to discharge the anti-tumor drugs out of the tumor cells [24], which makes cancer cell survival in a low concentration of drugs [25]. Elevated ABCG2 contributes to drug resistance against agents such as taxanes, tyrosine kinase inhibitors, doxorubicin, and mitoxantrone [26]. High expression of ABCG2 leads to drug resistance in a variety of cancers [27]. When inhibiting the expression of ABCG2, cancer cells gain sensitivity to therapeutic agents [28]. Several signaling pathways proved that regulating ABCG2 expression confers drug resistance. Suppression of the PI3K/AKT signaling pathway counteracts the protective effects of ABCG2 against the chemotherapeutic agent in human multiple myeloma [29]. Inhibition of the PI3K/AKT and the MAPK/ERK signaling pathway downregulates the ABCG2 expression in prostate cancer stem cells [30]. Also, SIRT1/CREB/ABCG2 pathway contributes to cisplatin resistance in gastric cancer stem cells [31]. Another cancer stem cell marker, aldehyde dehydrogenase (ALDH), has been reported that correlated to drug resistance [32]. The ALDH family includes several

subtypes of ALDH1, ALDH2, and ALDH3, which play an important role in maintaining the detoxification process by oxidizing aldehydes to corresponding carboxylic acids [33]. ALDH3A1 and ALDH1A1, also belonging to the ALDH family are markers of PCSCs, whose expression correlates with PCa progression [23, 34, 35]. Inhibition of the Wnt/beta-catenin signaling pathway represses ALDH3A1 expression, and then reduces temozolomide resistance in glioblastoma [17]. Next, C-X-C Motif Chemokine Receptor 4 (CXCR4) is another prostate cancer stem cell marker. High expression of CXCR4 associates with an increased risk of distant metastasis and local recurrence in PCa [36]. Interestingly, inhibition of the expression of CXCR4 resensitizes prostate cancer cells to docetaxel [37].

1.2.4 Signaling pathways in CSCs

Several signaling pathways play an essential role in maintaining the stemness properties of CSCs, including Hedgehog, Wnt/β-catenin, Notch pathway, and TGFβ/BMP [11]. They are dysregulated in different kinds of cancers via epigenetic modifications [38]. These aberrant epigenetic changes in such signaling pathways enhance tumor progression, invasion, metastasis, and resistance through maintaining CSCs [39]. The signaling pathways regulated by epigenetic modifications [11] are shown in **Figure 4**.

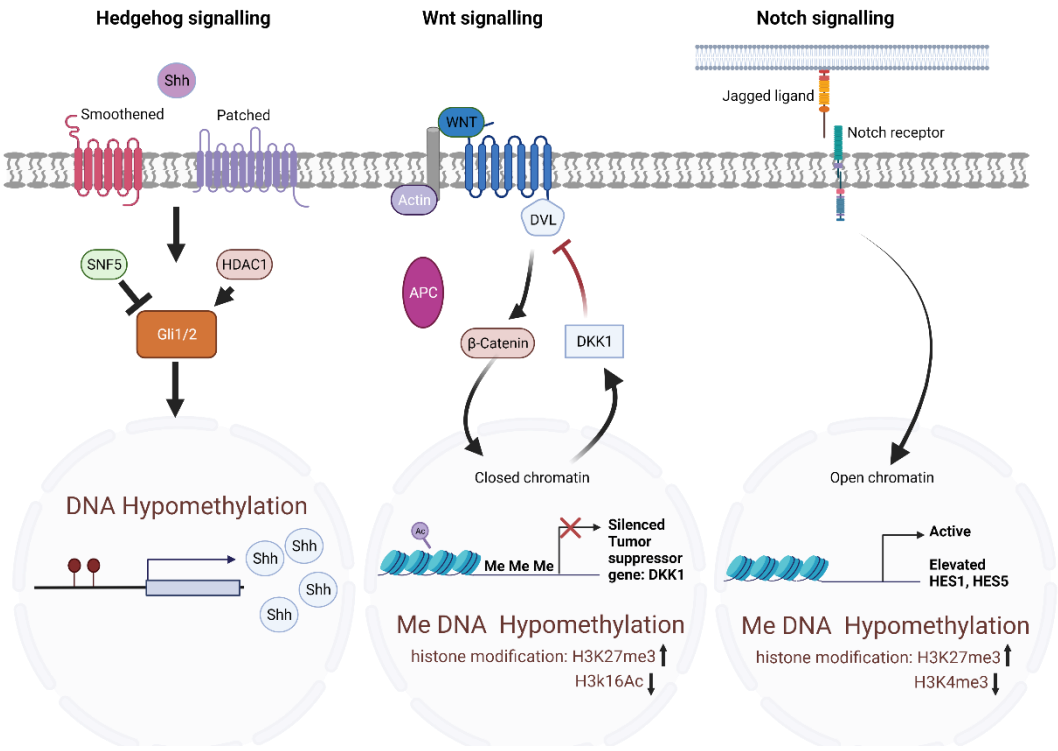

Figure 4. The major signaling pathways are regulated by epigenetic mechanisms in CSCs. Epigenetic dysregulation of signaling pathways in CSCs enables tumor cells to maintain self-renewal properties and stay in a drug-resistant state. The hedgehog signaling pathway is

activated via sonic hedgehog ligand (Shh) promoter hypomethylation, which is increased by the overexpression of histone deacetylases 1 (HDAC1), and decreased by the SWI/SNF chromatin-remodeling complex subunit (SNF5). Wnt signaling pathway is enhanced by inhibiting the expression of Dickkopf-related protein 1 (DKK1) through promoter hypermethylation, which enhances the H3K27me3, reduces acetylation at H3K16. DKK1 is an antagonist of Dishevelled (DVL) which is a cytoplasmic scaffold protein working in the Wnt signaling pathway. The notch signaling pathway is activated by enhancing the expression of hairy and enhancer of split-1 (HES1) and hairy and enhancer of split-5 (HES5) through promoter hypermethylation of STRAP. (Figure created with BioRender.com)

The Hedgehog signaling pathway is mainly involved in tissue homeostasis, regeneration of CSCs, embryonic development [40], and epithelial-to-mesenchymal transition of cells [41]. Hedgehog signaling is involved in the progression of different types of cancers, including basal cell carcinoma, gastrointestinal tumors, prostate cancer, breast cancer, glioblastoma, leukemia, and myeloma [42]. The Hedgehog network includes extracellular Hedgehog ligands, the transmembrane protein receptor PTCH (Patched 1), the transmembrane protein SMO (Smoothened), intermediate transduction molecules, and the downstream molecule GLI (Glioma-associated oncogene) [43]. The aberrant Hedgehog pathway plays an essential role in stem maintenance, self-renewal, and regeneration of CSCs for reasons that Hedgehog drives tumor growth and development and supports residual cancer cells after treatment [44]. When the Hedgehog ligand binds to PTCH, then rescue the suppression of SMO, and this whole cascade contributes to the translocation of GLI into the nucleus. Furthermore, the GLI family regulates the target genes of Hedgehog [45]. Also, the Hedgehog signaling pathway regulates different types of cancer stem cell markers or transcription factors, which are crucial for stemness properties and drug resistance, such as Oct4, Bmil, Sox2, ALDH1, Twist1, Wnt2, CCND1, CD44, SNAI1 (snail family zinc finger 1), CXCR4, C-MYC, ABCG2, C-MET, ABCB1, and Jagged 1 [44, 46, 47]. The Hedgehog pathway also regulates Nanog, which is a crucial transcription factor for CSCs to maintain stemness properties, self-renewal, and differentiation [48]. Activation of Hedgehog signaling pathway drives the CSCs in hepatocellular carcinoma [49], glioblastoma [50, 51], breast cancer [52, 53], colorectal adenocarcinoma [54], pancreatic cancer [55], and lung cancer [56].

Wnt/β-catenin signaling pathway plays a crucial role in the maintenance, expansion, and epithelial-mesenchymal transition of CSCs [57, 58]. The process that Wnt ligands bind to the co-receptors Frizzled and LRP 5/6 at the cell surface, stabilizes the cytoplasmic accumulation of β-catenin. The β-catenin then is transported into the nucleus,

activating the Wnt target genes, such as DKK1, Axin2, c-myc, cyclin D1, c-jun, which are important for the CSCs survival [59, 60]. Furthermore, Wnt signaling targets cancer stem cell markers, like CD44, CD24, EpCAM, and LGR5/GPR49 [59]. SOX2 regulates the activation of Wnt/β-catenin in CSCs, which promotes CSCs' dedifferentiation and drug resistance [61]. Enhancer of Zeste 2 (EZH2) also targets Wnt/β-catenin signaling and maintains the stemness of CSCs in glioblastoma [62].

Notch signaling pathway represents a kind of communication between cells that is essential for the regulation of stem cell proliferation, apoptosis, and cell fate during embryonic development [63] and is also crucial for proliferation, survival, self-renewal, differentiation, angiogenesis, and migration of CSCs [64-66]. Notch is a transmembrane receptor, including four types classified as Notch 1, Notch 2, Notch 3, and Notch 4. Activation of the receptors through binding to Notch ligands (Delta-like 1,3,4 and Jagged 1,2) releases the Notch intracellular domain into the nucleus and then influences the downstream genes [63]. Notch signaling pathway mediates the biological behaviors of CSCs such as self-renewal, differentiation, invasion, drug-sensitivity, and migration in hepatocellular carcinoma, colorectal carcinoma, pancreatic cancer, esophageal adenocarcinoma, and glioblastoma [63].

Transforming growth factor-beta (TGF-β) also has an active effect on forming CSCs and developing chemotherapeutic resistance [61]. TGF-β family ligands were activated by the assembly of a receptor complex with type I (main signal propagators) receptor components, and type II (activators) components. Receptor-phosphorylated SMAD proteins abbreviated R-SMAD can establish the transcriptional complexes, which are paired with other context-dependent transcription factors to regulate many different target genes [67]. TGF-β maintains CSCs' properties through enhanced cancer stem cell markers, such as CD133 in hepatocellular carcinoma [68, 69], and CD87 in lung cancer [70]. TGF-β pathway also influences the EMT progression through downregulating E-cadherin, and overregulating the levels of mesenchymal markers, like vimentin, N-cadherin, slug, fibronectin, and snail [70]. Keyvani-Ghamsari et al summarize the TGF-β/BMP signaling pathway in CSCs (**Figure 5**).

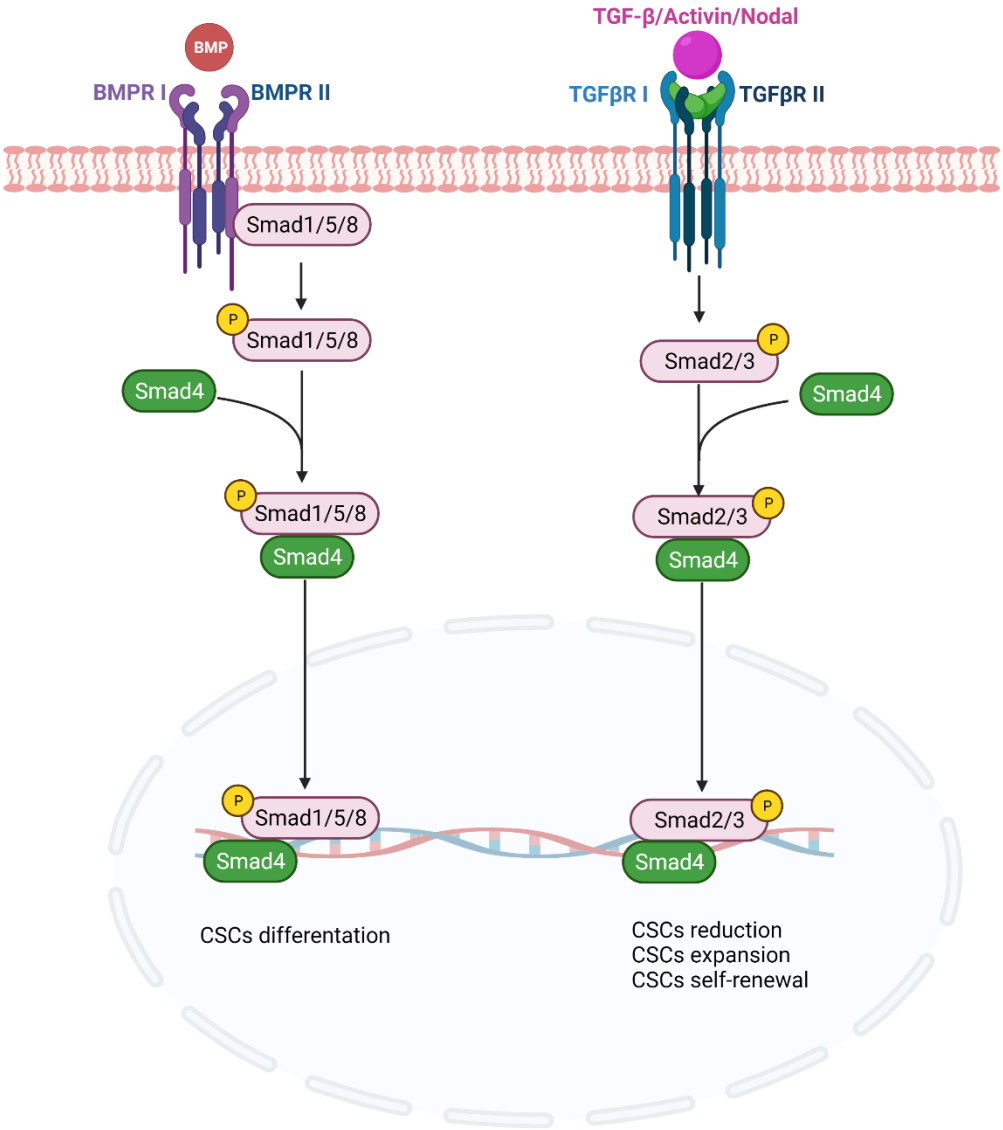

Figure 5. TGF-β/BMP pathway in CSCs. BMP (bone morphogenetic protein) signaling pathway mediates the CSCs differentiation. The TGF-β/Activin/Nodal signaling pathway plays a role in CSCs reduction, expansion, and self-renewal. (Figure created with BioRender.com)

1.2.5 MicroRNAs in CSCs

MicroRNAs (miRNAs), located in intergenic regions or introns of protein-coding genes, are non-coding RNAs that regulate genes through binding to the specific mRNAs [13]. For nuclear processing, first, primary miRNA transcripts (pri-miRNAs) are generated from miRNA genes with the assistance of RNA polymerase II. Then, the enzyme Drosha cleaves the stem-loop of the pri-miRNAs. DGCR8 (DiGeorge syndrome critical region gene 8) contains an RNA-binding domain and is thought to stabilize the pri-miRNAs by binding. Both Drosha and DGCR8 are building the microprocessor complex by which the precursor miRNAs (pre-miRNAs) are produced [71]. After that, pre-miRNAs are transported into the cytoplasm by Exportin 5, where pre-miRNAs are fur-

ther processed by the RNase III enzyme Dicer coupled to TRBP (transactivation response element RNA-binding protein). The terminal loop is removed to produce miRNA duplex molecules (miRNA/miRNA*). The 5p strand of a mature miRNA derives from the 5‘end of the pre-miRNA, and the 3p strand miRNA derives from the 3‘end of the pre-miRNA. In the end, either miRNA or miRNA* can be loaded into the Argonaut protein complex 1-4 (Ago1-4), the catalytic component of the miRISC (miRNA-induced silencing) complex. The miRNAs can target mRNAs through binding to the 3’UTRs or the open reading frames of the miRNAs [71]. There are two mechanisms by which miRNAs downregulate the target mRNA expression. One is to inhibit the translation of mRNAs to proteins. The other one is the degradation of the target mRNA through destabilization by decapping. Asadzadeh et. al has summarized the biogenesis and functions of miRNAs as shown in **Figure 6** [71].

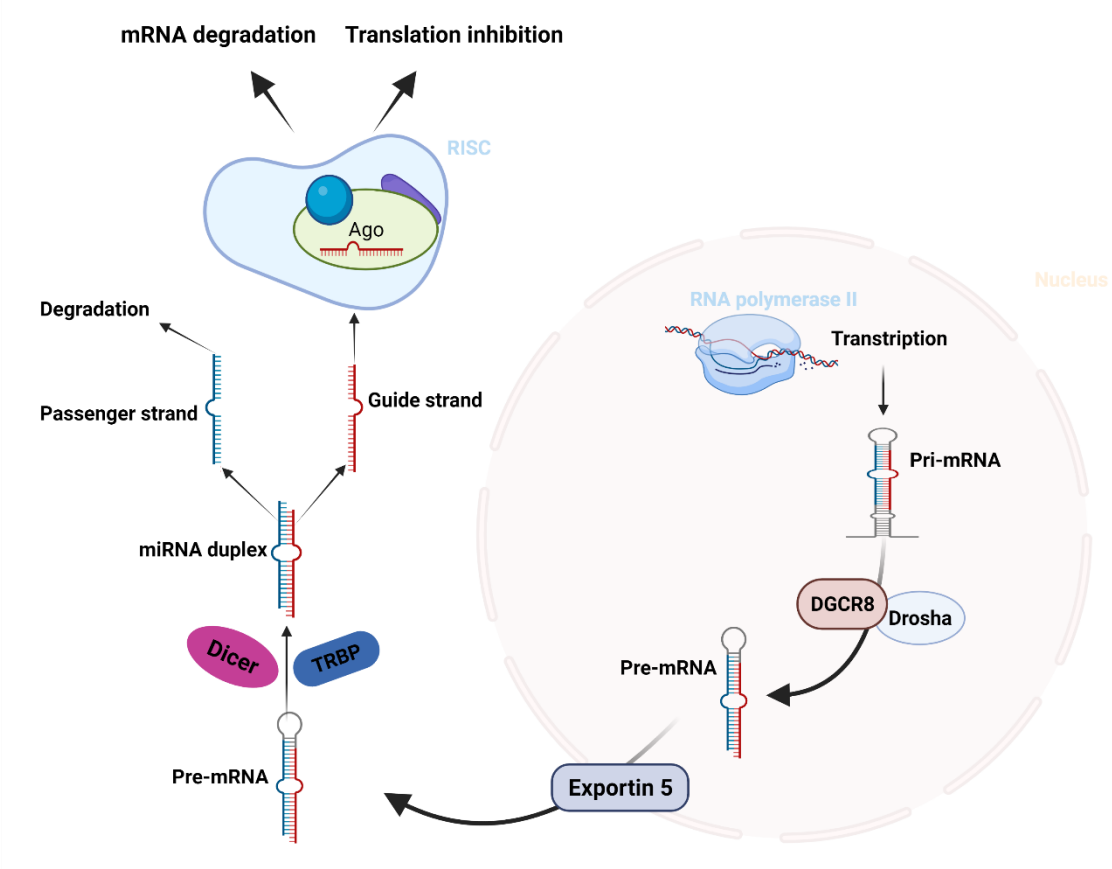

Figure 6. The biological origin and functions of miRNAs. The miRNA genes are transcribed by RNA polymerase II to form pri-miRNAs. The pri-miRNAs are then cleaved via the microprocessor complex (DGCR8 and Drosha) into stem-loop structure pre-miRNAs. Then those pre-miRNAs are exported to the cytoplasm with the assistance of Exportin 5. Furthermore, the pre-miRNAs are cleaved into mature miRNA through RNase III enzyme Dicer, which forms a complex with TRBP. The mature miRNA targeting mRNA is regulated by the RISC complex. The miRNAs regulate the specific genes by translation inhibition or degrading the mRNAs. DGCR8: DiGeorge syndrome critical region gene 8; miRNA: microRNA; mRNA: messenger RNA, pri-

miRNA: primary miRNA, pre-miRNA: precursor miRNA, RISC: miRNA-induced silencing complex, TRBP: transactivation response element RNA-binding protein. (Figure created with BioRender.com)

The miRNAs are released through apoptotic bodies when apoptosis happens in the extracellular space. MicroRNAs can be released through exosomes, AGO proteins, microvesicles, and high-density lipoproteins (HDL). Sohel et. al summarize the release mechanisms of circulating miRNAs [72] in **Figure 7**.

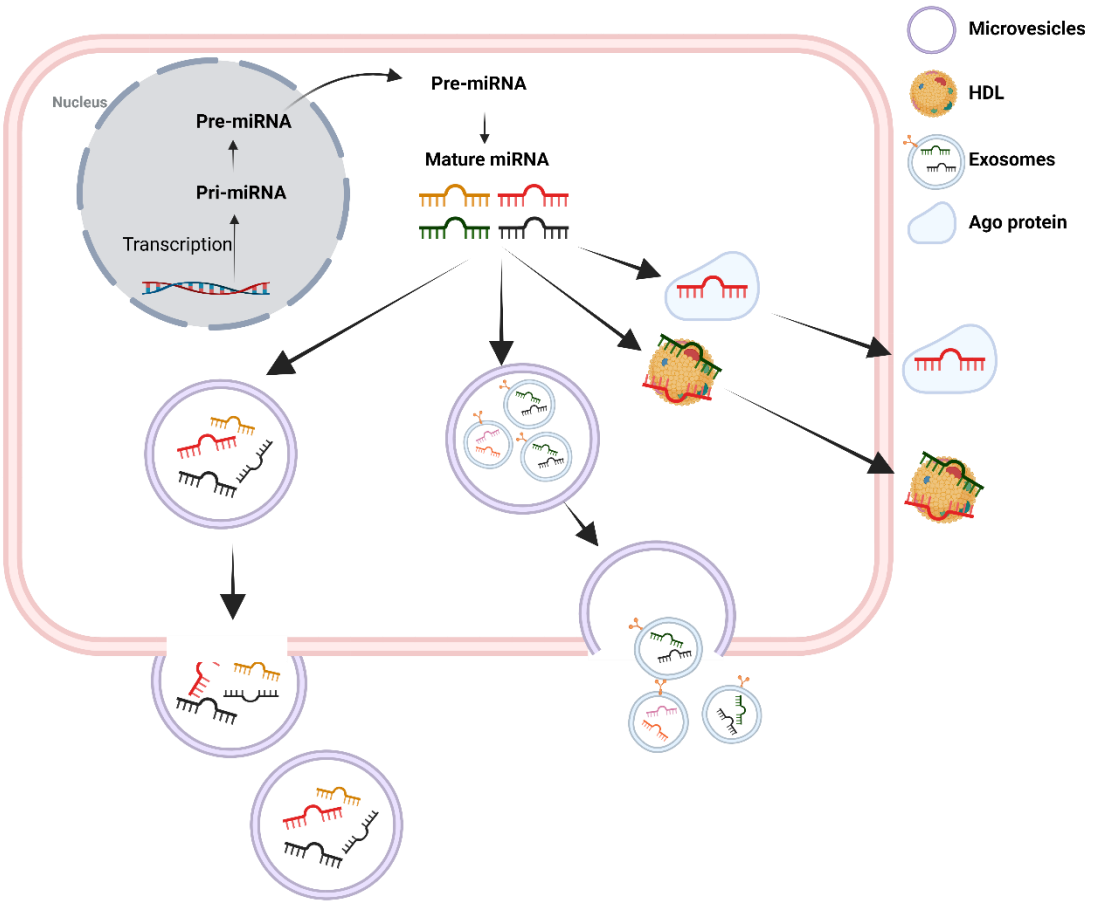

Figure 7. Release mechanisms of circulating miRNAs. First, miRNAs can be sorted and transported via exosomes through membrane invaginates. Second, the Ago proteins can process miRNAs by forming the miRISC complex, which can be released out of the cells. Third, healthy cells can generate microvesicles, which can convey miRNAs outside the cell through exocytosis. Fourth, the mature miRNAs can attach to high-density lipoproteins (HDL) to assemble a miRNA-HDL complex, which can be secreted out of the cells through exocytosis. (Figure created with BioRender.com).

It has been reported that CSCs enrich miRNAs with oncogenic features. Some miRNAs, are oncogenic miRNAs such as miR-10b, miR-20a, miR-21, miR-27, miR-29, miR-155, others are tumor suppressor miRNAs like miR-7, miR-34, miR-142, miR-145,

miR-200, miR-214, miR-448. They are related to the stemness properties of CSCs, tumor progression, or drug resistance [71, 73]. The oncogenic miRNAs, like miR-9, miR-215, are highly expressed and related to tumorigenesis, and drug resistance in CSCs. On the opposite, the tumor suppressor miRNAs, like let-7, miR-218, miR-16, miR-122, miR-34, and miR-152 are mainly downregulated in CSCs [71, 73].

MicroRNAs can regulate the CSCs signaling pathways, such as Notch, Wnt/β-catenin, and Hedgehog pathways, which are discussed in 1.2.4. The signaling pathways influenced by miRNAs [71] are shown in **Figure 8**.

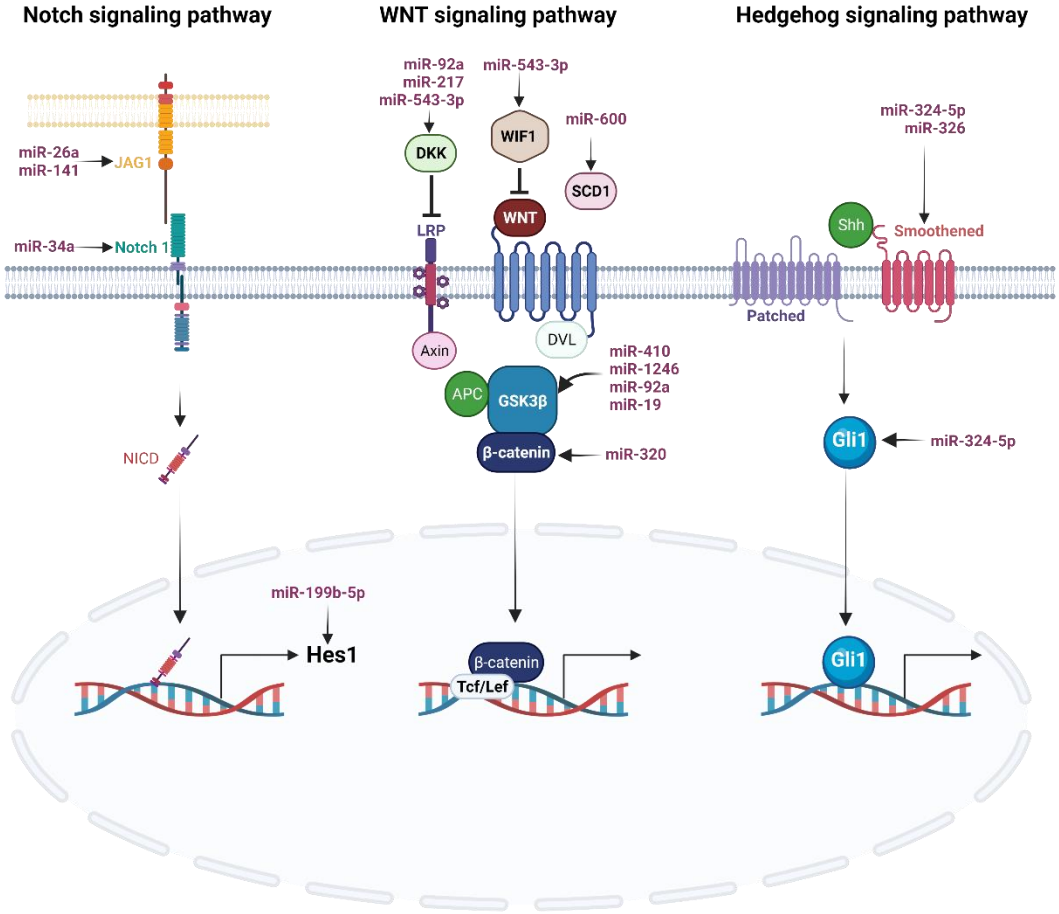

Figure 8. MicroRNAs involved in CSCs signaling pathways. The miRNAs miR-26a and miR-141 can regulate the Notch signaling pathway through targeting JAG1. Also, miR-34a and miR-199-5p target Notch1 and Hes1. The Wnt/β-catenin signaling pathway can be influenced by miR-92a, -217, -543-3p, -600, -410, -1246, -92a, -19, -320 via targeting DKK, WIF1, SCD1, GSK-3β, and β-catenin. In addition, miR-324 and miR-326 regulate the Hedgehog signaling by directly targeting Gli1 and smoothened mRNAs. (JAG1: Jagged1; Hes1: hairy and enhancer of split-1; NICD: Notch intracellular domain; DKK: dickkopf; WIF1: WNT Inhibitory Factor 1; DVL: Dishevelled; GSK3β: glycogen synthase kinase 3β; Tcf/Lef: T-cell factor/lymphoid enhancer factor; Gli1: glioma-associated oncogene homolog 1; miRNA: microRNA; mRNA: messenger

RNA; SCD1: stearoyl desaturase 1. (Figure created with BioRender.com)

1.3 Phytochemicals

1.3.1 Shikonin

Shikonin is one of the traditional Chinese medicines, which is derived from the roots of lithospermum erythrorhizon [74] and has anti-oxidant, anti-inflammatory, anti-thrombotic, and anti-cancer effects [75-77].

The chemical structure of shikonin is obtained from the PubChem database (https://pubchem.ncbi.nlm.nih.gov/compound/Shikonin) and shown in **Figure 9**.

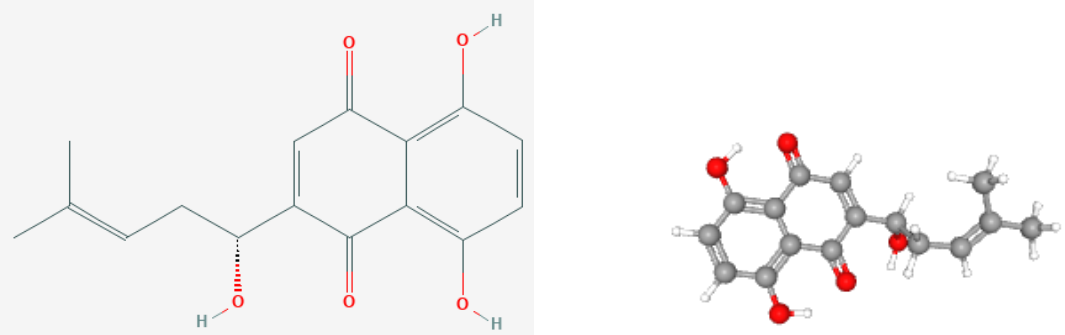

Figure 9. The structure of shikonin in 2-Dimensions and 3-Dimensions. The left graph shows the 2-dimensional structure of shikonin, the right graph shows the 3-dimensional structure.

Increasing evidence proves that shikonin induces autophagy by suppressing the AKT signaling pathway [78, 79], and impedes the growth of prostate cancer cells through modulating the androgen receptor [80]. Importantly, shikonin suppresses the viability [81] and proliferation of glioblastoma stem cells in a dose- and time-dependent manner, induces cell cycle arrest in G0/G1 and S phases, and promotes apoptosis [82]. Furthermore, an 18-months study shows that shikonin does not induce chemoresistance [83]. Taken together, we would like to investigate whether shikonin has anti-tumor effects on prostate cancer stem cells and whether shikonin is capable of reversing the drug resistance in our study.

1.3.2 Berbamine

Berbamine is a natural compound derived from the roots and barks of Berberis vulgaris

[84]. The chemical structure is from PubChem database

(https://pubchem.ncbi.nlm.nih.gov/compound/275182) and shown in **Figure 10**.

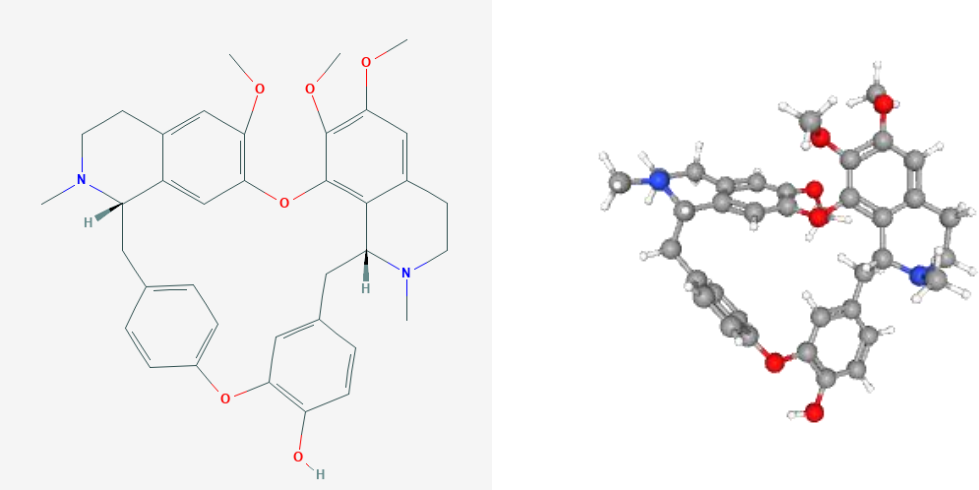

Figure 10. The structure of berbamine in 2-Dimensions and 3-Dimensions. The left graph shows the 2-dimensional structure of berbamine, the right graph shows the 3-dimensional structure.

Berbamine has anti-cancer activities in different types of cancers, such as chronic myeloid leukemia [85], breast cancer [86], and melanoma [87]. Promisingly berbamine can target the CSCs in glioblastoma [88]. Berbamine efficiently triggers apoptosis of leukemia stem cells through inhibiting phosphorylation of CaMKII γ [89]. The role of berbamine in prostate cancer stem cells and drug resistance will be investigated in this study.

2. Material and Methods

Parts of this chapter were already published in American Journal of Cancer Research [90]: Wang L, Stadlbauer B, Lyu C, Buchner A, Pohla H: Shikonin enhances the anti-tumor effect of cabazitaxel in prostate cancer stem cells and reverses cabazitaxel resistance by inhibiting ABCG2 and ALDH3A1. Am J Cancer Res 2020, 10:3784-3800.

2.1 Materials

2.1.1 Cell lines

The prostate cancer cell lines DU145, derived from a metastatic brain lesion and PC-3, derived from a metastatic bone marrow lesion, were used throughout the project. They were purchased from the DSMZ German Collection of Microorganisms and Cell Culture GmbH. The DU145 cancer stem cells (DU145 CSCs) and PC-3 cancer stem cells (PC-3 CSCs) were generated by the sphere formation assay as described in section 2.2.2.

2.1.2 Antibodies

Table 1. Antibody list

Antibodies	Clone	Company
APC-Annexin V	-	BD Biosciences, Heidelberg, Germany
Goat anti-mouse IgG H&L (Alexa Fluor® 488)	-	Abcam, Cambridge, UK
Goat anti-mouse IgG H&L (FITC)	-	Dianova, Hamburg, Germany
Goat anti-rabbit IgG H&L (Alexa Fluor® 647)	-	Abcam, Cambridge, UK
Goat anti-rabbit lgG H&L (Alexa Fluor® 488)	-	Invitrogen, Waltham, USA
Goat pAb to Rb lgG (HRP)	-	Abcam, Cambridge, UK
Mouse monoclonal ABCG2	BXP-21	Abcam, Cambridge, UK

Mouse monoclonal ABCG2antibody (APC)	5D3	BD Biosciences, Heidelberg, Germany
Mouse monoclonal CXCR4 monoclonal (PE)	12G5	BD Biosciences, Heidelberg, Germany
Mouse 23hosphor-Stat3 (Tyr705)	3E2	Cell Signaling Technology, Massachusetts, USA
Mouse Stat3	124H6	Cell Signaling Technology, Massachusetts, USA
Rabbit monoclonal Calnexin lgG	EPR3633(2)	Abcam, Cambridge, UK
Rabbit monoclonal CD9 lgG	EPR2949	Abcam, Cambridge, UK
Rabbit monoclonal HSP70 lgG	EPR16892	Abcam, Cambridge, UK
Rabbit monoclonal TSG101 lgG	EPR7130(B)	Abcam, Cambridge, UK
Rabbit monoclonal LIN28B lgG	EPR18717	Abcam, Cambridge, UK
Rabbit polyclonal ALDH3A1	-	Abcam, Cambridge, UK

2.1.3 Reagents and materials

Table 2. Reagent list

Reagents	Company
7-aminoactinomycin D	BD Biosciences, Heidelberg, Germany
A37 (ALDH1A1 inhibitor)	TOCRIS Bioscience, UK
ALDEFLUOR™ Kit	StemCell Technologies, Grenoble, France
AMD3100 (CXCR4 inhibitor)	Merck-Millipore, USA
B-27	Life Technology Grand Island, NY, USA
Berbamine	Selleckchem, Houston, Texas, USA
Bolt™ Antioxidant	Life technologies, Carlsbad, USA
Bolt™ LDS Sample Buffer (4x)	Life technologies, Carlsbad, USA

Bolt™ Sample Reducing Agent (10x)	Life technologies, Carlsbad, USA
Bolt™ MES SDS Running Buffer (20x)	Life technologies, Carlsbad, USA
BSA	Sigma, St. Louis, USA
BTYNB IMP1 Inhibitor (IGF2BP1 inhibitor)	Cayman CHEMICAL, ANN ARBOR, USA
Cabazitaxel	Selleckchem, Houston, Texas, USA
CB29 (ALDH3A1 inhibitor)	Sigma Aldrich, St. Louis, USA
CellTiter 96 Aqueous One Solution Cell Proliferation Assay	Promega, Madison, USA
CellTiter-Blue Cell Viability Assay	Promega, Madison, USA
Cryptotanshinone (CPT, p-STAT3 inhibitor)	Selleckchem, Houston, Texas, USA
Cytofix/ Cytoperm™ Kit	BD Biosciences, Heidelberg, Germany
DCFDA Cellular ROS Detection Assay Kit	Abcam, Cambridge, UK
DMEM	Life Technologies Europe, Bleiswijk, The Netherlands
EDTA	Ambion, USA
Epidermal growth factor (EGF)	Sigma Aldrich, St. Louis, USA
ExoQuick-TC™ Tissue Culture Media Exosome Precipitation Solution	System Biosciences, Palo Alto, CA, USA
FastStart Essential DNA Green Master kit	Roche, Penzberg, Germany
Fetal calf serum	Bio&Sell,GmbH, Feucht, Germany
Growth factor reduced Matrigel Basement Matrix	Corning, NY, USA
Human recombinant basic fibroblast growth factor (bFGF)	Sigma Aldrich, St. Louis, USA
Ibidi mounting medium	Ibidi, Martinsried, Germany
JC-1 mitochondrial membrane potential kit	Abcam, Cambridge, UK

Ko143 (ABCG2 inhibitor)	Tocris Biosciences, Bio-Techne GmbH, Wiesbaden-Neuenstadt, Germany
L-glutamine	Invitrogen, Life Technologies, Eugene Oregon, USA
Lipofectamine RNAiMAX Reagent	Invitrogen, Life Technologies, Eugene Oregon, USA
LIVE/DEAD® Fixable Blue Dead Cell Stain Kit	Invitrogen, Life Technologies, Eugene Oregon, USA
Minimal essential medium (MEM)	Invitrogen, Life Technologies, Eugene Oregon, USA
miRCURY® LNA® miRNA SYBR® Green PCR	Qiagen, Hilden, Germany
miRCURY® LNA® RT Kit	Qiagen, Hilden, Germany
miRCURY® Exosome Cell/Urine/CSF Kit	Qiagen, Hilden, Germany
miRNeasy Micro Kit	Qiagen, Hilden, Germany
miRNeasy Tissue/Cells Advanced Mini Kit	Qiagen, Hilden, Germany
mirVana miRNA mimic Negative Control	Ambion, USA
Molecular Probes® NucBlue® Fixed Cell Stain ReadyProbes® reagent (DAPI special formulation,)	Thermo Fisher Scientific, Waltham, USA
NCT-501(ALDH1A1 inhibitor)	Selleckchem, Houston, Texas, USA
OPTI-MEM reduced serum medium	Life Technologies, Paisley, UK
PBS	Invitrogen, Darmstadt, Germany
Phosphatase Inhibitor Cocktail 1-3	Sigma Aldrich, St. Louis, USA
Pierce™ BCA Protein Assay Kit	Thermo Fisher Scientific, Rockford, IL, USA
Reverse transcription system	Promega, Madison, USA
RIPA lysis buffer	Thermo Fisher Scientific, Waltham, USA
RNeasy Mini-Kit	Qiagen, Hilden, Germany

RPMI 1640 medium	Invitrogen, Darmstadt, Germany
SeeBlue® Plus2 Pre-Stained Protein Standard	Life Technologies, Thermo Fisher Scientific
Shikonin	Selleckchem, Houston, Texas, USA
Silencer® Select *GAPDH* positive control	Ambion, USA
Silencer® Select negative control	Ambion, USA
SNORD48	Qiagen, Maryland, USA
Sodium pyruvate	Invitrogen, Life Technologies, Eugene Oregon, USA
StemPro® Accutase®	Life Technologies, Thermo Fisher Scientific
SuperSignal™ West Pico PLUS Chemiluminescent Substrate	Thermo Scientific, Rockford, IL, USA
Triton X-100	Sigma Aldrich, St. Louis, USA
WZ811(CXCR4 inhibitor)	Selleckchem, Houston, Texas, USA

Table 3. Material list

Materials	Company
Blot Development Folders	Advansta, San Jose, CA, USA
Bolt™ 4-12% Bis-Tris Plus	Thermo Fisher Scientific, Carlsbad, CA, USA
Cryo Tube Vitals	Thermo Fisher Scientific, Roskilde, Denmark
FALCON 75 cm2 Flasks	Corning, NY, USA
FALCON 25 cm2 Flasks	Corning, NY, USA
iBind® 2 PVDF Regular Stacks	Thermo Fisher Scientific, Kiryat Shmona, Israel
IBind™ Flex Card	Thermo Fisher Scientific, Kiryat Shmona, Israel
iBind™ Flex Solution Kit	Thermo Fisher Scientific, Carlsbad, CA, USA
Ultra-Low Attachment 75 cm2 flasks	Corning, Kennebunk, ME, USA
16-well chambered coverslips	Thermo Fisher Scientific, NY, USA
40 µM nylon mesh	BD Biosciences, Heidelberg, Germany

Silicone inserts for migration assay	ibidi GmbH, Martinsried, Germany
The transwell inserts in 24-well plates (8.0 μm pores) for invasion assay	Falcon, Corning, NY, USA
Tissue Culture Plate, 6 Well	Corning, NY, USA
Tissue Culture Testplate 24	TPP, Switzerland
Tissue Culture TestPlate 96F	TPP, Switzerland

2.1.4 Primers

The primers for miRCURY LNA miRNAs of let-7a, let-7b, let-7d, let-7f, let-7g, let-7i, miR-98, miR-26a, miR-26b were designed and synthesized from Qiagen (Maryland, USA). The primers for our target genes were listed in **Table 4**.

Table 4. Primers list

Gene	Forward primer	Reverse primer
ABCG2	CAT CAA CTT TCC GGG GGT GA	CAC TGG TTG GTC GTC AGG AA
ACTB	CTG CCC TGA GGC ACT C	GTG CCA GGG CAG TGA T
ALDH1A1	TGT TAG CTG ATG CCG ACT TG	TTC TTA GCC CGC TCA ACA CT
ALDH3A1	GCA GAC CTG CAC AAG AAT GA	TGT AGA GCT CGT CCT GCT GA
CXCR4	TGG GTG GTT GTG TTC CAG TTT	ATG CAA TAG CAG GAC AGG ATG
GAPDH	CAT GGG TGT GAA CCA TGA	TGT CAT GGA TGA CCT TGG
HMGA1	CCA AGG GGC AGA CCC AAA AA	GCA AAG CTG TCC AGT CCCA
HMGA2	CAG GAA GCA GCA GCA AGA AC	GCC TCT TGG CCG TTT TTC TC
IGF2BP1	TGA CGA GGT TCC CCT GAA GA	GCA ACA ATT CTC GAT GGC CC
LIN28B	AAAGCACATTAGACCATGCGAG	CCCTCAGCTCCAAACTCGTG
PTEN	ATT CCC AGT CAG AGG CGC TA	CAC CTT TAG CTG GCA GAC CA
STARD13	CTG TCT CAG AAG GTC GGA CG	GCT TGT TGG ACA TGG AGT GC
STAT3	AGC AGC ACC TTC AGG ATG TC	GCA TCT TCT GCC TGG TCA CT

2.1.5 miRCURY LNA miRNA Mimics and Power Inhibitors

Table 5. miRCURY LNA miRNA Mimics and Power Inhibitors

microRNAs	Sequence 5‘-3‘
Let-7 Power inhibitor	C*A*A*C*C*T*M*C*T*A*C*C*T*C A*C*A*A*C*T*T*A*C*T*A*C*C*T*C A*C*A*A*W*C*T*A*C*T*A*C*C*T*C
Let-7a mimics	UGA GGU AGU AGG UUG UAU AGU U
Let-7b mimics	UGA GGU AGU AGG UUG UGU GGU U
Let-7i mimics	UGA GGU AGU AGU UUG UGC UGU U
miR-26 Power inhibitor	A*T*C*C*T*G*R*A*T*T*A*C*T*T*G*A
miR-26a mimics	UUC AAG UAA UCC AGG AUA GGC U
MiR-26b mimics	UUC AAG UAA UUC AGG AUA GGU

Note: All the mimics and inhibitors are designed and synthesized from Qiagen (Maryland, USA). The miRCURY LNA miRNA Power Inhibitors contain phosphorothioate bonds indicated by “*”. The inhibitors contain mixed DNA bases, which are indicated within the sequence (K = G, T; M = A, C; R = A, G; S = C, G; W = A, T; Y = C, T).

2.1.6 siRNAs

Table 6. *Silencer* ® Select siRNAs (ThermoFisher Scientific)

Target gene symbol	Sense strand (5'-3')	Anti-sense strand (5'-3')
ABCG2	CUCUGACGGUGAGAGAAAAtt	UUUUCUCUCACCGUCAGAGtg
ALDH3A1	GGAACUCAGUGGUCCUCAAtt	UUGAGGACCACUGAGUUCCct
CXCR4	CCUGUUUCCGUGAAGAAAAtt	UUUUCUUCACGGAAACAGGgt

2.1.7 Apparatus and software

Table 7. Apparatus and software

Apparatus and software	Company
BD CellQuest software (version 4.0.2)	BD Biosciences, Heidelberg, Germany
Confocol microscope SP5	Leica, Munich, Germany
Electrophoresis Power Supply-EPS 301	Amersham Biosciences, Sweden
Emax precision microplate reader	MWG Biotech, Ebersberg, Germany
FACSCalibur	Becton Dickinson, San Jose, CA, USA
Fiji ImageJ software	Homepage:https://imagej.net/software/fiji/ (Reference: [91])
FlowJo software (version 9.9.5).	Tree Star Inc., Ashland, OR, USA
Fluor-S™ Multilmager	BIO-RAD, USA
FLUOstar OPTIMA microplate reader	BMG LABTECH, Ortenberg, Germany
High-speed Centrifuge	Eppendorf, Hamburg, Germany
iBind® Flex Western Device	Thermo Fisher Scientific, Israel
iBlot® 2 Cell Transfer Device	Thermo Fisher Scientific, Kiryat Shmona, Israel
Light Cycler® 96	Roche, Penzberg, Germany
Lightcycler® 96 software (1.1 version)	Roche, Penzberg, Germany
LSRII flow cytometer	BD Biosciences, Ebersberg, Germany
NanoDrop 2000	Thermo Fisher Scientific, NY, USA
OPTIMA software version 2.0	BMG LABTECH
SPSS version 25.0	IBM, Armonk, NY, USA
Web-based Automated Cellular Analysis System	ACAS, MetaVì Labs, Bottrop, Germany
XCell SureLock™ Electrophoresis Cell	Invitrogen, USA

2.2 Methods

2.2.1 Cell culture

DU145 and PC-3 were grown in RPMI1640 supplemented with 10% fetal calf serum

(FCS), 1% minimal essential medium, 1 mM sodium pyruvate, and 2 mM L-glutamine under the condition of 5% CO2 at 37 ℃. The PCSCs were generated using CSC medium containing DMEM/F12 medium supplemented with 2% B-27, 10 ng/ml epidermal growth factor (EGF), and 10 ng/ml basic fibroblast growth factor (bFGF).

2.2.2 Sphere-forming assay

All the PCSCs were generated by the sphere-forming assay in CSC specific medium as described in 2.2.1. Initially, PCa cells (DU145 and PC-3) were harvested using 3-5 ml Accutase cell detach solution and incubated for 8-10 minutes at 37 ℃. Collected cells were counted using a hemocytometer. Then, around 3-10 × 10^5 cells were seeded in a 75 cm^2 low-attachment flask and cultured with 10 ml CSC specific medium for 7 days. Spheric PCSCs were harvested using Accutase cell detach solution. After dissociation, PCSC cells were filtered through a 40 µm nylon mesh, counted, and used for the different assays. For CSC enrichment, dissociated spheres were used for a second round of sphere formation.

2.2.3 Drug sensitivity assay

To evaluate the viability of PCa cells and PCSCs treated by different phytochemicals and drugs, the drug sensitivity assay was conducted using the CellTiter Blue Kit. Initially, cells were dissociated using Trypsin/EDTA for PCa cells or Accutase cell detach medium for PCSCs. After that, a total of 1-5 × 10^5 cells per well were seeded in 96-well plates and incubated overnight at 37 ℃ and 5% CO_2. The next day, the cell culture medium was discarded and exchanged with culture medium containing different concentrations of phytochemicals or other agents. The wells containing culture medium without cells were set up as background control, and the wells with cells but without phytochemicals or other agents were considered as the control group. Then, after 24 hours and 48 hours, 20 µl CellTiter Blue solution were added and the plate was incubated for one hour at 37 ℃ with 5% CO_2. Fluorescence was measured using the FLUOstar OPTIMA microplate reader at 560 (20) nm excitation and at 590 (10) nm emission. The data were collected and evaluated using the OPTIMA software version 2.0. of The logit regression model was used to calculate the half-maximal inhibitory concentration abbreviated as IC50.

2.2.4 Development of cabazitaxel-resistant DU145 cell line

To investigate the effect of phytochemicals or other agents on cabazitaxel-resistant PCa cells, we established a cabazitaxel-resistant DU145 cell line. At the beginning, a total of 1 × 10^6 DU145 cells were seeded in a 75 cm^2 flask with cabazitaxel at a concentration of 1 nM and 2 × 10^5 cells were seeded without cabazitaxel as a control. At confluency of the control cells, all cells were harvested and then seeded again. Once the DU145 cells gained resistance to 1 nM cabazitaxel, the cells were cultured with stepwise increasing cabazitaxel concentrations. The DU145 cells were cultured with cabazitaxel for at least eight months until a concentration of 6 nM cabazitaxel was reached. The cell viability assay was conducted to judge the resistance degree compared to the control cells cultured in parallel.

2.2.5 Cell proliferation assay

To determine the proliferative ability of PCa cells and PCSCs treated by phytochemicals or other agents, the cell proliferation assay was carried out using the CellTiter 96 Aqueous One Solution Kit. A total of 1-5 × 10^3 cells per well were seeded in 96-well plates and incubated overnight at 37 ℃ and 5% CO_2. The next day, the culture medium was exchanged with or without phytochemicals or other agents. The wells without cells were again used as background controls, while the wells with cells but without treatment were the control group. The proliferation would be assessed after 24 hours, 48 hours, or 72 hours with separate plates for different time points. A volume of 20 µl CellTiter 96 Aqueous One Solution was added to each well, and the plates were incubated for three hours at 37 ℃ and 5% CO_2. Finally, the data were collected using the Emax microplate reader at 490 nm for absorbance.

2.2.6 Apoptosis assay

To analyze the apoptosis rate of PCa cells and PCSCs caused by phytochemicals or other agents, the apoptosis assay was executed by flow cytometry. A total of 2-4 × 10^5 cells were seeded in 25 cm^2 flasks and incubated overnight at 37 ℃ and 5% CO_2. On the next day, the culture medium was exchanged with or without phytochemicals or other agents. After 5 days of incubation, the cells were harvested using 500 µl of Trypsin/EDTA for five minutes at 37 ℃ and 5% CO_2. Then, a volume of 100 µl Annexin V binding buffer was added to the cells. Afterwards 5 µl APC-conjugated Annexin V and 7-aminoactinomycin D (7-AAD) were added and the cells were incubated for 15 minutes at room temperature. Then, 100 µl Annexin V binding buffer was added again, the cells were put on ice, and measured using the FACSCalibur within one hour. For

each sample, a minimum of 1×10^4 cells was recorded. Data acquisition was done using BD CellQuest software and analyzed using FlowJo version 9.9.5. The Annexin V positive cells were considered as apoptotic cells.

2.2.7 Scratch wound healing assay

To evaluate the migration ability of PCa cells and PCSCs influenced by phytochemicals or other agents, the scratch wound healing assay was done using special 24-well µ-plates containing small 2-well silicone inserts per well. Those special inserts form a cell-free gap of 500 µm as space for the cells to migrate. The protective foil attached to the bottom of the µ-plate was removed by hand. Then, 70 µl of a cell suspension of 4 x 10^5 cells/ml culture medium were added to each small insert. The cells were incubated at 37 °C and 5% CO_2 for at least 24 hours until a confluent cell monolayer was achieved. The 2-well inserts were taken out with sterile tweezers and the cell layer was washed with PBS to remove cell debris and non-attached cells. Next, new culture medium with or without the phytochemicals at different concentrations was added to the cells. Pictures were taken at several time points like 0 h, 3 h, 6 h, 9 h, 21 h, 24 h, 27 h, and 30 h. The percent of covered area of the gap was assessed and analyzed by the Automated Cellular Analysis System based on the FastTrack AI image analysis algorithms.

2.2.8 Invasion assay

To investigate the invasiveness of PCa cells and PCSCs influenced by the phytochemicals or other agents, the invasion assay was done using the Boyden Chamber system with transwell inserts in 24-well plates coated with growth factor reduced Matrigel Basement Matrix (30 µg/100 µl/insert). The plates were incubated for at least four hours at 37 °C and 5% CO_2. The cells were harvested using Trypsin/EDTA, washed once with PBS, and resuspended in DMEM medium without FCS to reach a cell concentration of 4×10^5/ml. Before seeding the cells onto the Matrigel, the residual liquid should be discarded carefully from the Matrigel. A volume of 125 µl cells was seeded in the inserts, and another 125 µl FCS-free medium with or without phytochemicals were added. In the lower chamber, a volume of 750 µl medium containing 10% FCS was added. The plates were incubated for two days. Afterwards, the liquid in the inserts was pipetted out, and the Matrigel on the upper surface of the membrane was carefully wiped using pre-wetted cotton swabs to remove not migrated cells. Next, the inserts

were put into a 24-well plate containing 4% paraformaldehyde and incubated for 5 minutes to fix the cells, which had moved through the Matrigel to the lower surface of the membrane. Then, the inserts were stained in 1% crystal violet for 1 minute, washed with water, and dried on a paper towel at room temperature. The pictures were taken by a digital camera (three fields per insert) and the cells were counted using the Fiji Image J software. The number of cells in one picture was considered as invaded cell number.

2.2.9 Measurement of aldehyde dehydrogenase (ALDH)

To measure the ALDH expression influenced by phytochemicals in PCa cells and PCSCs, the ALDEFLUOR™ kit was used. At first, 3×10^5 cells were seeded in 25 cm^2 ultra-low attachment flasks with or without phytochemicals at different concentrations and cultured for 24 hours. After 24 hours, cells were dissociated using Accutase and washed once with PBS. To exclude dead cells, 5 µl 7-AAD was added and the cells were incubated for 15 minutes at room temperature. After being washed once with PBS, the cells were mixed with 400 µl ALDEFLUOR™ Buffer and transferred into flow cytometry tubes. Diethylaminobenzaldehyde (DEAB), a specific ALDH inhibitor was used as the control for background fluorescence and therefore, 1 µl DEAB reagent was added into an empty control tube and recapped immediately. One microliter activated ALDEFLUOR™ reagent (BODIPY-aminoacetaldehyde, BAAA) was added to the cells in the test tube. After being mixed well, 200 µl of the test samples were transferred immediately into the control tubes. The test and control samples were incubated for 45 minutes at 37 °C and 5% CO_2 and centrifuged for 5 minutes at 250 g. The supernatant was removed and the cells were resuspended in the 200 µl ALDEFLUOR™ Buffer, stored on ice, and measured using the FACSCalibur. Activated ALDEFUOR™ reagent (BAAA) is a fluorescent substrate for ALDH and diffuses into the cells. In the presence of ALDH BAAA will be converted into BODIPY-aminoacetate (BAA), which retains inside the cells and leads to increased fluorescence. The data were collected using BD CellQuest software and evaluated by FlowJo version 9.9.5.

2.2.10 Flow cytometry for protein detection

To characterize the PCSCs, the cancer stem cell markers were tested using flow cytometry. PCSCs were seeded in a 6-well ultra-low attachment plate, incubated using the specific CSC medium containing phytochemicals or other agents at different concentrations for 24 hours at 37 °C and 5% CO_2. Then, the cells were harvested, fixed,

and permeabilized using the Fixation/Permeabilization Solution Kit (Cytofix/Cytoperm™). Afterwards, cells were stained with APC-conjugated ABCG2 mouse monoclonal antibody, or PE-conjugated CXCR4 mouse monoclonal antibody, unconjugated STAT3 mouse monoclonal antibody, unconjugated mouse monoclonal phosphor-STAT3 antibody (Tyr705), and unconjugated LIN28B rabbit monoclonal antibody. The FITC-conjugated goat anti-mouse lgG + IgM (H+L) antibody and the Alexa Fluor 488-conjugated goat anti-rabbit lgG H&L antibody were used as secondary antibodies. To keep out the dead cells or debris, cells were stained with LIVE/DEAD® Fixable Blue Dead Cell Stain reagent. After that, at least 1×10^4 cells were measured using the LSR II or the FACSCalibur. Data processing was done with FlowJo version 9.9.5.

2.2.11 Quantitative real-time polymerase chain reaction (qRT-PCR)

RNA was isolated using the QIAGEN RNeasy® Mini Kit. A maximum of 5 x 10^6 cells were lysed with 350 µl RLT Buffer and centrifuged at 14,000 rpm for two minutes in a QIAshredder spin column placed in a 2 ml collection tube. To the lysate 350 µl 70% ethanol were added, mixed well, transferred to the RNeasy spin column in a 2 ml collection tube, and centrifuged at 10,000 rpm for 15 seconds. Flow-through was discarded. Then, 350 µl RW1 Buffer was added, the column was centrifuged again at 10,000 rpm for 15 seconds, and the flow-through was discarded. A volume of 80 µl DNase solution (10 µl DNase plus 70 µl RDD Buffer) was added into the column, incubated for 15 minutes at room temperature. Afterwards, 350 µl RW1 buffer was added, the column was centrifuged again, the flow-through discarded, 500 µl RPE Buffer was added, the column centrifuged again at 10,000 rpm for 15 seconds, and the flow-through discarded. Another 500 µl RPE Buffer was added, the column centrifuged at 10,000 rpm for 2 minutes, and the flow-through was discarded. Finally, the spin column was carefully removed from the collection tube, placed in a new 2 ml tube, centrifuged again, and transferred to a new 1.5 ml tube. A volume of 20-50 µl RNase-free water was added and the column was centrifuged at 10,000 rpm for 1 minute. The concentration of the eluted RNA was measured using the NanoDrop 2000.

A total of 1 µg RNA was used for the reverse transcription system. At first, the RNA was incubated at 70 °C for 10 minutes. The 20 µl reaction mix contains 4 µl 25 mM $MgCl_2$, 2 µl Reverse transcription 10× Buffer, 2 µl 10 mM dNTP, 0.5 µl Recombinant RNasin® Ribonuclease Inhibitor, 15 U AMV Reverse Transcriptase, 0.5 µg oligo(dT) primer, 1 µg RNA template, and PCR-grade water. The reaction mix was incubated at

42 ℃ for 15 minutes, at 95 ℃ for 5 minutes, and then for at least 5 minutes at 4℃. The cDNA was diluted and stored at -20 ℃ for further experiments.

The real-time PCR procedure was performed using the LightCycler® 96 and the FastStart Essential DNA Green Master kit. A 10 µl reaction mix containing 5 µl FastStart Essential DNA Green Master, 1 µl nuclease-free water, 1 µl of each forward and reverse primer at 5 pmol respectively, and 2 µl diluted cDNA template was set up. The parameters were as follows: a hot start with 95 °C for 10 minutes, then 40 cycles beginning with a denaturation step at 95 ℃ for 10 seconds, followed by annealing at 60 °C for 10 seconds, and final extension at 72 °C for 10 seconds. Then, a melting process was set up at 95 °C for 10 seconds, followed by 65 °C for 1 minute, and 97 °C for 1 second. Data were analyzed using the LightCycler® 96 software SW 1.1. The relative expression was estimated using the $2^{-\Delta\Delta Ct}$ method. Normalization was done using the internal controls *GAPDH* and *ACTB*. The primer list was provided in **Table 4**.

2.2.12 Confocal immunofluorescence microscopy

To detect the correlation of cancer stem cell markers, confocal fluorescence microscopy was performed using the confocal Leica SP5 and 365 nm wavelength for excitation and 420 nm wavelength for emission. First, a total of 2×10^4 cells were seeded in a 16-well chambered coverslip and incubated for 24 hours. The next day, the cells were fixed, permeabilized, and blocked using 4% formaldehyde for 10 minutes, 0.1% Triton X-100 for 5 minutes, and 3% BSA for 1 hour at room temperature, respectively. Then, the cells were incubated with the primary rabbit polyclonal antibody ALDH3A1 at 5 µg/ml and the mouse monoclonal antibody ABCG2 at a dilution of 1:50 at 4 ℃ overnight. Afterwards, the cells were washed three times with PBS and incubated with the secondary antibodies (goat anti-rabbit IgG (H+L) conjugated with Alexa Fluor 647 for ALDH3A1 and goat anti-mouse IgG (H+L) conjugated with Alexa Fluor 488 for ABCG2) in a dilution of 1:200 for 1 hour at room temperature in the dark. After a further washing step with PBS for three times, 200 µl NucBlue® Fixed Cell Stain ReadyProbes® solution (DAPI) was added per well for 20 minutes at room temperature in the dark for bright nuclear staining. Then the Ibidi Mounting Medium solution was used to cover the cells, followed by the coverslip. A negative control was set up with only the secondary antibodies.

2.2.13 Assessment of reactive oxygen species (ROS)

To determine ROS generation of PCa cells and PCSCs treated with phytochemicals or other agents, the Cellular ROS Assay Kit was used. The cell permeant reagent 2',7' – dichlorofluorescein diacetate (DCFDA) enters the cells, is then deacetylated by cellular esterases to a non-fluorescent substance, which is later oxidized by ROS into 2', 7' – dichlorofluorescein (DCF), a highly fluorescent substance. At first, a total of 3-4 × 10^6 cells were cultured and obtained on the day before the experiment. Then, cells were harvested using Trypsin/EDTA, seeded in a clear bottom 96-well plate with 2.5 × 10^4 per well, and incubated overnight at 37 ℃ and 5% CO_2. On the following day, cells were washed once with 1× Buffer (provided in the kit),100 µl 25 µM DCFDA solution was added, and the cell suspension was incubated in the dark for 45 minutes at 37 ℃ and 5% CO_2. After washing three times with 1× Buffer, cells were treated with the phytochemicals for 6 hours. ROS was measured using the FLUOstar OPTIMA microplate reader immediately at 485 nm for excitation and 535 nm for emission. The antioxidant N-acetyl-L-cysteine (NAC) was used as ROS inhibitor at a concentration of 1 mM in a 4-hour pre-treatment step.

2.2.14 Evaluation of the mitochondrial membrane potential

To further evaluate the apoptosis mechanism induced by phytochemicals in PCa cells and PCSCs, the mitochondrial membrane potential was measured using the JC-1 mitochondrial membrane potential kit. A total of 1.5 × 10^4 cells were seeded in a 96-well plate and incubated overnight at 37 ℃ and 5% CO_2. The next day, cells were washed once with PBS, and cultured with normal medium containing non-phenol red RPMI 1640 and the phytochemicals in different concentrations for 48 hours at 37 ℃ and 5% CO_2. Afterwards, cells were stained with 20 µM JC-1 solution for 10 minutes at 37 ℃ and 5% CO_2 and measured using the FLUOstar OPTIMA microplate reader at 530±15 nm for the monomeric form showing a green fluorescence and 590±17.5 nm for the aggregate form showing a red fluorescence. The monomeric form represents the injured mitochondria with low membrane potential, and the aggregate form represents the normal mitochondrial potential. The data were analyzed and presented by the ratio of monomer form to aggregate form.

2.2.15 Downregulation of cancer stem cell markers

To downregulate the cancer stem cell markers, inhibitors and small interfering RNAs (siRNAs) were used. Ko143 was an inhibitor of ABCG2 and used at a concentration of 1 µM. CB29 was an inhibitor of ALDH3A1 and used at 32 µM. Two inhibitors of CXCR4

were applied namely AMD3100 at 10 µM and WZ811 at 5 µM. For ALDH1A1, also two inhibitors were applied, NCT-501 at 10 µM and A37 at 10 µM. Moreover, the Silencer® Select siRNAs were designed and synthesized to silence *ABCG2*, *ALDH3A1, and CXCR4* shown in **Table 6**. Silencer® Select negative control and Silencer® Select *GAPDH* positive control were used as controls. Cells were transfected using the Lipofectamine RNAiMAX Reagent.

2.2.16 Small RNA-sequencing

A total of 36 samples were prepared to analyze the expression of different miRNAs, including the control group, berbamine group, cabazitaxel group, and berbamine plus cabazitaxel group in DU145 cells, caba-DU145 cells, and DU145 CSCs with repeating three times. Small RNA-sequencing was done by IMGM Laboratories GmbH.

The total RNAs including small RNAs were isolated using the miRNeasy Mini Kit. A DNAse digestion step was included and the RNA was eluted in 40 µl RNase-free water. Then, an aliquot of each total RNA sample was used to calculate the RNA concentration and purity using NanoDrop. The total RNA samples were analyzed on the 2100 Bioanalyzer using RNA 6000 Nano LabChip Kits (Agilent Technologies).

Next, Library preparation was conducted with the NEBNext® small RNA Library Prep Kit for Illumina. Before normalization, the quality and quantity of each small RNA library sample were evaluated as an intermediate control step. For this purpose, the High Sensitivity DNA LabChip Kit on the 2100 Bioanalyzer (Agilent Technologies) was used to analyze the quality of the libraries. Furthermore, all libraries were quantified using the highly sensitive fluorescent dye-based Qubit® ds DNA HS Assay Kit. The single small RNA libraries were pooled into a sequencing library pool. An equal amount of DNA was used per sample. The sequencing library pool was purified by gel electrophoresis to remove adapter dimers. The purified sequencing library pool was quantified using the highly sensitive fluorescent dye-based Qubit® ds DNA HS Assay Kit (Thermo Fisher Scientific). Furthermore, it was quality controlled using the High Sensitivity DNA LabChip Kit on the 2100 Bioanalyzer. After quantification, the final sequencing library pool was diluted to 2.25 nM, followed by denaturation with NaOH. This ensures the presence of single-stranded DNA fragments for cluster generation. The final sequencing library pool consists of single-stranded fragments with sequencing adapters, sequencing primer binding sites, and indices.

The next-generation sequencing was performed as follows. The complete sequencing library pool was initially sequenced on a NextSeq® 500 high output (HO) flowcell. Clus-

tering of the library pool was performed at a final concentration of 1.8 pM and with a 1% PhiX v3 control library spike-in on the NextSeq® 500 sequencing system (Illumina). Cartridge loading was conducted following the manufacture's recommendations for NovaSeq® 6000 according to the standard workflow using an SP flowcell. Template amplification and clustering were performed onboard the NovaSeq® 6000 applying the exclusion amplification (ExAmp) chemistry. The ExAmp workflow is an Illumina proprietary method and ensures that only single DNA templates are bound within single wells of the patterned NovaSeq® flow cells and are almost instantaneously amplified. Thereby, evenly spaced monoclonal clusters are generated on the flow cell. For cluster generation and subsequent sequencing of the subpool, one single-read 75 cycles (75bp SR) run was performed using an SP flow cell. Cluster generation and sequencing were operated under the control of the NovaSeq® Control Software (NVCS) v1.6.0. After cluster generation, sequencing primers hybridize to the adapter sequences at the end of the fragments and sequencing was performed.

Primary image processing on the NextSeq® 500 instrument was performed using Real Time Analysis 2.4.11 Software (RTA), while on the NovaSeq® 6000 instrument Real Time Analysis 3.4.4 Software (RTA) was used. For both sequencers, primary data analysis was performed using the bcl2fastq 2.20.0.422 software package. The Illumina Sequence Analysis Viewer (SAV) 2.4.7 was applied for imaging and evaluation of the sequencing run performance.

The CLC Genomics Workbench 12.0.3 was applied for in-depth analysis of differential expression and annotation of reads. Excel 2010 was utilized for filtering differentially expressed small RNAs.

Read data were imported into the CLC Genomics Workbench. Failed reads are indicated by a flag within the quality score header information inside the fastq file, specifying if a read has passed the sequencer-inherited quality filters or not. These were removed from the data set during data import. Read counts and quality for each sample were evaluated with the CLC Genomics Workbench "QC for Sequencing Reads" tool. The similarity between different samples based on global expression profiles was assessed by projection analysis. A principal component analysis was carried out within the CLC Genomics Workbench and results were visualized. Small RNAs were extracted and counted by the CLC Genomics Workbench tool. Two small RNA databases, miRbase Release 22 and Homo_sapiens. GRCh38.ncrna were used to annotating and merging the small RNAs.

Baggerly's test was applied to calculate the significant differential expression of small

RNAs. The CLC Genomics Workbench tool "Proportion-based Statistical Analysis" was used to analyze the statistically significant expression of small RNAs. A small RNA is classified as induced in a specific comparison if its FDR-corrected p-value is < 0.01 and if it has a Weighted proportions FC value ≥ 2.0. Analogously, a small RNA is classified as repressed if its corrected p-value is < 0.01 and its Weighted proportions FC is ≤ -2.0.

Venn diagrams were prepared to show the overall number of differentially expressed small RNAs in all pairwise comparisons and their overlaps between the different cell lines (DU145, Caba-DU145, and DU145 CSCs). Thereby, all differentially expressed small RNAs were detected in any pairwise comparisons and any of the biological replicates were included.

2.2.17 Individual miRCURY LNA miRNA PCR assay

RNAs were extracted using the miRNeasy advanced Mini kit. At first, a total of 2×10^5 cells were seeded in a 6-well plate overnight. After incubation with or without drugs for 48 hours, RNAs were extracted. A volume of 260 µl RLT buffer was mixed with the cells, and transferred to a QIAshredder Mini Spin Column, centrifuged at 14,000 rpm for 2 minutes. Then, a volume of 80 µl AL buffer was added and the suspension was incubated for 3 minutes at room temperature, transferred to gDNA Eliminator Spin, centrifuged at 10,000 rpm for 30 seconds, and flow-through was saved. Next, a volume of 340 µl isopropanol was added and mixed by pipetting, transferred to the RNeasy Mini column, centrifuged for 15 seconds at 10,000 rpm, and the flow-through was discarded. The reagents were added one by one as follows: 700 µl RWT buffer for 15 seconds at 10,000 rpm, 500 µl RPE buffer for 15 seconds at 10,000 rpm, 500 µl 80% Ethanol for 2 minutes for 10,000 rpm. The RNeasy Mini spin columns were placed in new 2-ml collection tubes and centrifuged at 14,000 rpm for 1 minute. Finally, the RNeasy Mini spin columns were placed in new 1.5 ml collection tubes, and 30 µl RNase-free water was directly added to the center of the spin column membrane, incubated for 1 minute, and centrifuged for 1 minute at 14,000 rpm.

For cDNA synthesis, the miRCURY LNA RT kit was applied. The reverse transcription master mix was prepared on ice as follows: 2 µl 5× miRCURY SYBR Green RT Reaction Buffer, 4.5 µl RNase-free water, 1 µl 10× miRCURY RT Enzyme Mix, 0.5 µl Synthetic RNA spike-in, 2 µl template RNA at 5 ng/ µl. Incubation was done for 60 minutes at 42 ℃, 5 minutes at 95 ℃, and then immediately cooled to 4 ℃.

For the PCR procedure, the miRCURY LNA miRNA PCR assay was performed based on the instructions of QIAGEN, and its mechanism is shown in **Figure 11**.

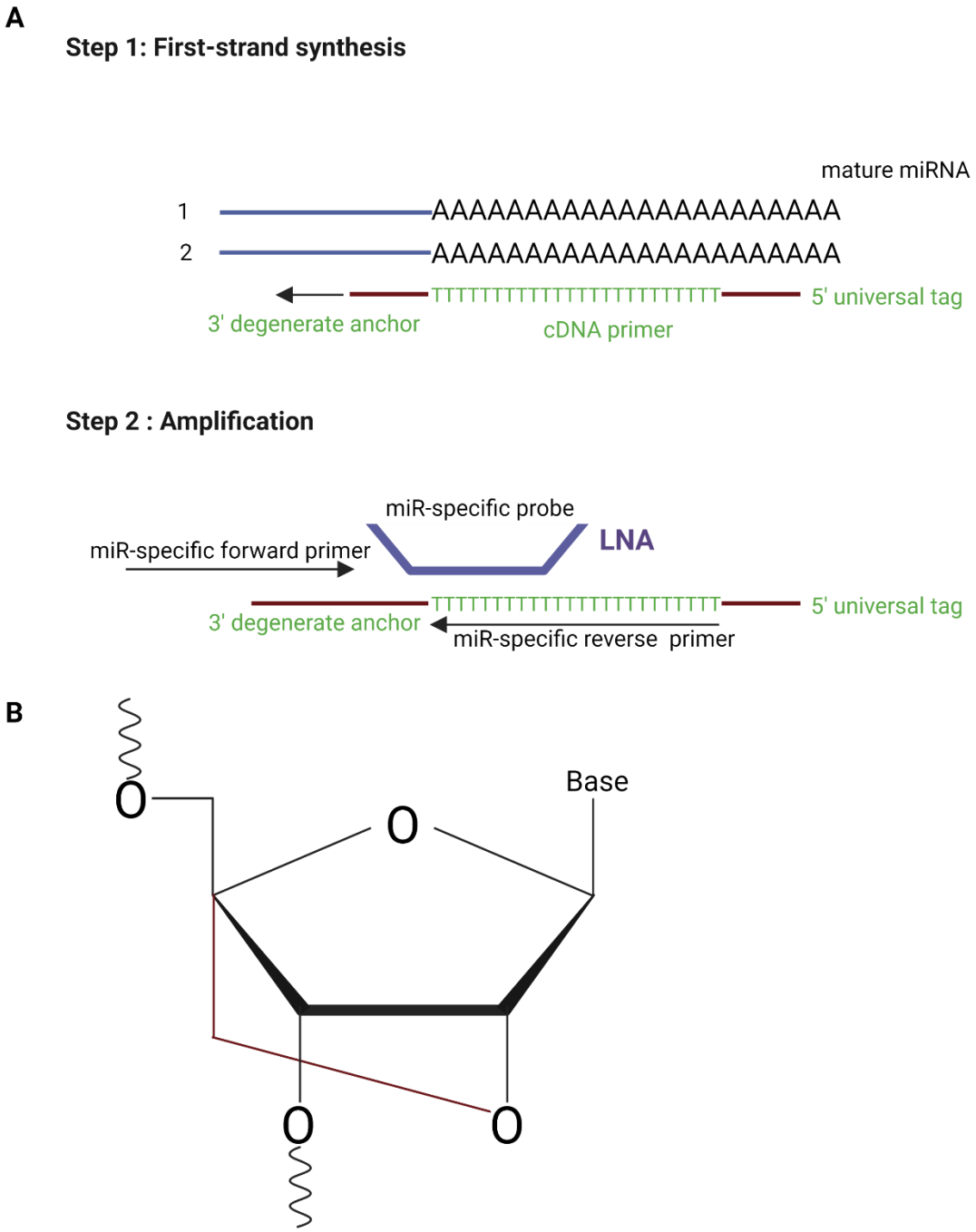

Figure 11. The mechanism of miRCURY® LNA® miRNA PCR System. A. The whole process of miRCURY LNA miRNA PCR assay. Step 1: cDNA synthesis using a poly(T) primer with a 3' degenerate anchor and a 5' universal tag. Step 2: Real-time PCR amplification. As shown in Step 2, the cDNA template is amplified by two miRNA-specific, LNA-enhanced forward and reverse primers. **B.** The structure of locked nucleic acids (LNA). LNA is a high-affinity RNA analog in which the ribose ring is "locked" in the ideal conformation for Watson-Crick binding.

When hybridized to complementary DNA or RNA strands, LNA oligonucleotides display unusual thermal stability. The melting temperature (Tm) of the duplex augments by 2 to 8 °C for each incorporated LNA monomer. In addition, LNA oligonucleotides can be designed shorter than normal DNA or RNA oligonucleotides and still retain a high Tm, which is essential for detecting small or highly similar targets (Figure created with BioRender.com).

For the miRCURY LNA miRNA PCR assay, the cDNA was diluted 60 times by adding 590 µl RNase-free water to the 10 µl RT reaction mix. Then, 5 µl 2× miRCURY SYBR Green Master Mix, 1 µl resuspended PCR primer mix, 3 µl cDNA template, 1 µl RNase-free water were added, mixed thoroughly, centrifuged briefly, and measured using the LightCycler®96 instrument using the following cycling program: 95 ℃ for 2 minutes, and two-step cycling of 45 cycles: 95 ℃ for 10 seconds, followed by 56 ℃ for 60 seconds. Data were analyzed using the LightCycler® 96 software SW 1.1 and the relative expression was calculated using the $2^{-\Delta\Delta Ct}$ method. SNORD48 was used as an internal control.

2.2.18 Cell transfection

Mimics of let-7a, let-7b, let-7i, miR-26a, miR-26b, inhibitors of let-7, miR-26, and mimic negative control were synthesized and purchased from Qiagen (Table 5). The structures and applications of miRCURY LNA miRNA mimics and inhibitors were described by Qiagen and Hum et al. [92] shown in **Figure 12 and Figure 13**. The miRCURY LNA miRNA mimics are designed as triple-RNA strand and ensures specific mimicry without off-target miRNA activity. miRCURY LNA miRNA inhibitors are antisense oligonucleotides with a perfect sequence match to their targets. In the experiments, the so-called miRCURY LNA power inhibitors were used. These inhibitors have a phosphorthioate modified backbone and are therefore highly resistant to enzymatic degradation and more stable. The second advantage is, that these inhibitors can be taken up without a transfection reagent. Inhibitors were used to identify and validate miRNA targets. The Silencer® select siRNAs for ABCG2, ALDH3A1, CXCR4 were synthesized and purchased from Ambion. Silencer® Select GAPDH positive control and Silencer® Select negative control were used as controls.

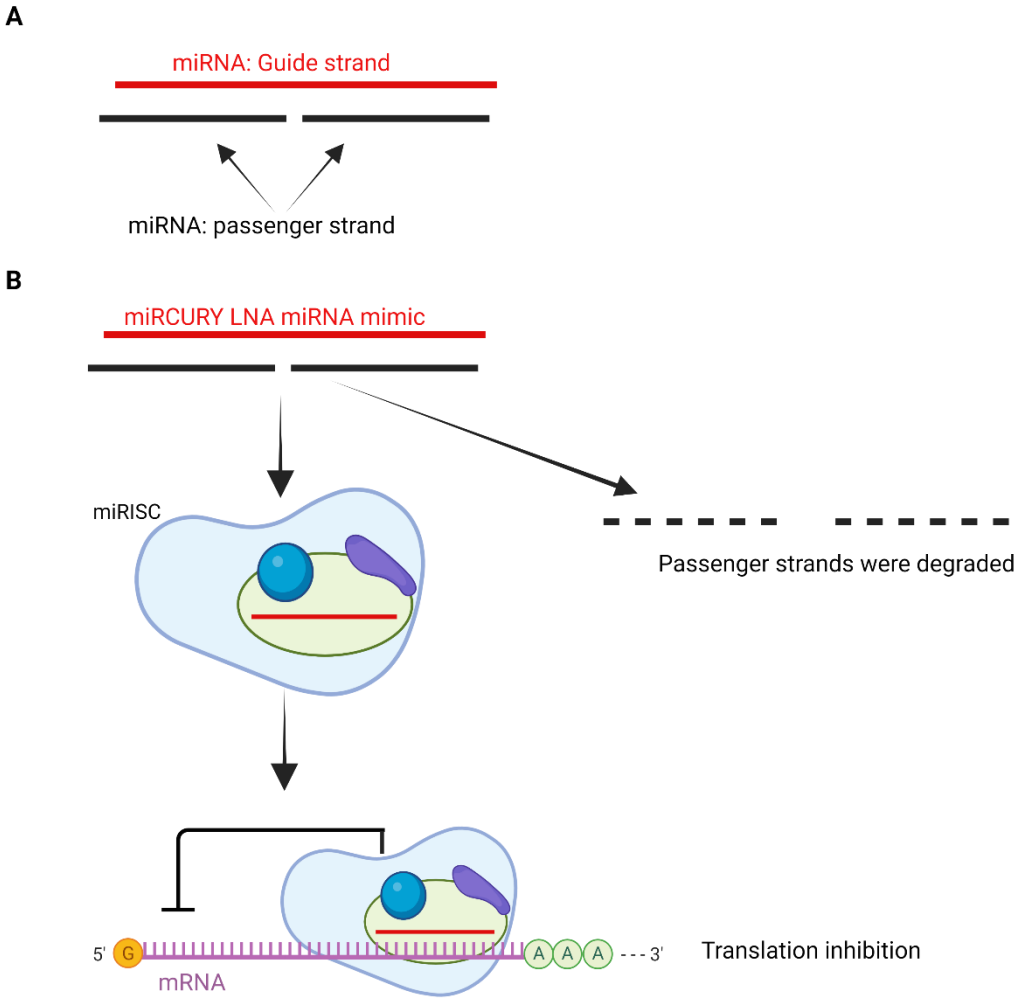

Figure 12. The structure of mimics. A. miRCURY LNA miRNA mimics are made of three RNA strands, including an unmodified miRNA (guide) strand which exactly matches the miRBase annotation and two LNA-modified RNAs strands which match the miRNA strand (passenger). **B.** Only the miRNA (guide) strand is integrated by the RNA-induced silencing complex (RISC). The two passenger strands are rapidly degraded after displacement from the miRNA strand. (Figure created with BioRender.com).

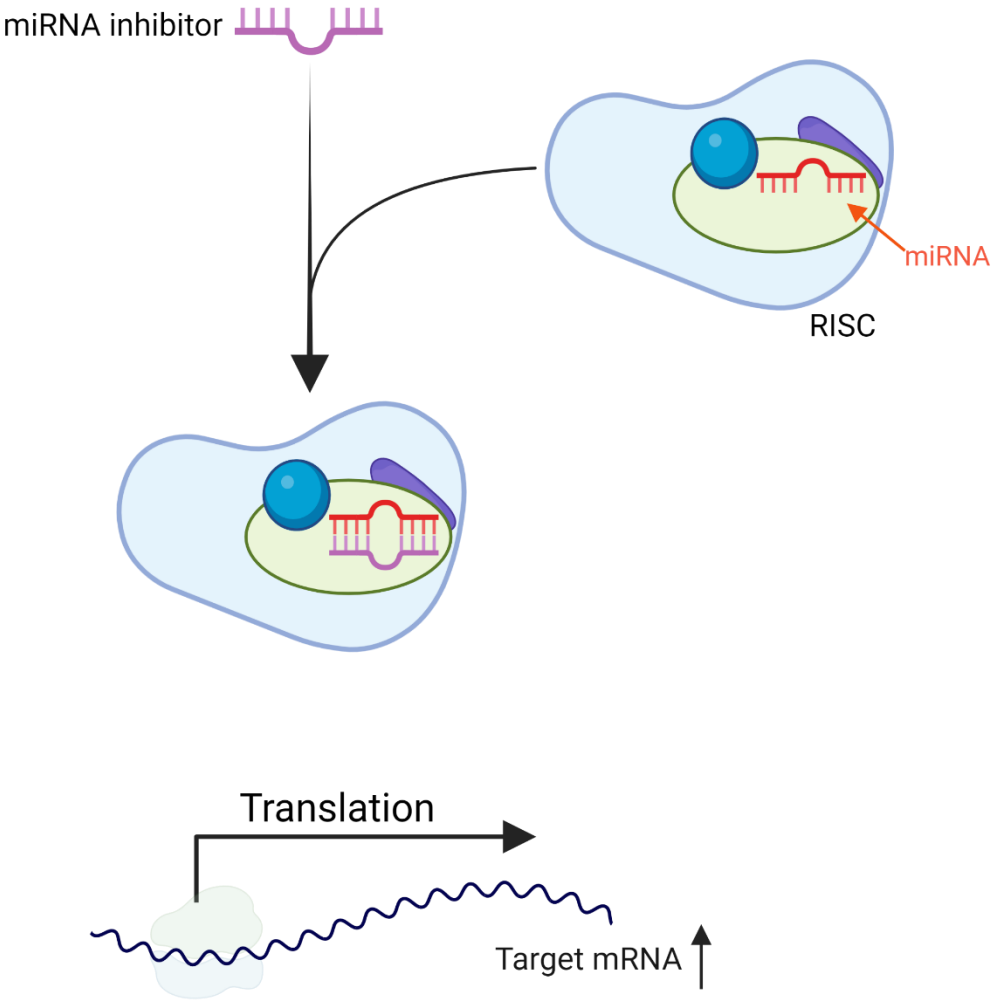

Figure 13. Function of the miRNA inhibitor. The miRNA inhibitor integrates into the RISC complex and perfectly matches the specific miRNA. The miRNA loses its ability to inhibit the translation of the target mRNA. (Figure created with BioRender.com)

Cell transfection was performed using lipofectamine RNAiMAX reagent as the manufacturer's protocol described. Briefly, a total of 1×10^5 cells were seeded in the 24-well plate with a duplicate well for each group. After reaching 70-80 % confluence, the cells were transfected. First, 3 µl lipofectamine RNAiMAX reagent was mixed in 50 µl OPTI-MEM medium as lipofectamine reagent. Second, 1 µl mimics at 30 µM, inhibitors at 30 µM, or siRNAs at 10 µM was mixed with 50 µl OPTI-MEM as target reagent. Third, the mixture of lipofectamine reagent and target reagent was vortexed and incubated for 5 minutes at room temperature. A volume of 50 µl was taken out from the mixture and added to the cells in one well. After 48 h incubation, cells were collected and used for further experiments.

2.2.19 Extraction of exosomes

The exosomes were extracted using the ExoQuick-TC Kit as described by the manufacturer's instructions. Briefly, supernatant derived from DU145 cells, caba-DU145 cells, and DU145 CSCs was collected and centrifuged at the speed of 3000 g for 15 minutes to remove cells and cell debris. Then, the supernatant was transferred to sterile vessels and was added to ExoQuick-TC in the ratio supernatant: ExoQuick-TC = 5:1, mixed well, and refrigerated overnight at 4 ℃. The tubes should not be rotated during incubation and should stay upright. The next day, ExoQuick-TC/supernatant mixture was centrifuged at 1500 g for 30 minutes. Afterwards, the supernatant was discarded and centrifuged again at 1500 g for 5 minutes. All traces of fluid were removed by aspiration. The exosomal pellet was resuspended in 100-200 µl RIPA lysis buffer (1 ml RIPA mixed with 10 µl Phosphatase Inhibitor Cocktail 2, 10 µl Phosphatase Inhibitor Cocktail 3, and 10 µl Protease Inhibitor Cocktail 1), incubated for 15 minutes on ice, followed by centrifugation at 14,000 rpm for 15 minutes. The supernatant containing the proteins was transferred into a new tube. The protein concentration was determined using the Pierce™ BCA Protein Assay Kit. Then, the samples were used for western blotting to validate the exosomal markers.

2.2.20 Western blot analysis

Exosomal proteins obtained from 2.2.19, were validated by Western Blot analysis using Bolt™ 4-12% Bis-Tris Plus gels and XCell SureLock™ Electrophoresis (Invitrogen). For sample preparation, a total of 60 µg proteins were was given to 5 µl Bolt™ LDS Sample Buffer (4×), 2 µl, Bolt™ Reducing Agent (10×), and deionized water up to a total volume of 20 µl. Then, the samples were heated at 70 ℃ for 10 minutes. Next, the gel tank was filled with 1× Bolt™ MES SDS running buffer. Samples were added into Bolt Mini Gels in a volume of 20 µl per well containing 60 µg proteins. The SeeBlue Plus2 Pre-Stained Protein Standard was used as a marker. A volume of 400 µl Bolt™ Antioxidant was added to the cathode chamber. The electrophoresis was run at 180 V for 40 minutes.

The iBlot™ 2 Dry Blotting System was used to transfer the proteins onto the PVDF membrane as the manufacturer's introductions. Briefly, the iBlot 2 Transfer Stacks with gels containing proteins were assembled onto the iBlot 2 Gel Transfer Device. Then, the P0 protocol (20 V for 1 minute, 23 V for 4 minutes, and 25 V for 3 minutes) was started to transfer the proteins onto the PVDF membrane.

Furthermore, the iBind™ Flex Western System was applied for antibody binding. First, the 1× iBind Flex Solution was prepared with 500 µl 100× Additive, 10 ml iBind Flex 5× Buffer, and 39.5 ml distilled water. Second, the iBind™ Flex Card was placed on the stage and 10 ml of 1 × iBind™ Flex solution was applied across the Flow Region. The membrane was situated on top of the pooled solution with the protein-side down, and the low molecular weight region closest to the stack. With the Blotting Roller, any air bubbles were removed. The lid of the iBind™ Flex device was closed and the latch handle lowered to lock the lid. The following solutions were added sequentially to each well: 0.7 ml of the primary antibody in the first line, 2 ml iBind™ Flex Solution in the second line, 0.7 ml of the secondary antibody in the third line, and 6 ml iBind™ Flex Solution in the fourth line. The well cover was closed and the reaction was incubated overnight at 4 ℃. Afterwards, the membrane was rinsed in water and proceeded to the immunodetection protocol.

For the immunodetection, the SuperSignal West Pico Chemiluminescent substrate was prepared with a 1:1 ratio of enhancer to peroxide. The membrane was incubated in the substrate solution for 5 minutes. Membranes were put into the Blot Development Folders and the signals were detected using the Fluor-S™ Multilmager (120 seconds exposure under the module of Blotting/High Resolution).

2.2.21 Detection of exosomal microRNAs

The exosomes were extracted using miRCURY® Exosome Cell/Urine/CSF Kit. First of all, the supernatant was collected from the cell culture, centrifuged at 3,000 g for 10 minutes to remove the cells and debris. For a 1 ml sample, a volume of 400 µl Precipitation Buffer was added, vortexed to mix thoroughly, and incubated for 60 minutes at 4 ℃. Then, the samples were centrifuged at 10,000 g for 30 minutes at 20 ℃. The supernatant was removed, centrifuged for 5 seconds at 10,000 g, and the supernatant removed again. A volume of 100 µl Resuspension Buffer was added to the pellet, vortexed for 15 seconds. To minimize the risk of RNase contamination, the exosomes were directly proceeded to the miRNeasy Micro Kit to purify the total RNA.

A volume of 700 µl QIAzol Lysis Reagent was added to the exosomes, transferred into the QIAshredder homogenizers, centrifuged at 14,000 rpm for 2 minutes, and incubated for 5 minutes at room temperature. A volume of 140 µl chloroform was added to the samples, mixed thoroughly for 15 seconds, incubated for 3 minutes at room temperature, and centrifuged at 12,000 g for 15 minutes at 4 ℃. The upper aqueous phase was transferred to a new collection tube then 1.5 volumes of 100% ethanol was added,

mixed thoroughly by pipetting. A volume of 700 µl sample was then added into the RNeasy MinElute spin column in a 2 ml collection tube, and centrifuged at 9,000 g for 15 seconds at room temperature, followed by discarding the flow-through. Then, 700 µl RWT Buffer was added onto the RNeasy MinElute spin column and centrifuged for 15 seconds at 9,000 g. The flow-through was discarded. Next, 500 µl RPE Buffer was added, centrifuged for 15 seconds at 9,000 g, and the flow-through was discarded again. Furthermore, 500 µl of 80% ethanol was added, centrifuged for 2 minutes at 9,000 g, and the flow-through was discarded. The spin column was placed into a new collection tube, centrifuged again at 14,000 rpm, for 5 minutes, the flow-through was discarded, and the spin column was placed in a new 1.5 ml collection tube, 14 µl RNase-free water was added to the center of the spin column membrane, and the column centrifuged for 1 minute at 14,000 rpm to elute the RNA.

The miRCURY LNA RT kit was used for cDNA synthesis, and the individual miRCURY LNA miRNA PCR assay was performed for the PCR procedure as described in 2.2.17.

2.2.22 Statistics

The experiments were independently repeated three times, and the numerical data were stored and analyzed using Microsoft Excel. The statistical difference was calculated using IBM SPSS Statistics 25. Figures were generated using GraphPad Prism 7 and the data expressed as mean plus SEM (standard error of the mean). The values from two different groups were calculated using the statistical method of the Mann-Whitney U test. The correlation between the cancer stem cell markers in the confocal microscopy experiment was determined using the Pearson product-moment correlation coefficient. The two-sided p-value less than 0.05 was considered as significant.

3. Results

3.1 The influence of shikonin on cancer stem cells

Note: This part was already published in the American Journal of Cancer Research [90]: Wang L, Stadlbauer B, Lyu C, Buchner A, Pohla H: Shikonin enhances the antitumor effect of cabazitaxel in prostate cancer stem cells and reverses cabazitaxel resistance by inhibiting ABCG2 and ALDH3A1. Am J Cancer Res 2020, 10:3784-3800.

3.1.1 Shikonin inhibits cell viability and proliferative ability in PCa cells and PCSCs

To obtain the PCSCs, the sphere-forming assay was carried out as described in 2.2.2. The differentiated non-stem-like cells do not form spheres in serum-free medium under low-adherent conditions and die, while the CSCs could form spheres showing self-renewal properties [93]. **Figure 14** shows the development of CSC spheres within ten days.

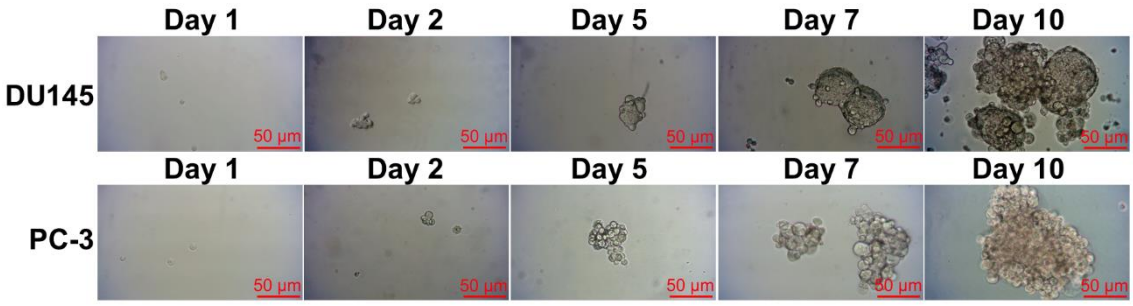

Figure 14. Sphere forming assay. DU145 cells and PC-3 cells were cultured in specific CSC medium for ten days. The photos were taken with a digital microscope camera at 100x magnification (Figure adapted from Wang et al. [90]).

Several experiments were carried out to explore the influence of shikonin on the PCa cells and PCSCs. First of all the CellTiter Blue Cell Viability assay was performed as described in 2.2.3. DU145 and PC-3, and their corresponding sphere cells were treated with different concentrations of shikonin for 24 and 48 hours. The results demonstrated that shikonin inhibited cell viability in a dose-dependent manner (**Figure 15A-B**). The IC50 concentrations of shikonin were calculated using the statistical method of the logit regression model, which were 0.75 µM for DU145 cells, 4 µM for DU145 CSCs, 5 µM for PC-3 cells, 7 µM for PC-3 CSCs.

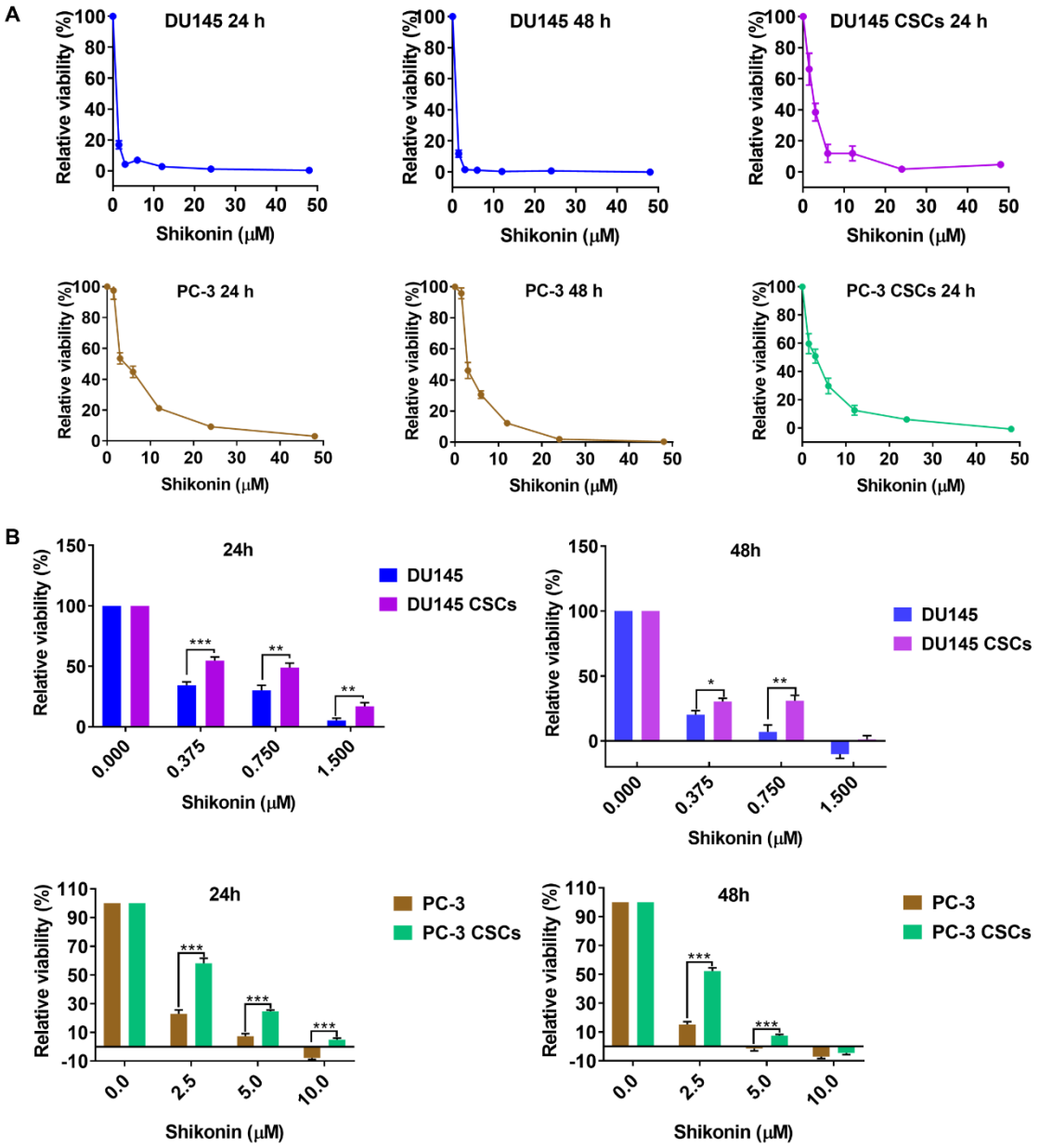

Figure 15. Shikonin represses cell viability in PCa cells and PCSCs. **A.** CellTiter-Blue Cell Viability Assay for DU145 cells and PC-3 shown for 24 hours and 48 hours, and PCSCs for 24 hours. Shikonin repressed the cell viability of DU145 cells, PC-3 cells, DU145 CSCs and PC-3 CSCs. **B**. CellTiter-Blue Cell Viability Assay demonstrated that DU145 CSCs and PC-3 CSCs were more resistant to shikonin than DU145 cells and PC-3 cells. The data were acquired from three separate experiments and calculated as means ± SEM. *p < 0.05; **p < 0.01; ***p < 0.001. (Figure adapted from Wang et al. [90])

An inhibitory influence of shikonin on the proliferation rate was noticed as well using different concentrations of shikonin (0.5× IC50, 1x IC50, 2× IC50, **Figure 16A-B**). Results showed that DU145 CSCs and PC-3 CSCs were more resistant to shikonin than DU145 cells and PC-3 cells (**Figure 15B** and **Figure 16B**), which suggested that those

spheric CSCs were similar to drug-resistant cells.

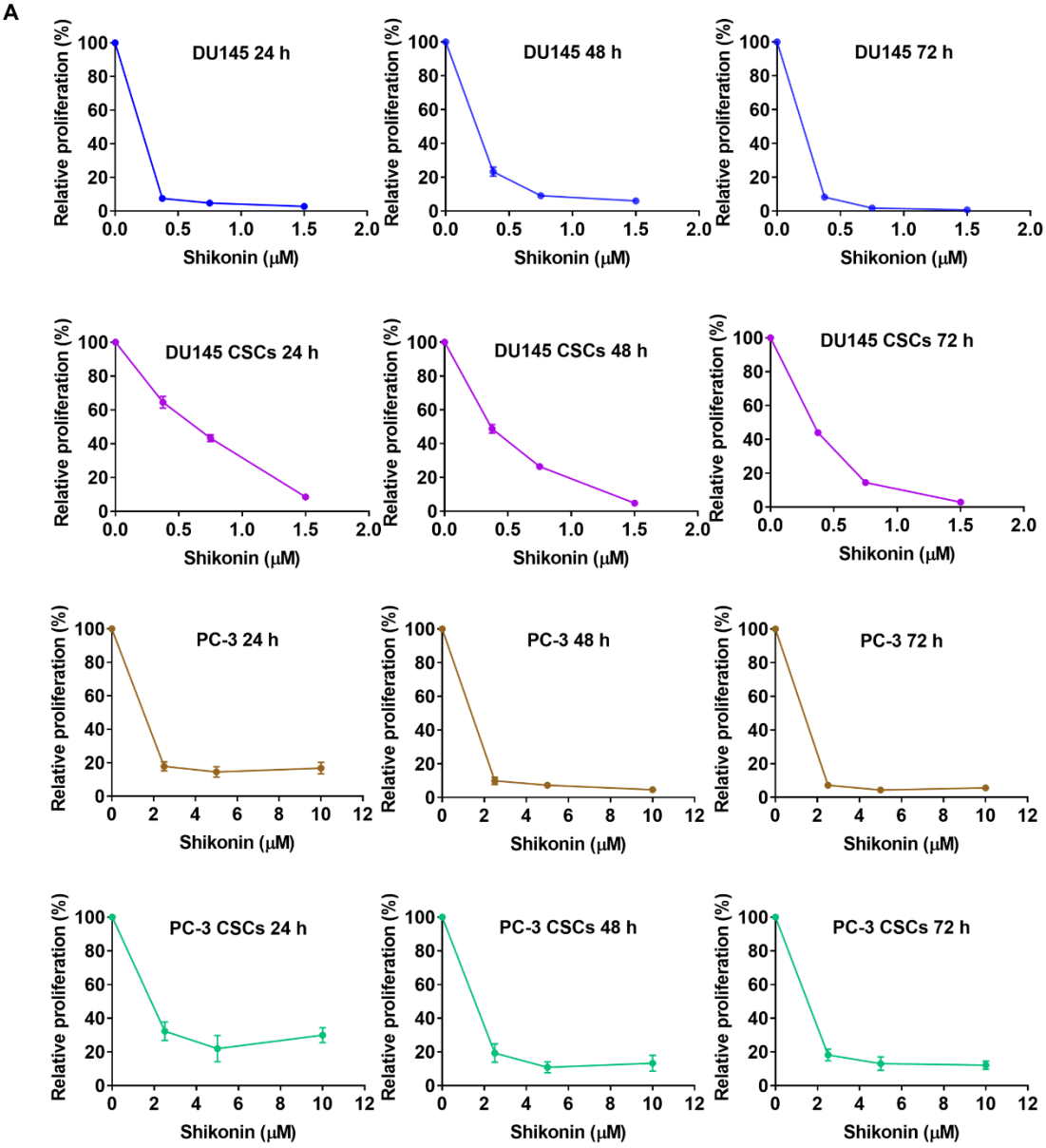

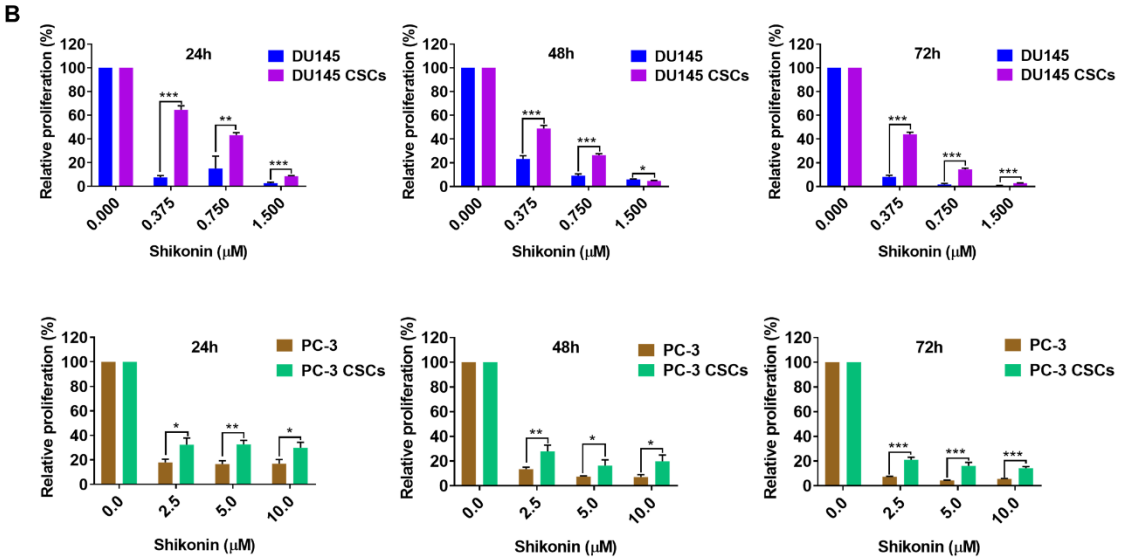

Figure 16. Shikonin suppresses the proliferative ability in PCa cells and PCSCs. A. Proliferation assay showed that shikonin repressed the proliferation of DU145 cells, PC-3 cells, DU145 CSCs, and PC-3 CSCs. **B**. Proliferation assay showed that DU145 CSCs and PC-3 CSCs were more resistant to shikonin compared to DU145 cells and PC-3 cells. The data were acquired from three separate experiments and calculated as means ± SEM. *p < 0.05; **p < 0.01; ***p < 0.001. (Figure adapted from Wang et al. [90])

3.1.2 Shikonin inhibits the migration and invasive ability in PCa cells and PCSCs

The influence of shikonin on migration and invasion of PCa cells and PCSCs was also tested. Migration was done using the wound healing assay as described in 2.2.7. During treatment with different concentrations of shikonin, microscope photos were captured 6-7 times within 33 hours. The results showed that shikonin suppressed the migration ability of DU145 cells, PC-3 cells, DU145 CSCs, and PC-3 CSCs (**Figure 17A-C**).

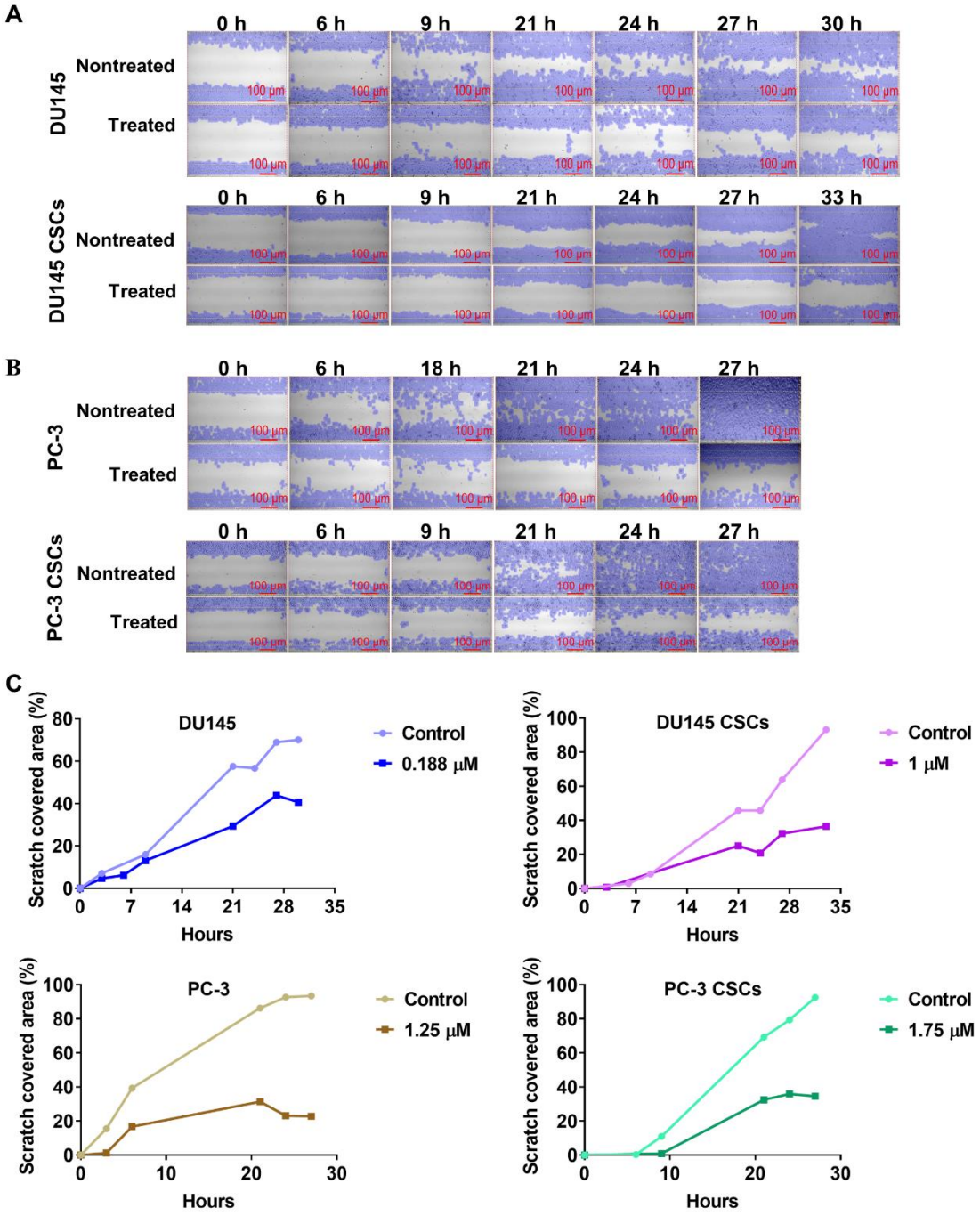

Figure 17. Shikonin inhibits the migration ability in PCa cells and PCSCs. A and **B**. Scratch wound healing assays showed that shikonin inhibited the migration of DU145 at 0.188 µM, DU145 CSCs at 1 µM, PC-3 cells at 1.25 µM, PC-3 CSCs at 1.75 µM. Pictures were captured by a digital microscope camera at 40x magnification. The percent of covered areas of the gap was assessed and analyzed by the Automated Cellular Analysis System based on the FastTrack AI image analysis algorithms. **C**. The graphs show the percentage of the covered area of the scratch wound at different time points of culture with and without shikonin (Figure adapted from Wang et al. [90]).

The invasion assay demonstrated that the number of invaded cells was decreased sig-

nificantly in the group with higher concentrations of shikonin both in the adherent cells and cancer stem cells (**Figure 18A-B**), indicating that shikonin can inhibit invasion remarkably in PCa cells and PCSCs.

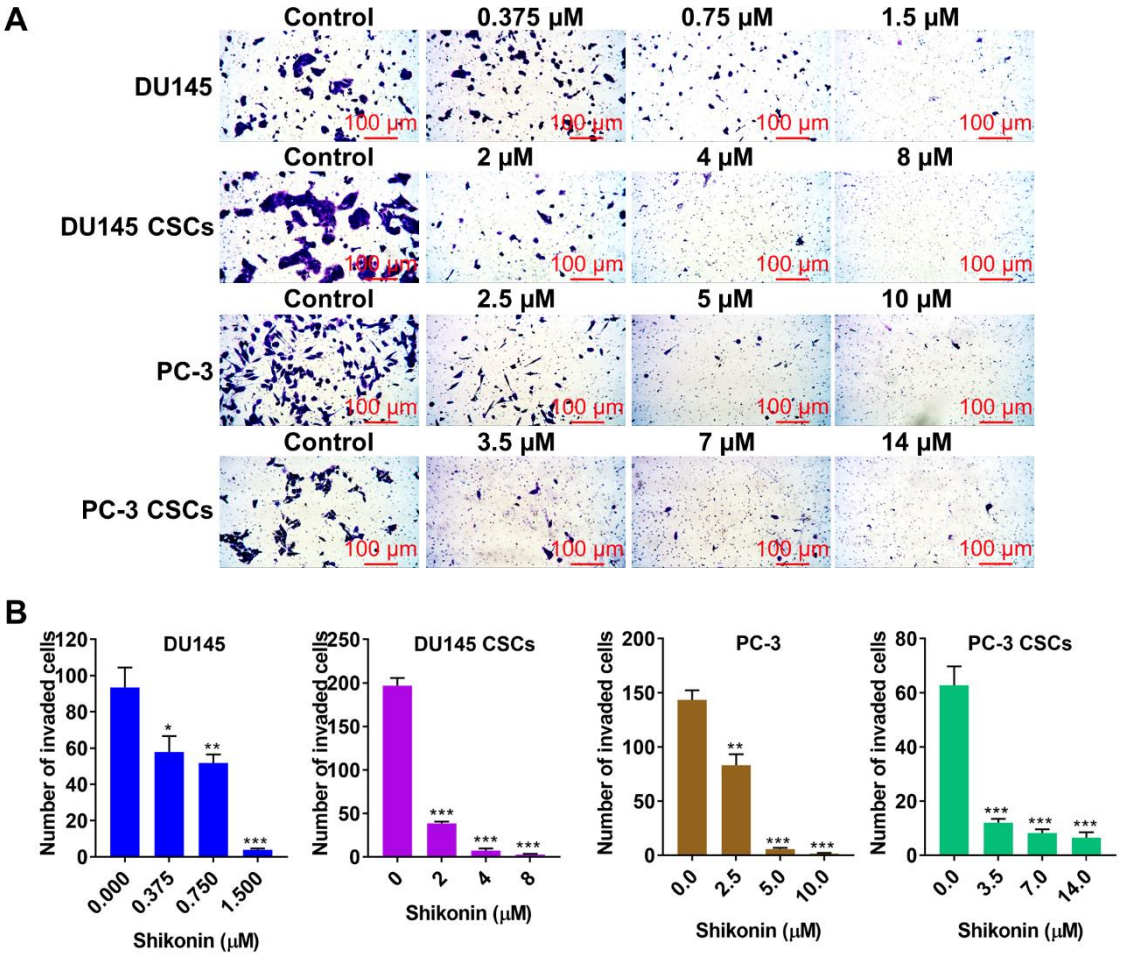

Figure 18. Shikonin inhibits the invasion of PCa cells and PCSCs. **A**. Invasion assay: shikonin inhibited the invasiveness of DU145 cells, PC-3 cells, and their corresponding CSCs. From every transwell insert pictures were taken with the digital microscope camera at 40x magnification (three fields per insert) and cells were counted using the Fiji Image J software. **B**. The bar charts demonstrate the number of invaded cells, calculated as means ± SEM The data were acquired from three separate experiments. *p < 0.05; **p < 0.01; ***p < 0.001 (Figure adapted from Wang et al. [90]).

3.1.3 Shikonin augments the anti-cancer effect of cabazitaxel

Afterwards, the viability, proliferation, apoptosis, and invasion assays were carried out again to examine whether shikonin could enhance the anti-cancer effect of cabazitaxel. We determined the IC50 of cabazitaxel for 48 hours, which was 3 nM using the method of the logit regression model (**Figure 19**).

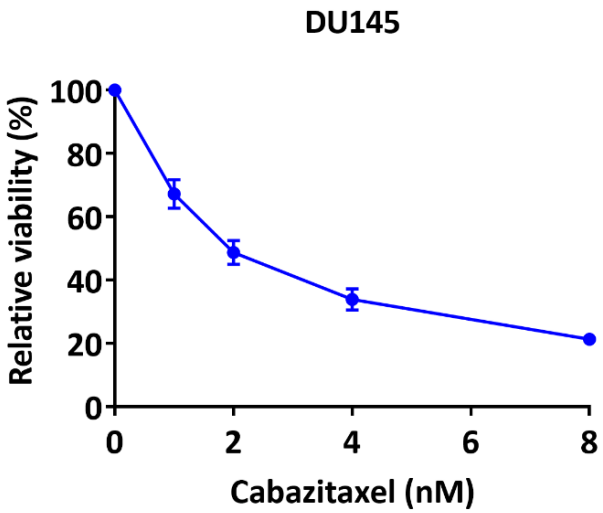

Figure 19. Cabazitaxel inhibits the viability of DU145 cells. CellTiter-Blue Cell Viability Assay demonstrated that cabazitaxel inhibited the cell viability in a dose-dependent manner in DU145 cells treated for 48 hours. The IC50 was calculated using the logit regression model (= 3 nM) (Figure adapted from Wang et al. [90]).

DU145 cells and DU145 CSCs were cultured with shikonin at a concentration of 0.75 µM combined with cabazitaxel at different concentrations (0.375 nM, 0.75 nM, 1.5 nM, and 3 nM) for 48 hours. The combination of shikonin and cabazitaxel contributed to a notable decline in viability (**Figure 20**) and proliferation (**Figure 21**) of DU145 cells and DU145 CSCs in contrast to cabazitaxel alone. As also shown shikonin alone repeatedly demonstrated a significant decrease in viability and proliferation.

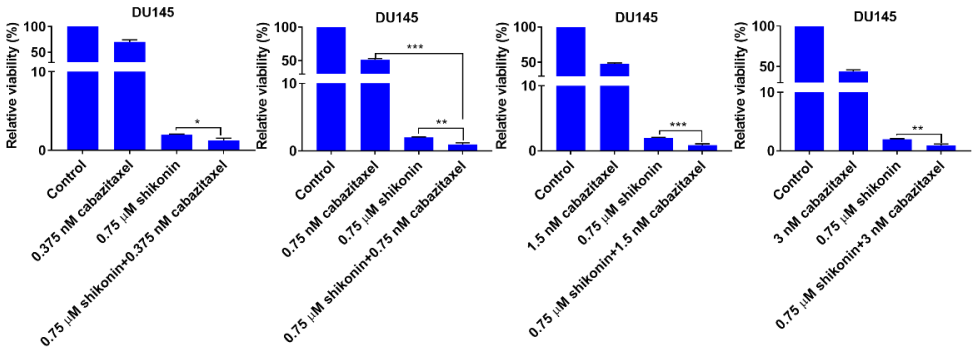

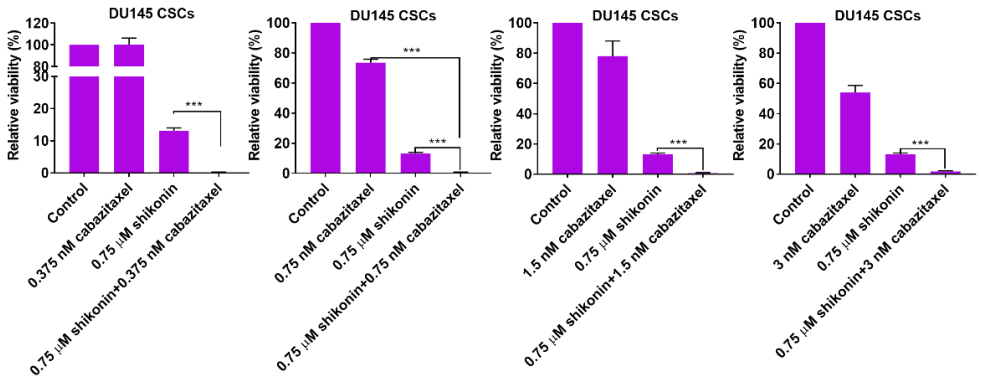

Figure 20. Shikonin promotes the anti-tumor effect of cabazitaxel in the viability assay. Shikonin (0.75 μM) combined with different concentrations of cabazitaxel enhanced the cytotoxic effect of cabazitaxel in contrast to the single-agent group. The viability was measured after 48 h treatment. The data were acquired from three separate experiments and calculated as means ± SEM. *p < 0.05; **p < 0.01; ***p < 0.001 (Figure adapted from Wang et al.[90].

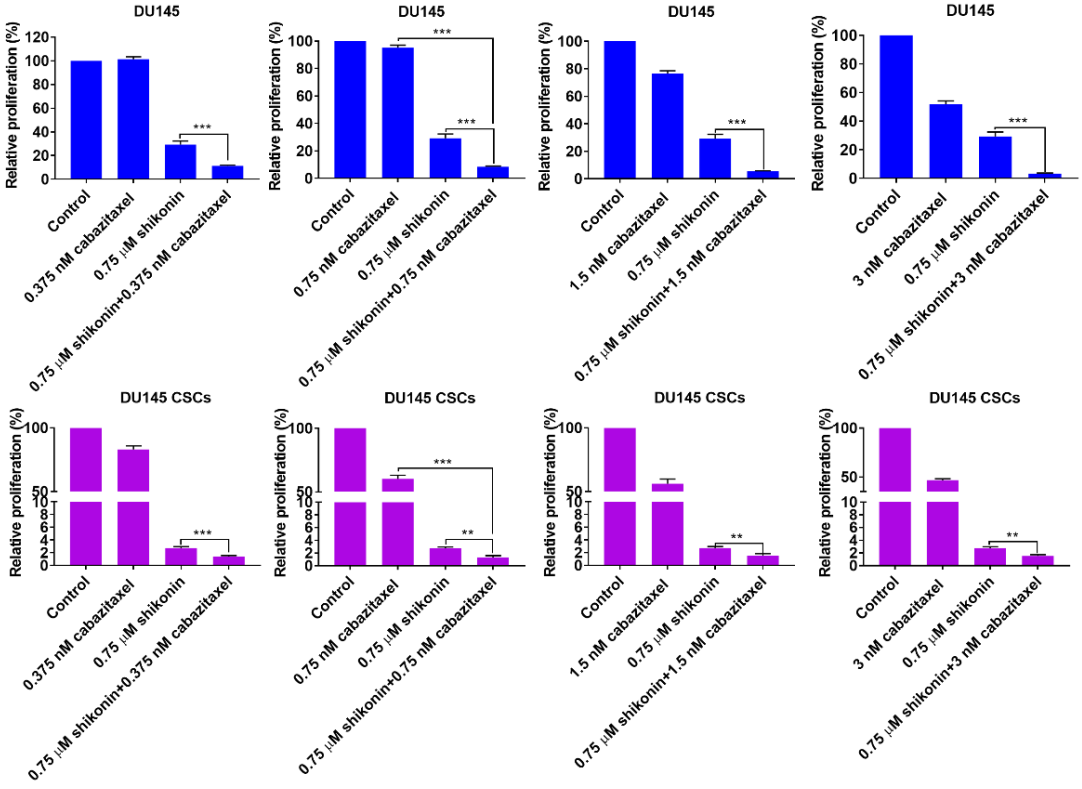

Figure 21. Shikonin enhances the anti-tumor effect of cabazitaxel in the proliferation assay. Shikonin (0.75 μM) combined with different concentrations of cabazitaxel enhanced the anti-proliferative effect in contrast to the single-agent group. The proliferation was determined after 48 h treatment. The data were acquired from three separate experiments and calculated as means ± SEM. *p < 0.05; **p < 0.01; ***p < 0.001 (Figure adapted from Wang et al. [90].

Similarly, the apoptosis assay demonstrated that shikonin plus cabazitaxel induced more apoptotic events than in the single-agent group as we anticipated. (**Figure 22**). Also, in the invasion assay a notably higher inhibition was seen in the combination treatment (**Figure 23**).

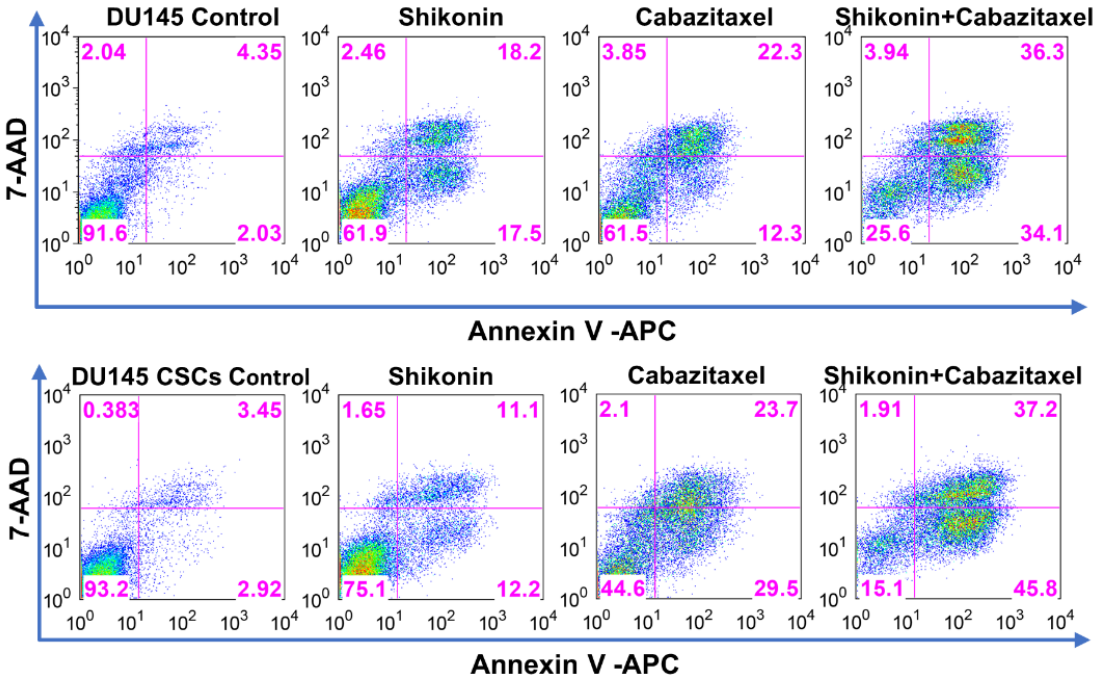

Figure 22. Shikonin augments the anti-tumor effect of cabazitaxel in the apoptosis assay. Shikonin (0.75 μM) plus cabazitaxel (1.5 nM) induced a higher apoptosis rate in contrast to the single-agent group. Apoptosis was measured as described in 2.2.6. The percentage of Annexin V positive cells was considered as apoptotic cells. (Figure adapted from Wang et al. [90]).

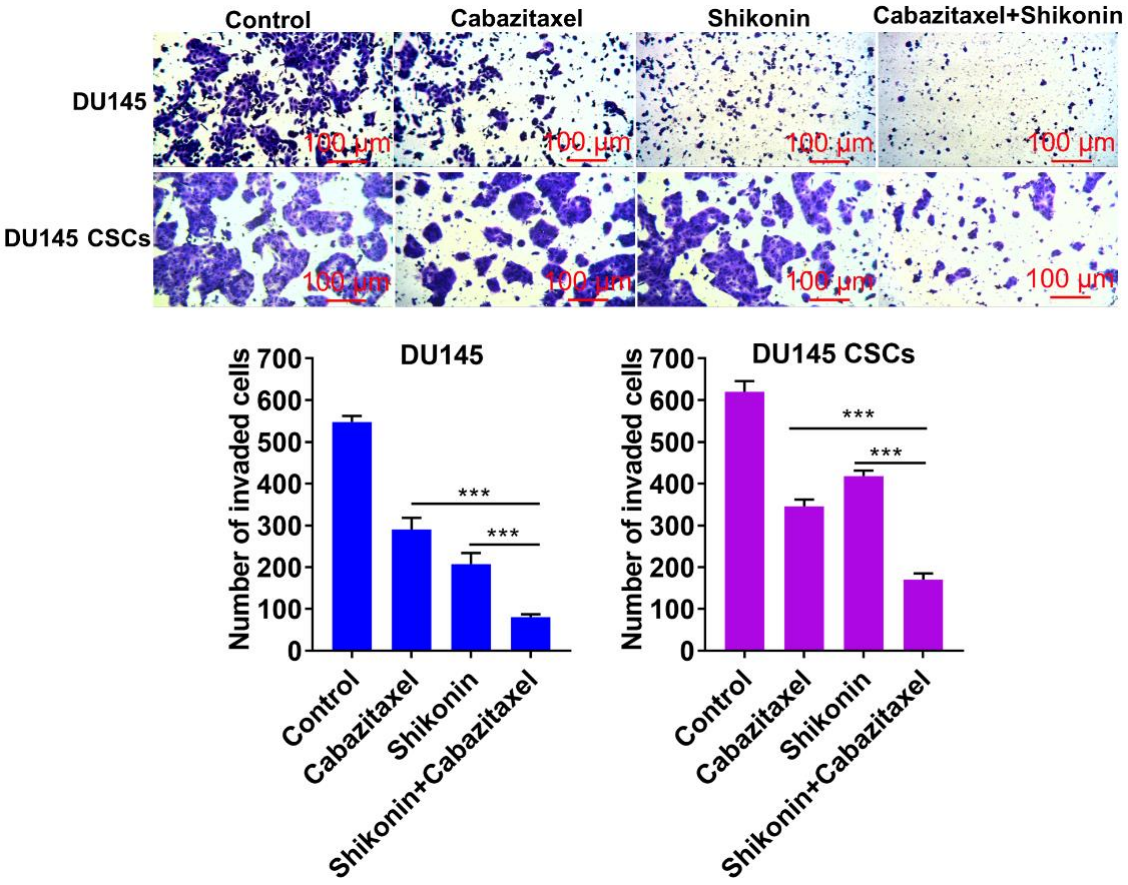

Figure 23. Shikonin augments the anti-tumor effect of cabazitaxel in the invasion assay. Shikonin (0.75 µM) plus cabazitaxel (1.5 nM) enhanced the inhibitory effect in DU145 cells and DU145 CSCs to a greater extent than in the single-agent group. From every transwell insert photos were taken with the digital microscope camera at 40x magnification (three fields per insert) and were analyzed using the Fiji Image J software. The bar charts demonstrate the number of invaded cells, calculated as means ± SEM. The data were acquired from three separate experiments. *p < 0.05; **p < 0.01; ***p < 0.001 (Figure adapted from Wang et al. [90].

3.1.4 Shikonin generates ROS and dysregulates mitochondria membrane potential

To show the influence of shikonin alone on the apoptosis rate, apoptosis assays were done with both cell lines and their corresponding PCSCs. Results indicated that shikonin significantly induced apoptosis in DU145, DU145-CSC, PC-3, and PC-3 CSC (**Figure 24)**.

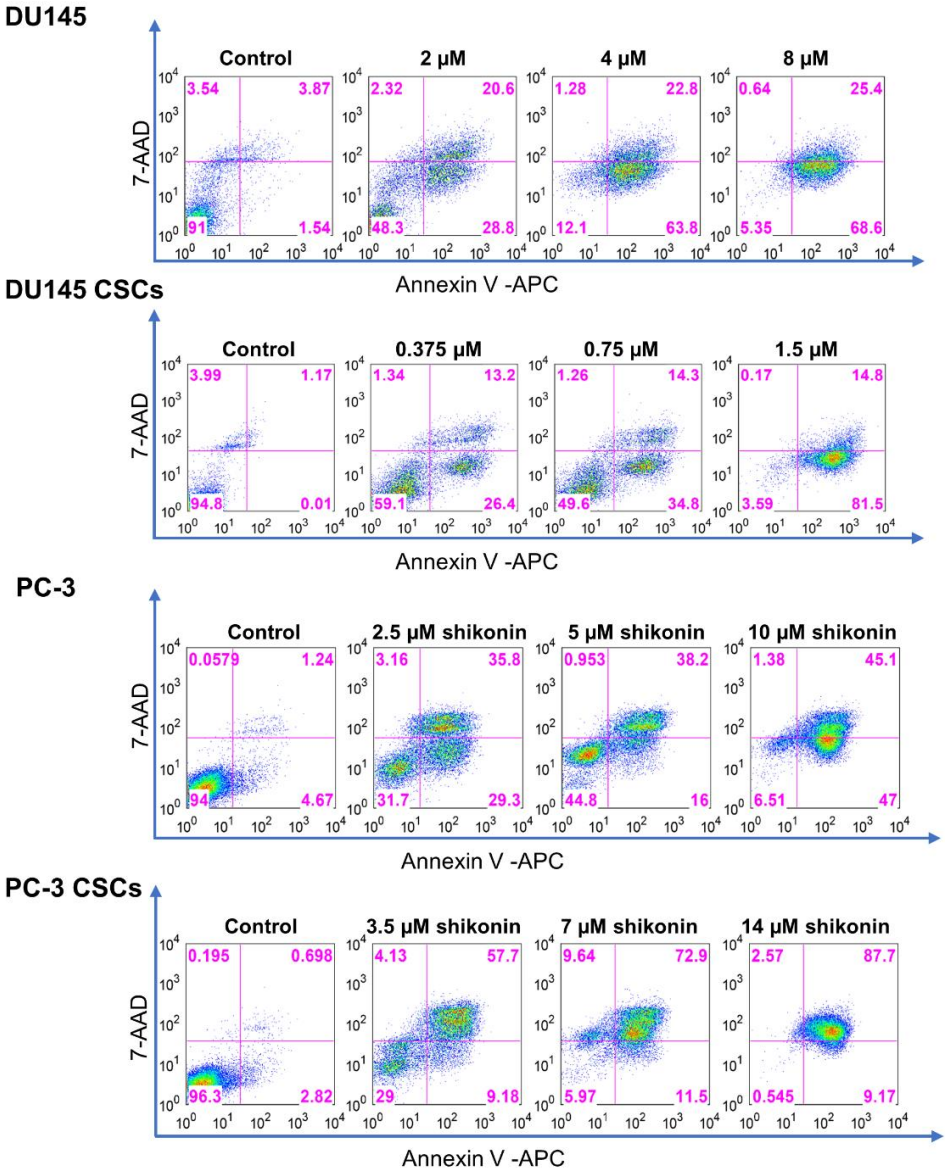

Figure 24. Shikonin induces apoptosis in PCa cells and PCSCs. The apoptosis assay revealed that shikonin induced apoptosis in DU145 cell line, DU-145 CSC, PC-3 cell line, and PC-3 CSC. The Annexin V positive cells were considered as apoptotic cells (Figure adapted from Wang et al. [90]).

Next, to investigate the mechanisms of apoptosis induced by shikonin, we performed the ROS assay. The generation of ROS was reported to be an essential mechanism of apoptosis progression in different types of cancers [94-97] and was conducted as described in 2.2.13. The ROS assay indicated that shikonin extremely enhanced the ROS production (**Figure 25**).

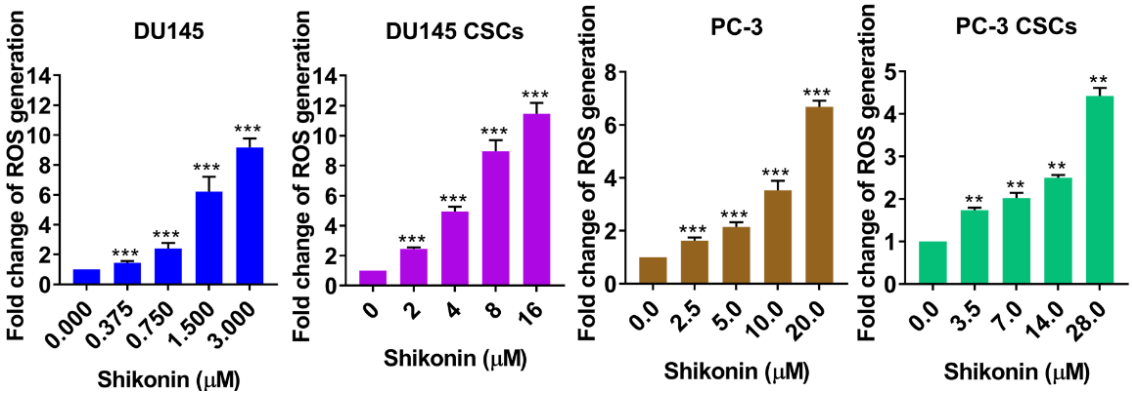

Figure 25. Shikonin generates ROS in PCa cells and PCSCs. Shikonin induced ROS production in a concentration dependent manner during 6 hours incubation. The data were acquired from three separate experiments and calculated as means ± SEM. *p < 0.05; **p < 0.01; ***p < 0.001 (Figure adapted from Wang et al. [90]).

The effect of ROS generation can be reversed by pre-treatment with N-acetyl-L-cysteine (NAC), which is an inhibitor of ROS as described in 2.2.13. NAC decreased the effect of shikonin on cell viability as we anticipated (**Figure 26**), which suggested that shikonin targeted cell viability through ROS generation.

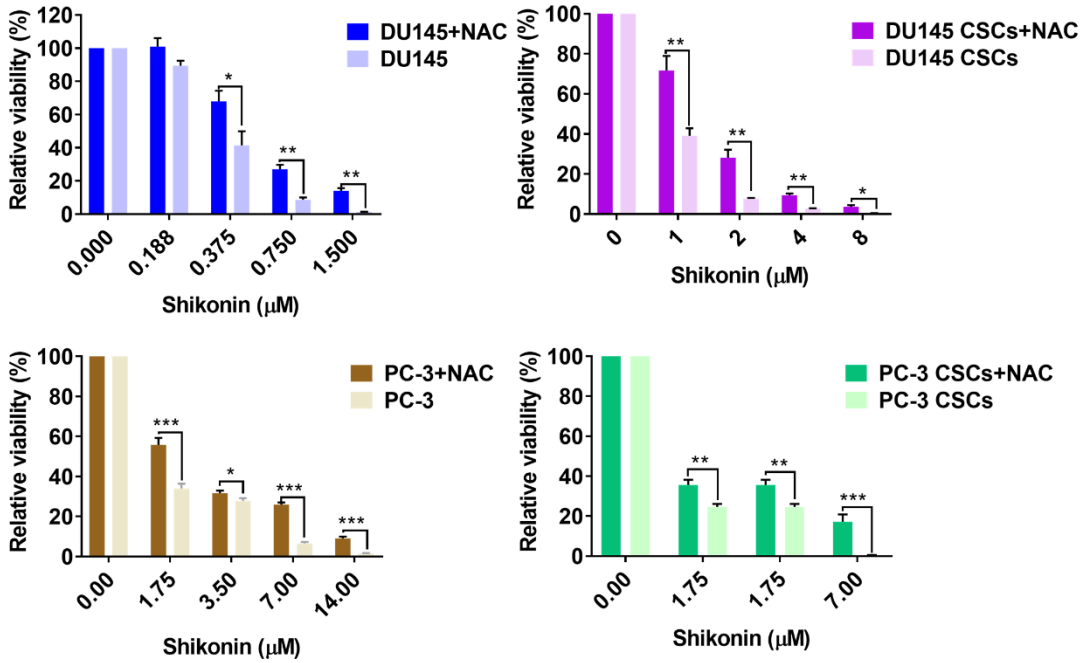

Figure 26. NAC decreased the shikonin-induced anti-cancer effect in PCa cells and PCSCs. CellTiter-Blue Cell Viability Assay showed that pretreatment with the ROS scavenger NAC at 1 mM for 4 hours reduced the cell viability. The data were acquired from three separate experiments and calculated as means ± SEM. *p < 0.05; **p < 0.01; ***p < 0.001 (Figure adapted from Wang et al. [90])

Furthermore, the JC-1 mitochondrial membrane potential assay was conducted to see whether shikonin could dysregulate mitochondrial membrane potential based on the fact that ROS influences the mitochondrial functions as described in 2.2.14. The results showed that shikonin greatly diminished the JC-1 aggregate monomer ratio, which meant the mitochondrial membrane potential was disrupted. Pre-treatment with NAC reversed the dysregulation of the membrane potential and verified the conclusion that shikonin dysregulated the mitochondrial function through ROS generation (**Figure 27**).

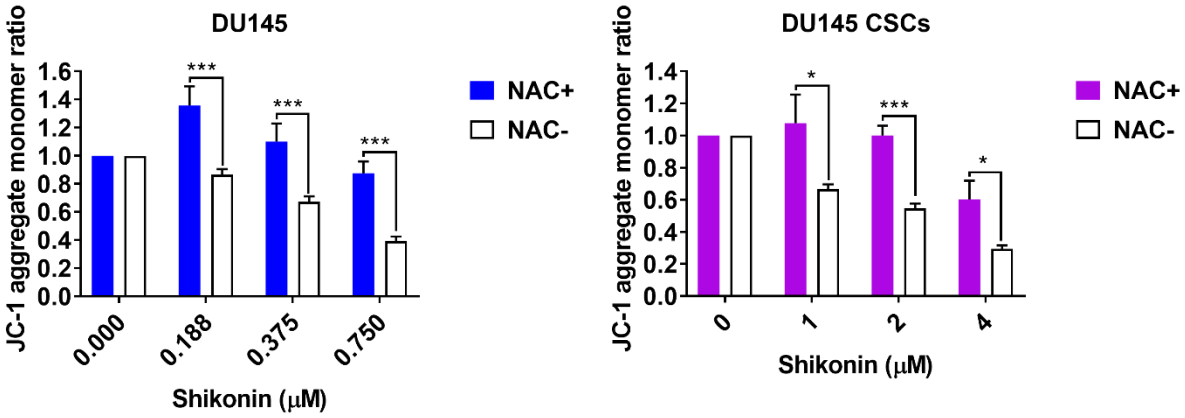

Figure 27. Shikonin causes mitochondrial dysfunction in PCa cells and PCSCs. JC-1 mitochondrial membrane potential assay demonstrated that shikonin disrupted the mitochondrial membrane potential along with higher concentration. Pre-treatment with NAC inhibits this dysregulation. The data were acquired from three separate experiments and calculated as means ± SEM. *p < 0.05; **p < 0.01; ***p < 0.001 (Figure adapted from Wang et al. [90]).

3.1.5 Shikonin suppresses the expression of ABCG2 and ALDH3A1 in PCSCs

Drug-resistance can be driven by different CSC markers for example ALDH and ABCG2. To measure these markers the ALDEFLUOR kit, flow cytometry, and qRT-PCR were conducted as described in 2.2.9, 2.2.10, and 2.2.11. The ALDEFLUOR assay demonstrated that shikonin inhibited the expression level of ALDH in PCSCs (**Figure 28**). Also, the expression level of ABCG2 was inhibited shown by flow cytometry using APC-conjugated ABCG2 antibody (**Figure 29A**). Similarly, in the qRT-PCR assay it was shown that shikonin inhibited *ABCG2* and *ALDH3A1* in PCSCs (**Figure 29B**).

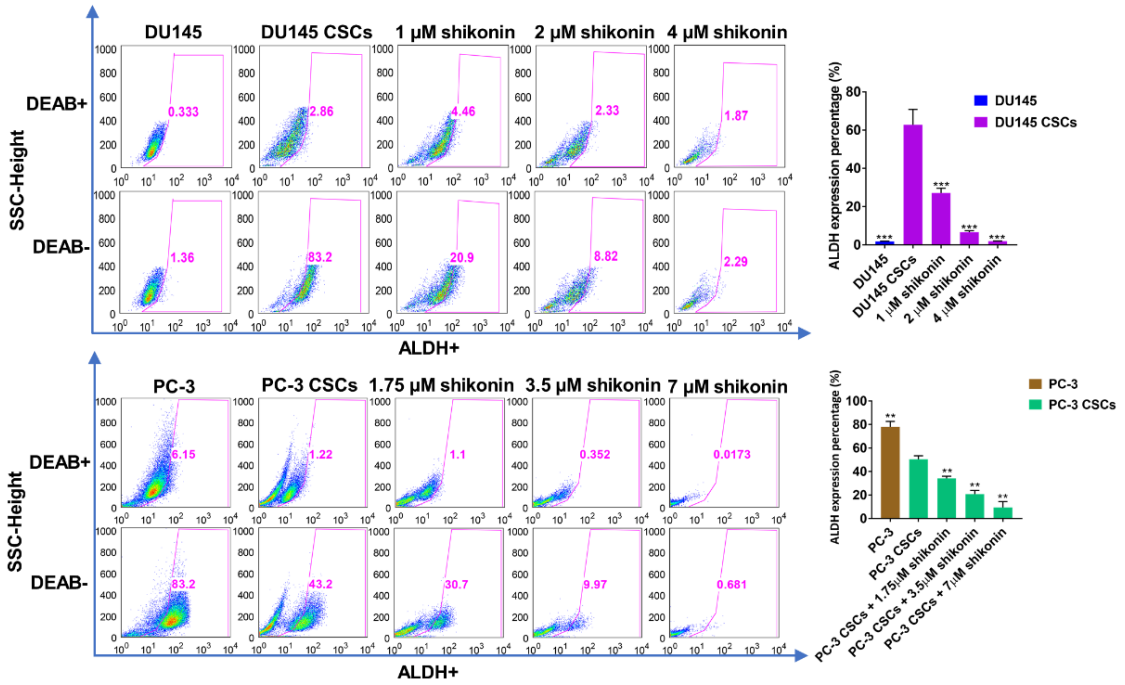

Figure 28. Shikonin inhibits the expression of ALDH. Using the ALDEFLUOR kit it was observed that ALDH expression was decreased by shikonin in DU145 CSCs and PC-3 CSCs. DEAB, the ALDH inhibitor, was applied as a control. The data were acquired from three separate experiments and calculated as means ± SEM. *p < 0.05; **p < 0.01; ***p < 0.001 (Figure adapted from Wang et al. [90]).

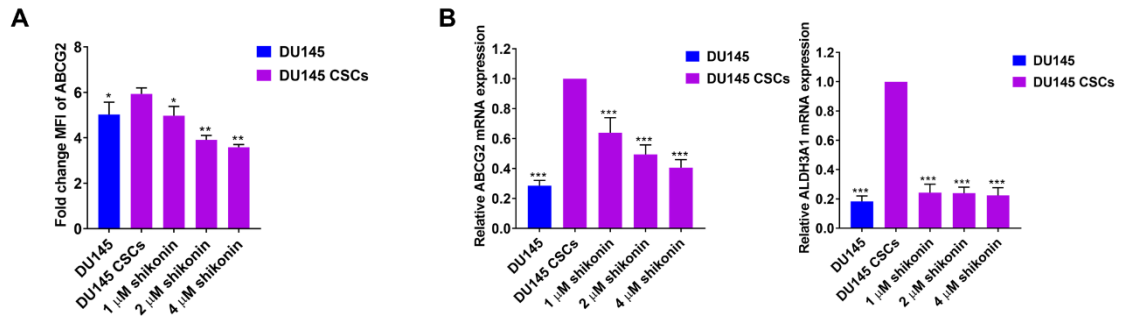

Figure 29. Shikonin inhibits the expression of ABCG2 and ALDH3A1 in PCSCs. A. Results from flow cytometry showed that ABCG2 expression was decreased by shikonin. **B**. Results from qRT-PCR indicated that shikonin also suppressed *ABCG2* and *ALDH3A1.* The data were acquired from three separate experiments and calculated as means ± SEM. *p < 0.05; **p < 0.01; ***p < 0.001 (Figure adapted from Wang et al. [90]).

To investigate a possible correlation between the two CSC markers, ALDH3A1 and ABCG2, regulated by shikonin, confocal fluorescence microscopy, and siRNAs experiments were performed. The siRNA experiments demonstrated that downregulation of ALDH3A1 could not influence the expression level of ABCG2 (**Figure 30B**), while

downregulation of ABCG2 significantly decreased the expression level of ALDH3A1 (**Figure 30C**). The confocal microscopy experiment verified the co-existence of ABCG2 and ALDH3A1. Both the Pearson correlation coefficient and the overlap coefficient were around 0.9 (**Figure 30A**). In general, the results suggested that ABCG2 and ALDH3A1 were at least co-expressed in DU-145 CSCs and that shikonin can inhibit the expression of ALDH3A1 by downregulating ABCG2.

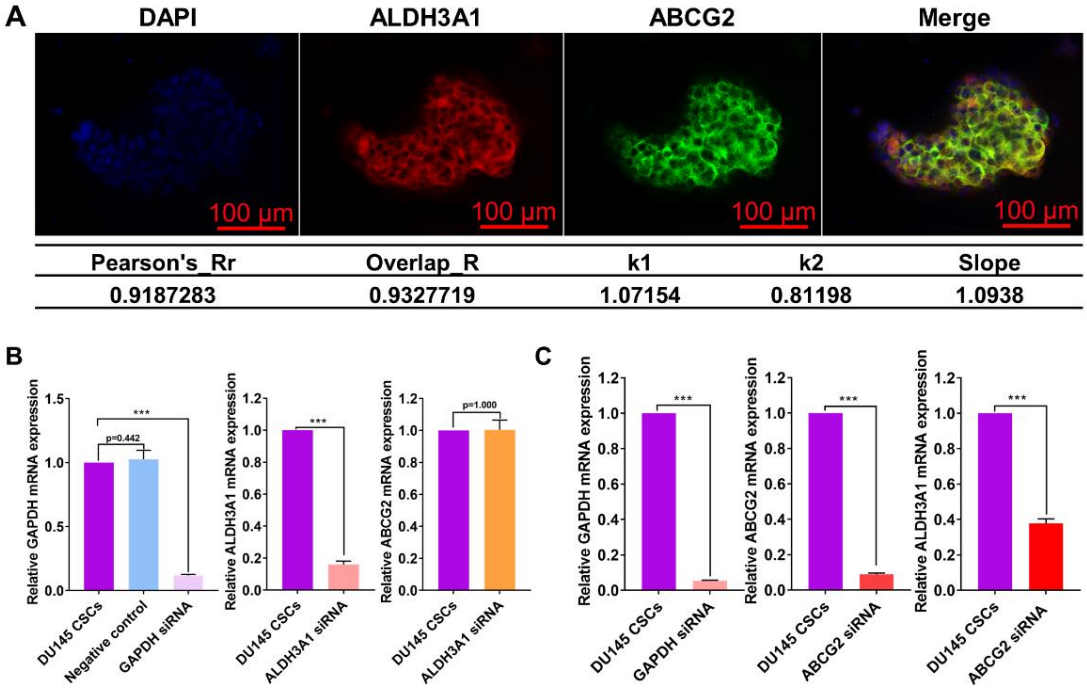

Figure 30. The correlation between ABCG2 and ALDH3A1 in DU145 CSCs. **A**. Confocal microscopy indicated the co-existence of ALDH3A1 and ABCG2. Pearson correlation coefficient and overlap coefficient were calculated using the colocalization finder module from the Image J software and were mounted around 9.2 and 9.3, respectively. **B**. DU145 CSCs were transfected with siRNA for *ALDH3A1* and cultured for 48 hours. qRT-PCR showed no influence on the expression of ABCG2. The *GAPDH* siRNA was applied as a positive control. **C**. In contrast, silencing of *ABCG2* led to downregulation of *ALDH3A1*. The data were acquired from three separate experiments and calculated as means ± SEM. *p < 0.05; **p < 0.01; ***p < 0.001 (Figure adapted from Wang et al. [90]).

3.1.6 Downregulation of ABCG2 and ALDH3A1 re-sensitizes caba-DU145 cells to cabazitaxel

Based on our above results, we hypothesized that shikonin can re-sensitize drug-resistant cells by regulating the expression level of ABCG2 and ALDH3A1. To verify this, a cabazitaxel-resistant PCa cell line (caba-DU145) was established as described in 2.2.4. **Figure 31** showed that caba-DU145 cells were more resistant than DU145

cells.

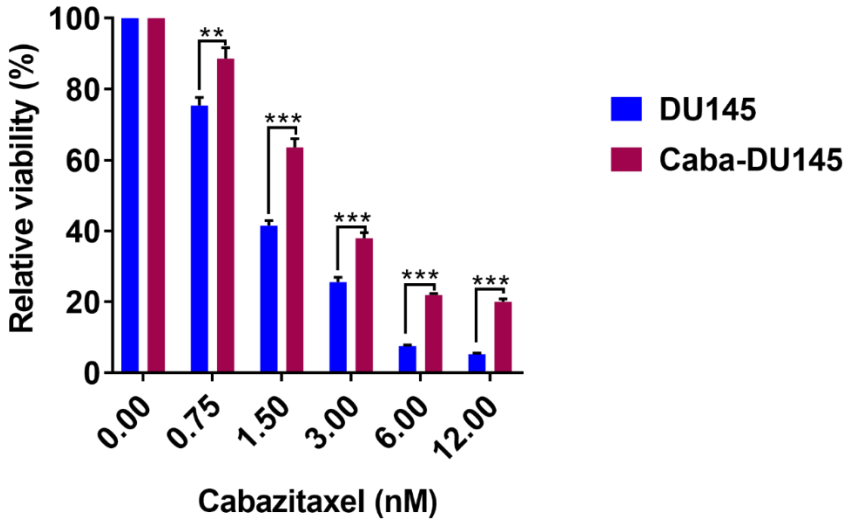

Figure 31. The generation of cabazitaxel-resistant DU145 cell line. Viability assay: the cabazitaxel-resistant DU145 cell line showed significantly higher viability than the parental DU145 cell line. The data were acquired from three separate experiments and calculated as means ± SEM. *p < 0.05; **p < 0.01; ***p < 0.001**.** (Figure adapted from Wang et al. [90]).

Then, caba-DU145 cells were pretreated with 1 μM ABCG2 inhibitor Ko143 or 32 μM ALDH3A1 inhibitor CB29 for five days. Afterwards, cell viability and proliferation were assessed following treatment with cabazitaxel. When suppressing ABCG2 and ALDH3A2 caba-DU145 cells became more sensitive to cabazitaxel as shown for both the viability (**Figure 32A** and **Figure 33A**), and the proliferation (**Figure 32B and Figure 33B**).

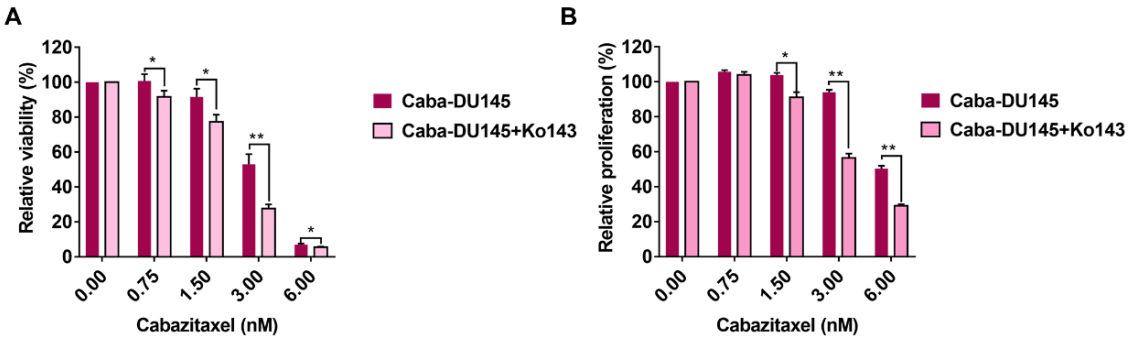

Figure 32. Inhibition of ABCG2 sensitizes caba-DU145 cells to cabazitaxel. Viability assay (**A**) and proliferation assay (**B**) demonstrated that inhibition of ABCG2 following pre-treatment with Ko143 strengthened the anti-cancer effect of cabazitaxel. The data were acquired from three separate experiments and calculated as means ± SEM. *p < 0.05; **p < 0.01; ***p < 0.001 (Figure adapted from Wang et al. [90]).

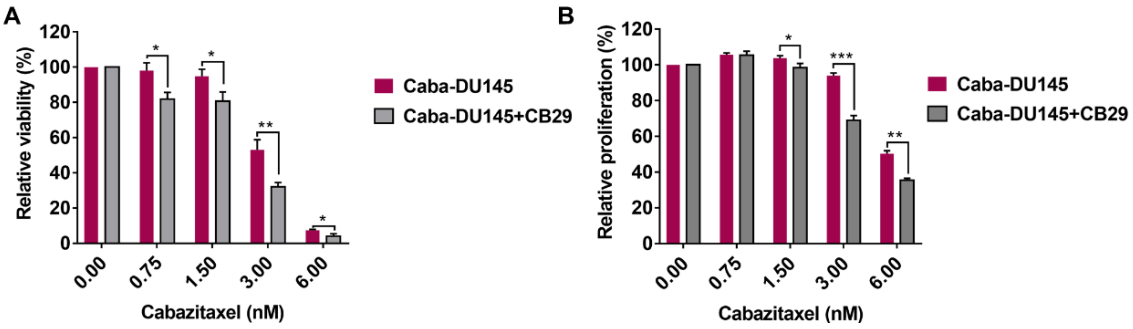

Figure 33. Inhibition of ALDH3A1 sensitizes caba-DU145 cells to cabazitaxel. Viability assay(**A**) and proliferation assay (**B**) demonstrated that inhibition of ALDH3A1 following pretreatment with CB29 strengthened the anti-cancer effect of cabazitaxel. The data were acquired from three separate experiments and calculated as means ± SEM. *p < 0.05; **p < 0.01; ***p < 0.001 (Figure adapted from Wang et al. [90]).

Moreover, in the apoptosis assay it could be demonstrated that inhibition of ALDH3A1 and ABCG2 increased the rate of apoptosis as we expected (**Figure 34**).

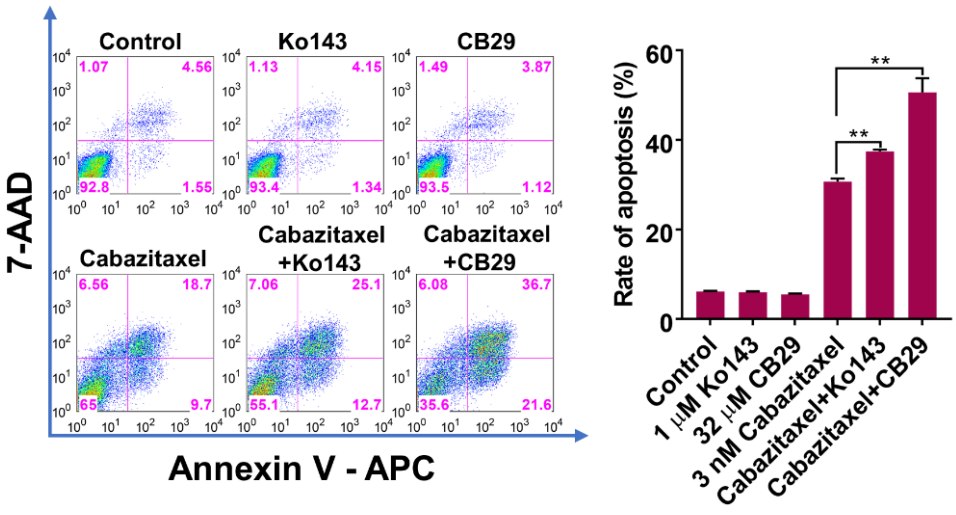

Figure 34. Downregulation of ABCG2 and ALDH3A1 sensitizes caba-DU145 cells to cabazitaxel as shown in the apoptosis assay. Inhibition of ABCG2 and ALDH3A1 following pretreatment with Ko143 and CB29 led to an enhanced apoptosis rate in caba-DU145 cells. The Annexin V positive cells were considered as apoptotic cells. The data were acquired from three separate experiments and calculated as means ± SEM. *p < 0.05; **p < 0.01; ***p < 0.001 (Figure adapted from Wang et al. [90]).

To confirm the re-sensitizing effect of shikonin to cabazitaxel in caba-DU145 cells, we combined shikonin with cabazitaxel. Even at a low concentration of shikonin (0.375 µM), an increased apoptosis rate was observed in caba-DU145 cells compared to treatment with cabazitaxel alone (**Figure 35**).

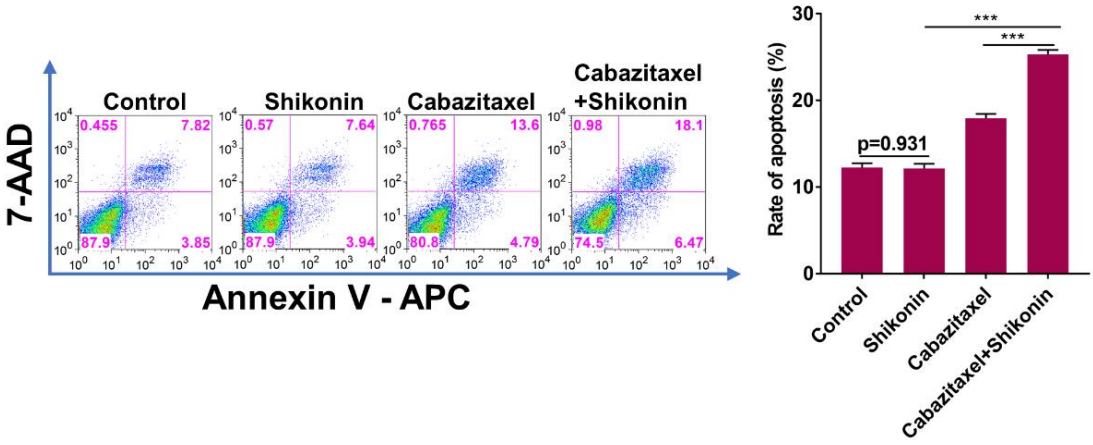

Figure 35. Shikonin re-sensitizes caba-DU145 cells to cabazitaxel. The apoptosis assay showed that shikonin at 0.375 µM re-sensitized the caba-DU145 cells to cabazitaxel (3 nM). The Annexin V positive cells were considered as apoptotic cells The data were acquired from three separate experiments and calculated as means ± SEM. *p < 0.05; **p < 0.01; ***p < 0.001 (Figure adapted from Wang et al. [90]).

Taken together, shikonin shows an anti-cancer effect on PCa cells and PCSCs via mediating ROS generation and dysregulating the mitochondria membrane potential. Furthermore, shikonin re-sensitizes cabazitaxel-resistant PCa cells to cabazitaxel through inhibiting the expression of ABCG2 and ALDH3A1. It seems that the combination of cabazitaxel and shikonin shows a synergistic effect. Therefore, shikonin is a highly promising phytochemical to treat not only PCa in general but also CRPC patients resistant to cabazitaxel.

3.2 The influence of berbamine on cancer stem cells

3.2.1 Berbamine has anti-tumor effects on PCSCs

We generated prostate cancer stem cells (PCSCs) using the sphere-forming assay as shown in **Figure 14**. PCa cells (DU145 and PC-3) and PCSCs (DU145 CSC and PC-3 CSC) were treated with berbamine in different concentrations for 24 hours and 48 hours. CellTiter Blue Cell Viability Assay showed that berbamine repressed the cell viability of PCa cells and PCSCs in a dose-dependent manner (**Figure 36A-B**). The IC50 concentrations of berbamine were calculated using the statistical method of the logit regression model, which were 23 µM in DU145 cells, 9 µM in DU145 CSCs, 40 µM in PC-3 cells, 12 µM in PC-3 CSCs.

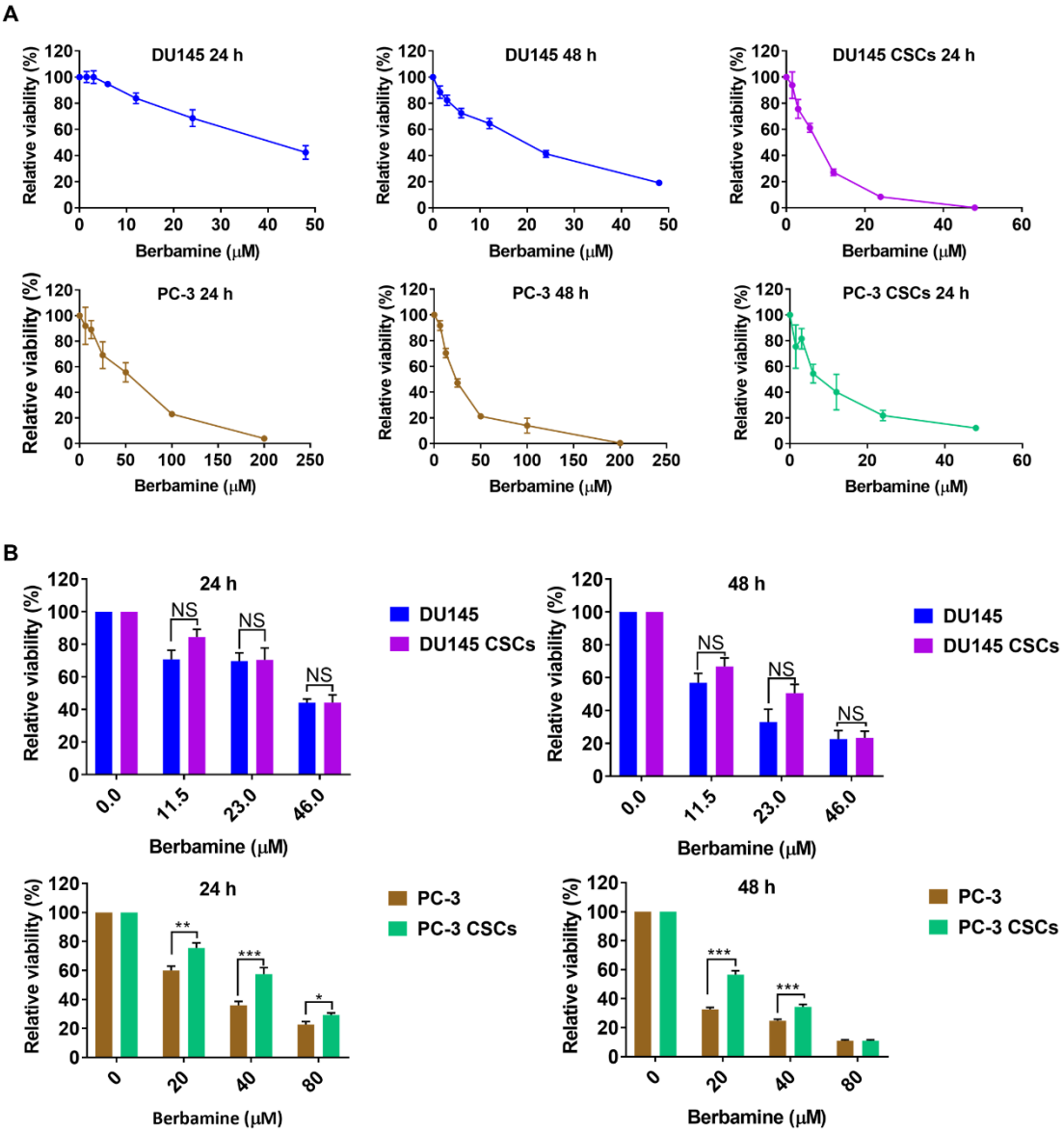

Figure 36. Berbamine inhibits the viability in PCa cells and PCSCs. A. CellTiter-Blue Cell Viability Assay for DU145 and PC-3 shown for 24 and 48 hours, and PCSCs for 24 hours. Berbamine repressed the viability of DU145 cells, PC-3 cells, DU145 CSCs and PC-3 CSCs in a dose-dependent manner. **B**. CellTiter-Blue Cell Viability Assay: PC-3 CSCs were much more resistant to berbamine than PC-3 cells, while there was no difference between DU145 CSCs and adherent DU145. The data were acquired from three separate experiments and calculated as means ± SEM. *p < 0.05; **p < 0.01; ***p < 0.001, NS: not significant.

An inhibiting influence of berbamine on the proliferation rate was noticed as well using different concentrations of berbamine (0.5× IC50, 1x IC50, 2× IC50, **Figure 37A-B**). Results showed that PC-3 CSCs were much more resistant to berbamine than PC-3 cells. However, there was no difference between DU145 CSCs and adherent DU145 cells (**Figure 36B** and **Figure 37B**).

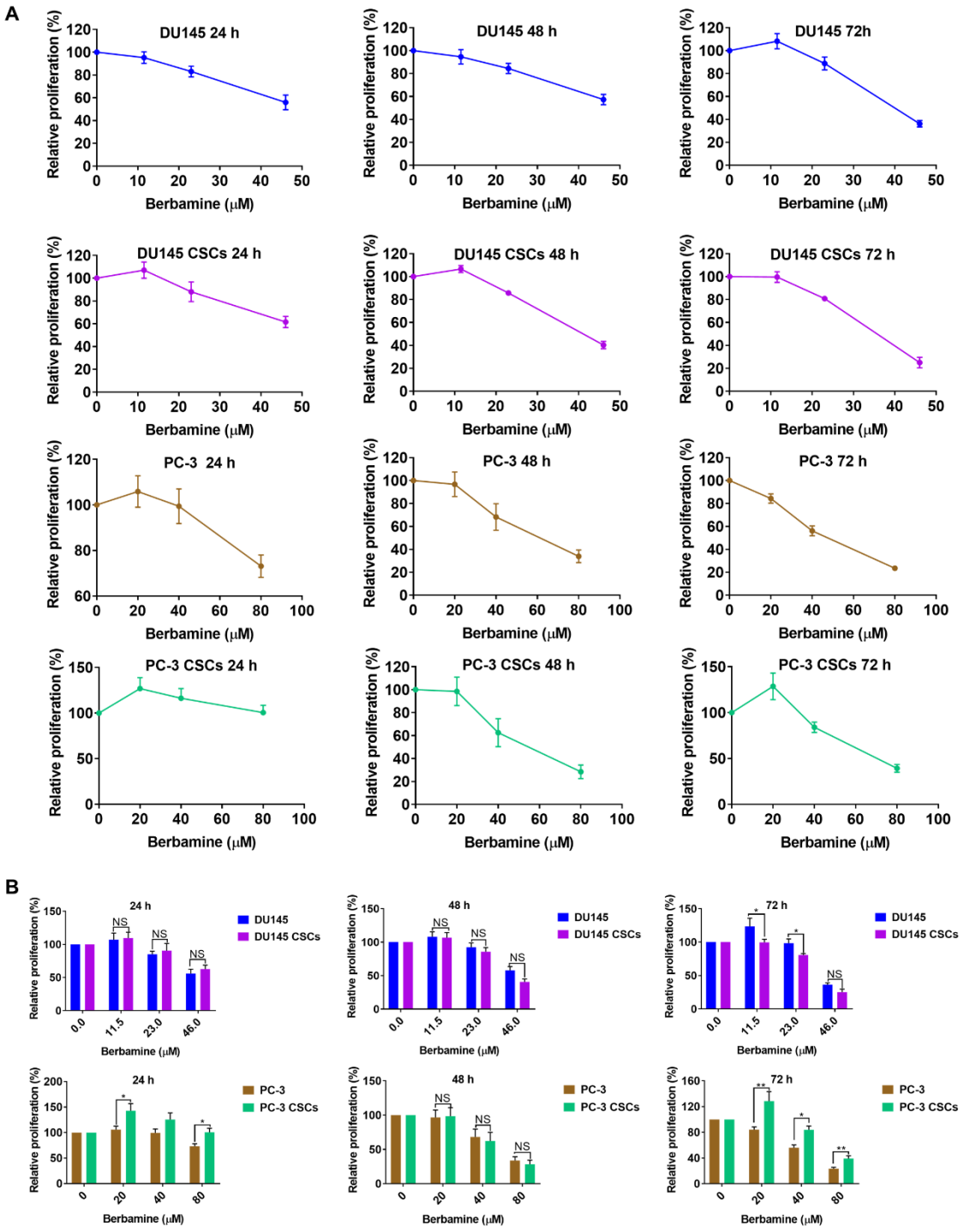

Figure 37. Berbamine inhibits the proliferation of PCa cells and PCSCs. **A**. Proliferation assay showed that berbamine repressed the proliferation of DU145 cells, PC-3 cells, DU145 CSCs and PC-3 CSCs. **B**. Proliferation assay showed that PC-3 CSCs were much more resistant to berbamine than PC-3 cells, while there was no difference between DU145 CSCs and DU145 cells. The data were acquired from three separate experiments and calculated as means ± SEM. *p < 0.05; **p < 0.01; ***p < 0.001, NS: not significant.

We also evaluated the influence of berbamine on migration and invasion. Migration was evaluated again using the assay described in section 2.2.7. After treatment with berbamine in different concentrations, pictures were taken at different time points. Berbamine inhibited the ability to migrate of DU145 cells, PC-3 cells, DU145 CSCs, and PC-3 CSCs to the center of the gap (**Figure 38A-B**).

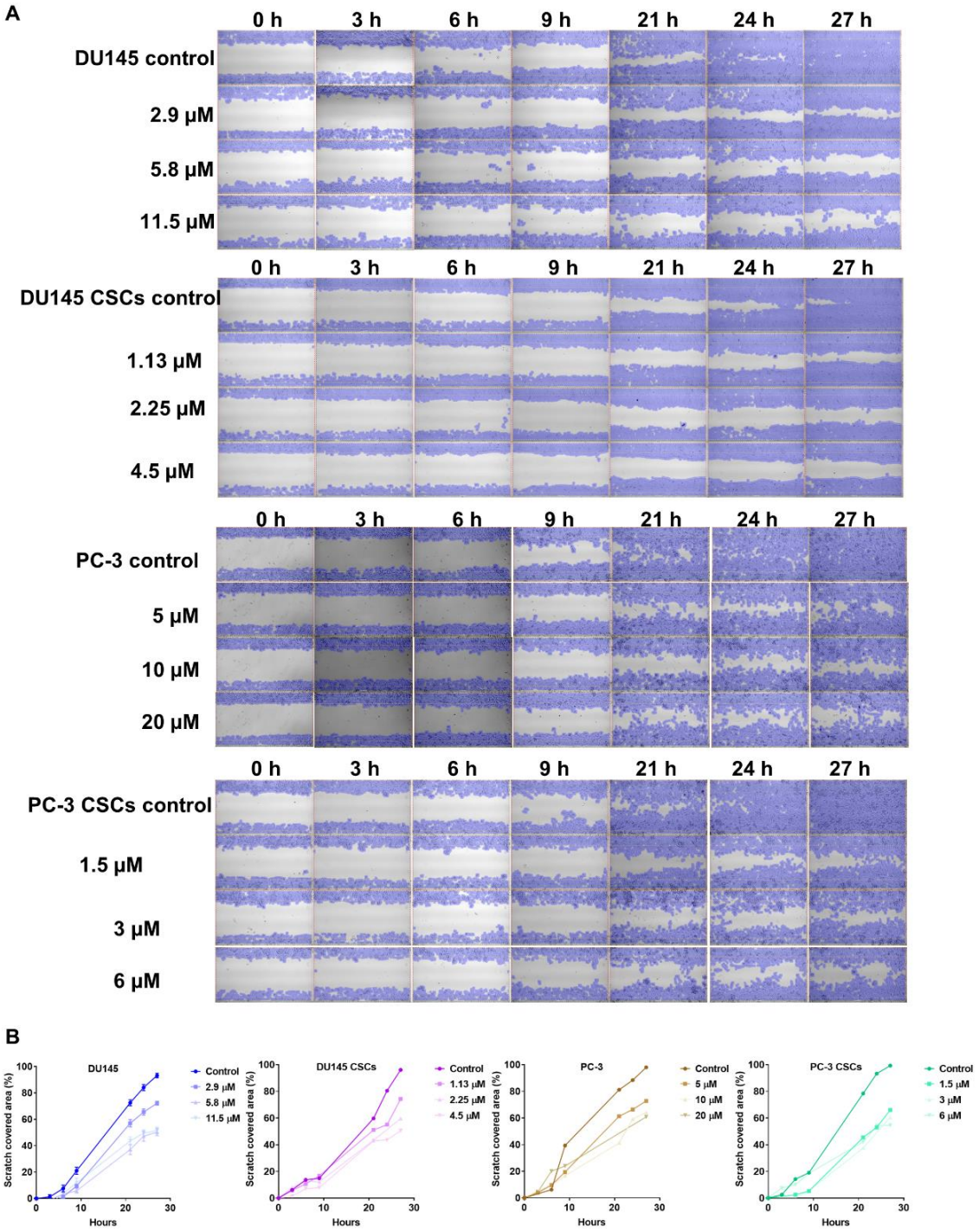

Figure 38. Berbamine inhibits migration ability in PCa cells and PCSCs. A. The scratch wound healing assay showed that berbamine inhibited the migration of DU145 cells (at 2.9 μM, 5.8 μM, and 11.5 μM), DU145 CSCs (at 1.13 μM, 2.25 μM, 4.5 μM), PC-3 cells (at 5 μM, 10 μM,

20 µM), PC-3 CSCs (at 1.5 µM, 3 µM, 6 µM). Pictures were captured with a digital microscope camera at 40x magnification at different time points. The percentage of the covered area of the gap was calculated using the Automated Cellular Analysis System based on the FastTrack AI image analysis algorithms. **B**. The graphs show the percentage of the covered area of the scratch wound at different time points of culture with or without berbamine.

The invasion assay demonstrated that the number of invaded cells was decreased significantly in the group with higher concentrations of berbamine both in the adherent cells and cancer stem cells (**Figure 39A-B**), indicating that berbamine can inhibit invasion remarkably in PCa cells and PCSCs.

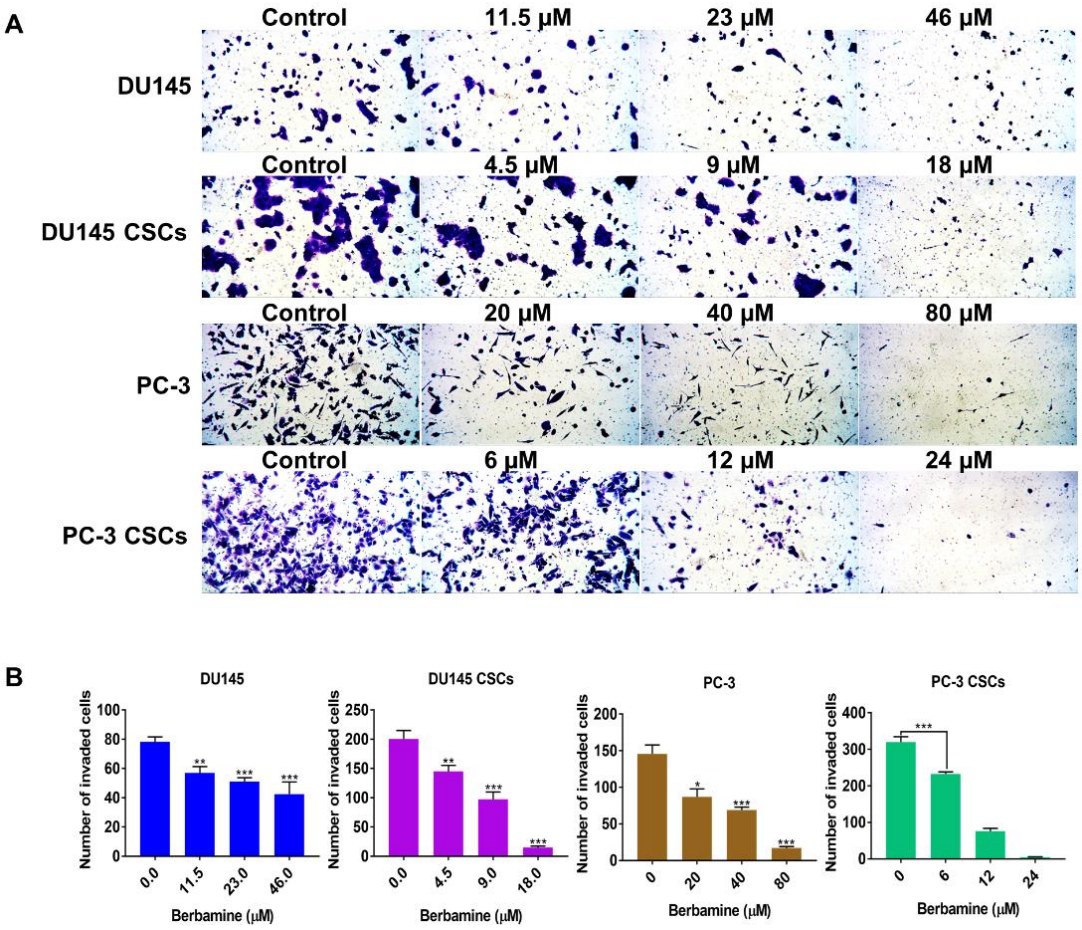

Figure 39. Berbamine inhibits invasiveness in PCa cells and PCSCs. A. Invasion assay: berbamine inhibited the invasiveness of DU145 cells, PC-3 cells, DU145 CSCs, and PC-3 CSCs. Pictures were taken from every insert by the digital microscope camera at 40x magnification (three fields per insert). Then, cells were counted using the Fiji Image J software. The number of cells in one picture was considered as invaded cell number. **B.** The bar charts show the number of invaded cells. The data were acquired from three separate experiments and calculated as means ± SEM. *p < 0.05; **p < 0.01; ***p < 0.001, NS: not significant.

Cell apoptosis analysis showed that berbamine induced a higher rate of apoptosis along with higher concentrations compared to the untreated group (**Figure 40**).

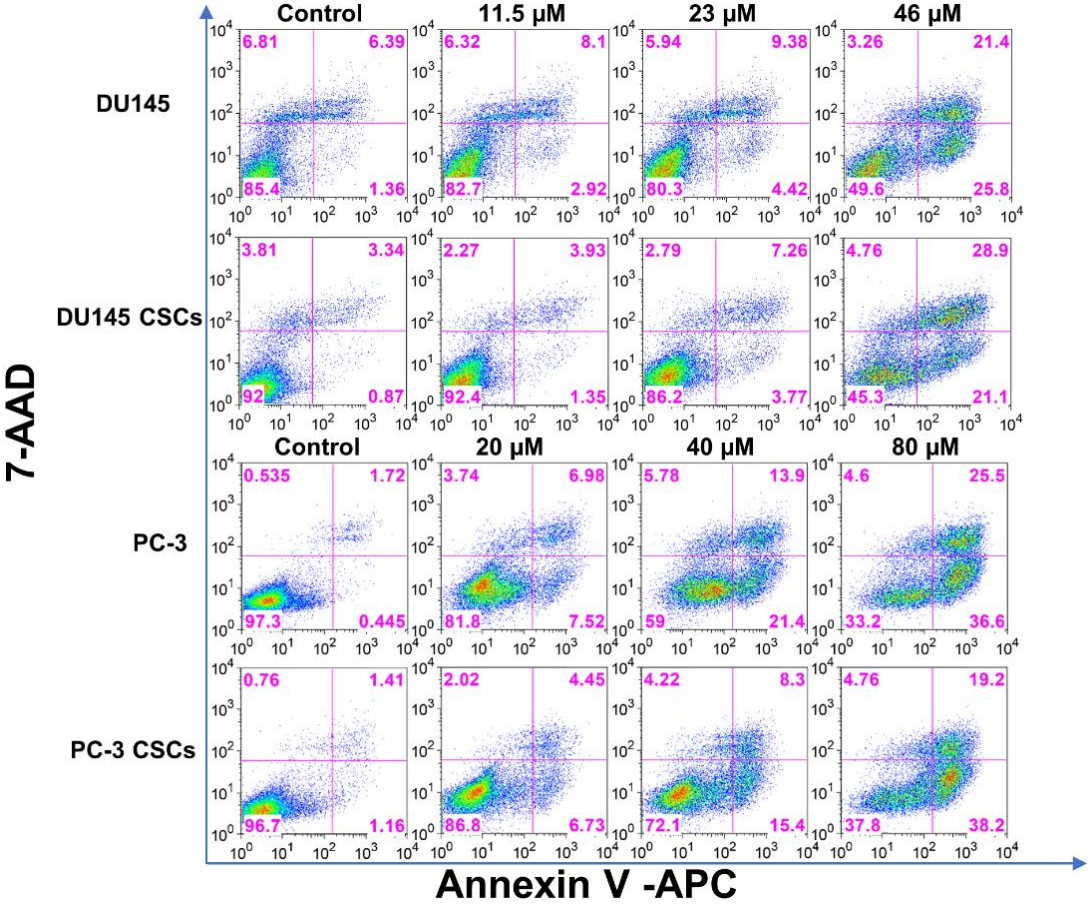

Figure 40. Berbamine induces apoptosis in PCa cells and PCSCs. Apoptosis assay showed that berbamine induced the apoptosis of DU145 cells, PC-3 cells, DU145 CSCs, and PC-3 cells. Annexin V positive cells were considered as apoptotic cells. The experiment was repeated independently three times.

3.2.2 Berbamine enhances the toxicity of cabazitaxel on PCa and PCSCs

The viability, proliferation, invasion, and apoptosis assays were carried out again to examine whether berbamine could augment the anti-cancer effect of cabazitaxel. We determined the IC50 concentration of cabazitaxel, which was 3 nM using the method of the logit regression model (**Figure 19**). Afterwards, DU145 cells and DU145 CSCs were treated with berbamine at the concentration of 23 μM combined with different concentrations of cabazitaxel for 48 hours. The combination of berbamine and cabazitaxel resulted in a remarkable decrease both in viability (**Figure 41**) and proliferation (**Figure 42**) compared to cabazitaxel alone in DU145 cells and DU145 CSCs.

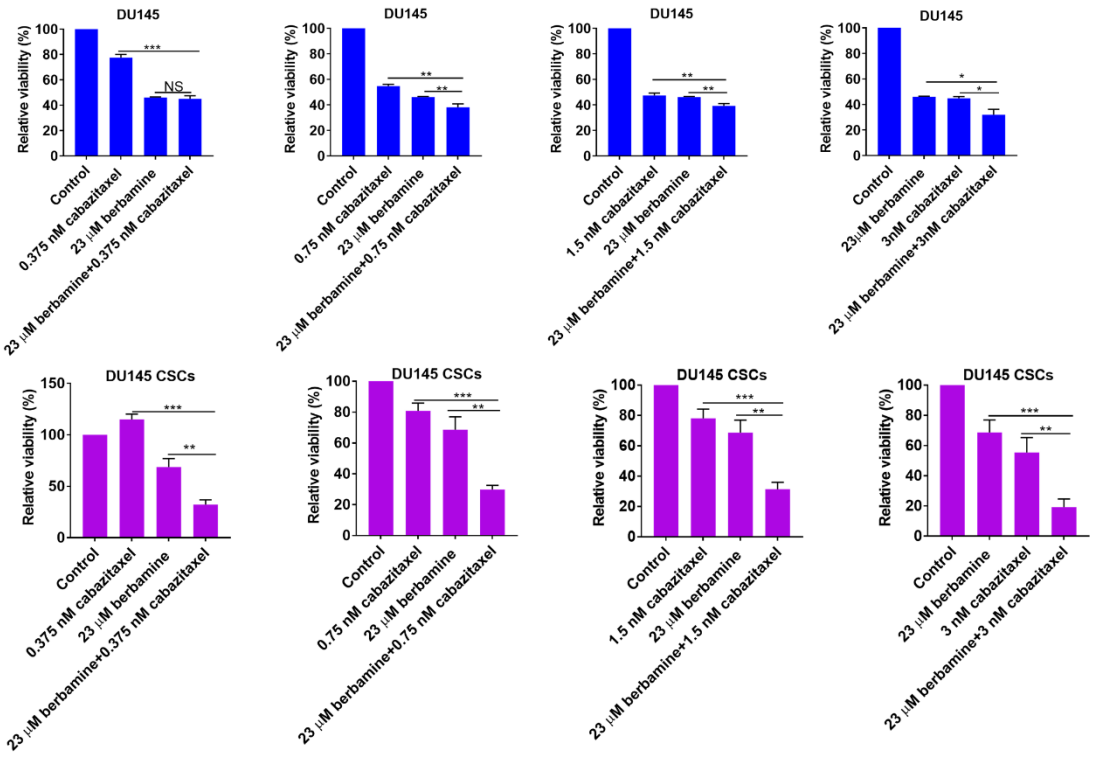

Figure 41. Berbamine enhances the anti-tumor effect of cabazitaxel in the viability assay. CellTiter-Blue Cell Viability Assay: the combination of berbamine (23 μM) and different concentrations of cabazitaxel enhanced the cytotoxic effect compared to cabazitaxel alone. The viability assay was measured after 48 hours. The data were acquired from three separate experiments and calculated as means ± SEM. *p < 0.05; **p < 0.01; ***p < 0.001.

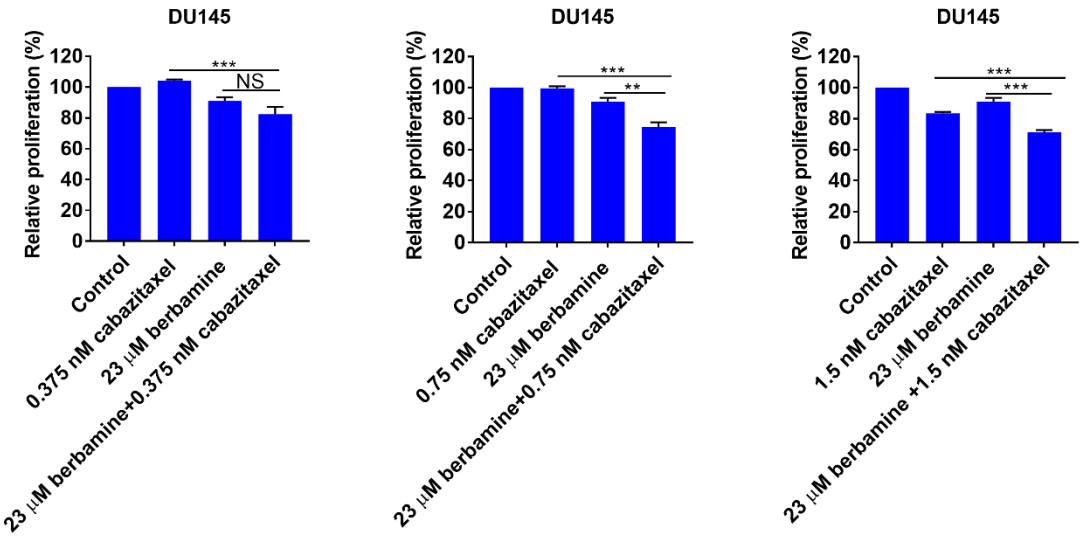

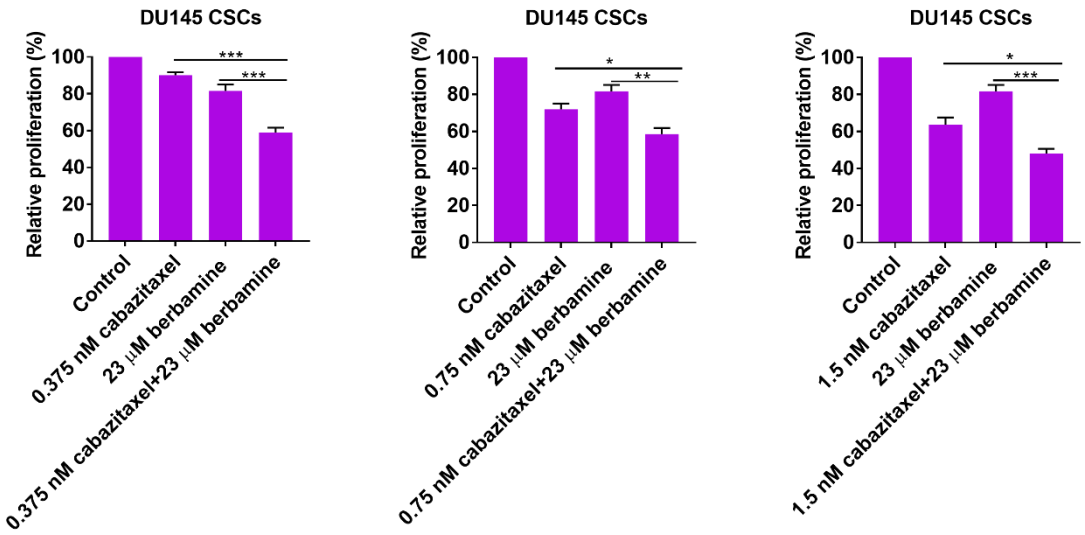

Figure 42. Berbamine enhances the anti-tumor effect of cabazitaxel in the proliferation assay. The proliferation assay demonstrated that the combination of berbamine (23 µM) with different concentrations of cabazitaxel decreased proliferation compared to cabazitaxel alone. The proliferation was determined after 48 hours. The data were acquired from three separate experiments and calculated as means ± SEM. *p < 0.05; **p < 0.01; ***p < 0.001.

Also, a notably higher inhibition was observed within the combination group in the invasion assay (**Figure 43**).

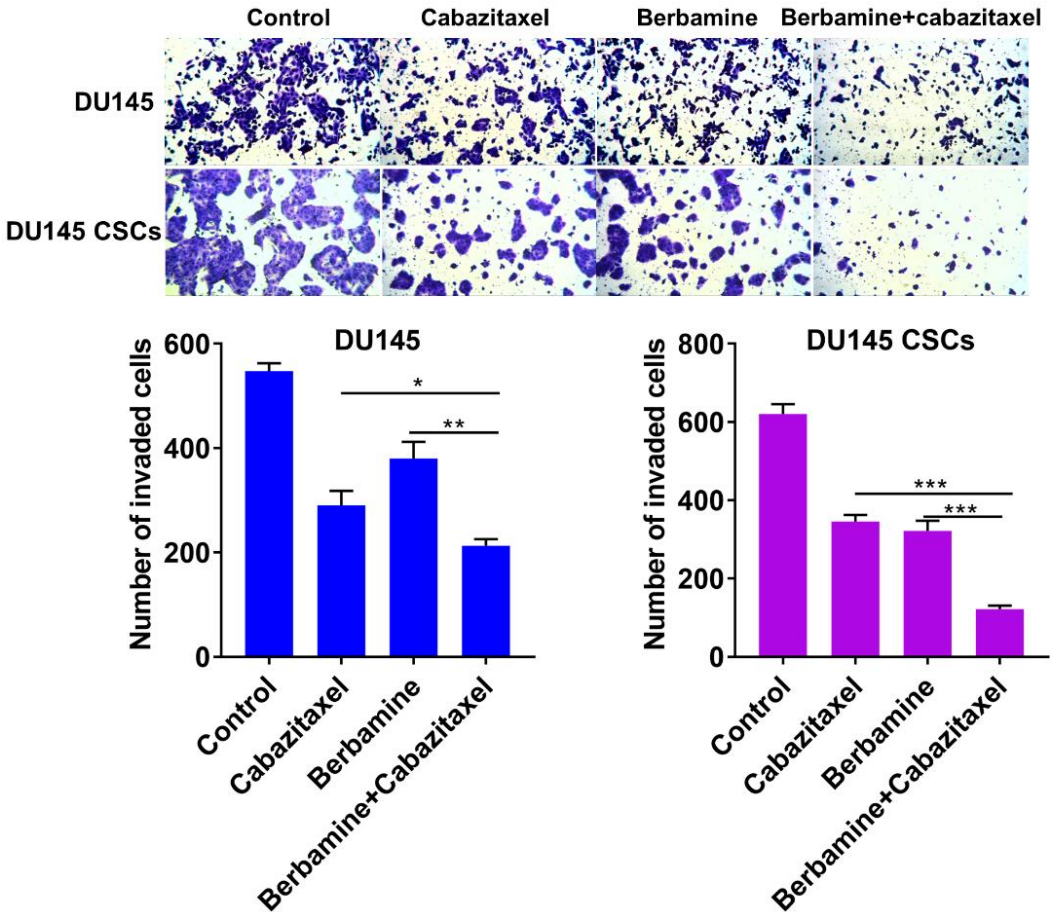

Figure 43. Berbamine enhances the anti-tumor effect of cabazitaxel in the invasion assay. In the treatment group berbamine plus cabazitaxel the invasiveness of DU145 cells and DU145 CSCs was reduced compared to cabazitaxel alone. The pictures were taken by the digital microscope camera at 40x magnification (three fields per insert) and analyzed using the Fiji Image J software. The bar graphs demonstrate the number of invaded cells. The data were acquired from three separate experiments and calculated as means ± SEM. *p < 0.05; **p < 0.01; ***p < 0.001.

Even the apoptosis assay demonstrated that the percentage of apoptotic cells was higher after treatment with berbamine plus cabazitaxel compared to cabazitaxel and berbamine alone (**Figure 44**). Altogether, berbamine increased the cytotoxic effect of cabazitaxel in PCa cells and PCSCs.

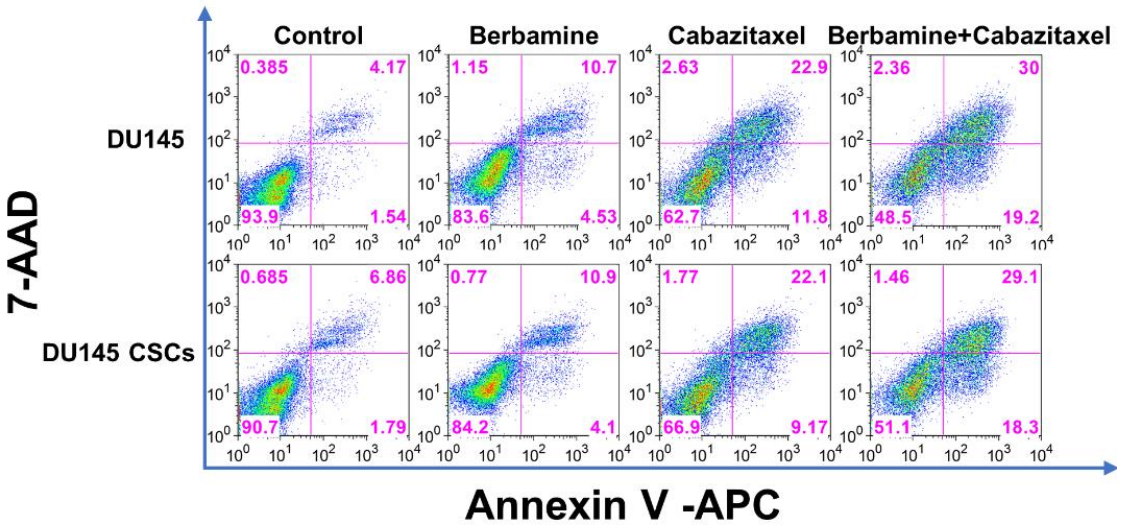

Figure 44. Berbamine enhances the anti-tumor effect of cabazitaxel in the apoptosis assay. The results of the flow cytometry experiment demonstrated that berbamine plus cabazitaxel enhanced the apoptosis rate. Annexin V positive cells were considered as the percentage of apoptotic cells.

3.2.3 Berbamine reverses the cabazitaxel-resistant state by downregulating ABCG2 and CXCR4

The prostate cancer stem cell markers have the capacity of driving drug resistance, and cancer relapse [23]. Therefore, we want to know if berbamine can influence the expression of some known cancer stem cell markers. Flow cytometry showed that berbamine inhibited the expression of the cancer stem cell marker ALDH (**Figure 45**), ABCG2 (**Figure 46A**), and CXCR4 (**Figure 46A**) in DU145 CSCs and PC-3 CSCs. Importantly, elevated levels of ALDH, ABCG2, and CXCR4 were observed in DU145 CSCs compared to DU145 as we expected. The qRT-PCR demonstrated similar results that berbamine inhibited the expression of *ALDH1A1*, *ABCG2*, and *CXCR4*. Also, DU145 CSCs expressed higher levels of *ALDH1A1*, *ABCG2*, and *CXCR4* than DU145 cells (**Figure 46B**).

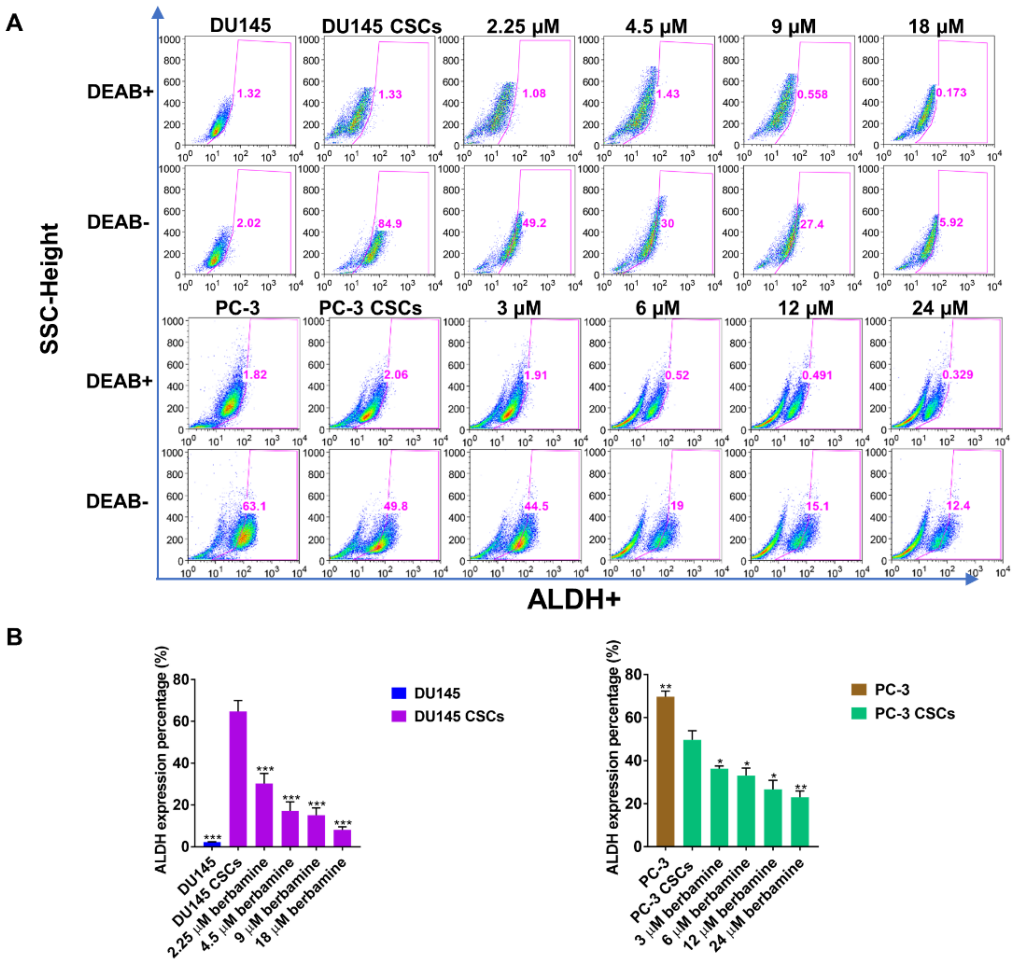

Figure 45. Berbamine downregulates the levels of ALDH. **A**. The ALDEFLUOR kit was used to demonstrate that berbamine suppresses the expression of ALDH in DU145 CSCs and PC-3 CSCs. The ALDH inhibitor DEAB was used as a control. **B**. The bar charts summarize the expression level of ALDH for the different concentrations of berbamine in PCSCs and adherent PCa cells. The data were acquired from three separate experiments and calculated as means ± SEM. *p < 0.05; **p < 0.01; ***p < 0.001.

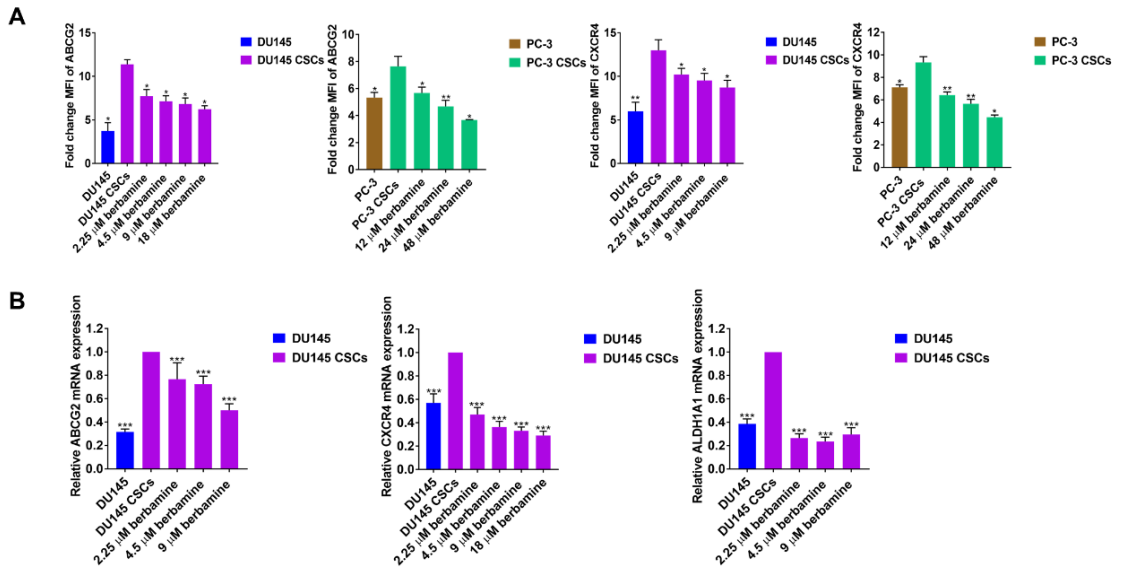

Figure 46. Berbamine downregulates ABCG2, CXCR4, and ALDH1A1. **A.** Flow cytometry: berbamine inhibited the expression of ABCG2 and CXCR4 in DU145 CSCs and PC-3 CSCs. PCSCs expressed more ABCG2 and CXCR4 than adherent cells. **B**. qRT-PCR analysis: berbamine inhibited the expression of *ABCG2*, *CXCR4*, and *ALDH1A1* mRNA as observed on the protein level by flow cytometry. DU145 CSCs expressed higher levels of *ABCG2*, *CXCR4*, than DU145 cells. The data were acquired from three separate experiments and calculated as means ± SEM. *p < 0.05; **p < 0.01; ***p < 0.001.

Next, to explore if blocking the expression of ALDH1A1, ABCG2, and CXCR4 could sensitize to cabazitaxel in cabazitaxel-resistant DU145 cells, the caba-DU145 cell line was generated as described in 2.2.4 (**Figure 31**). Caba-DU145 cells were treated with cabazitaxel combined with the ABCG2 inhibitor Ko143 at the concentration of 1 μM, with the CXCR4 inhibitors WZ811 and AMD3100 (5 μM and10 μM, respectively), or with the ALDH1A1 inhibitors A37 at 10 μM and NCT-501 at 5 μM. The results show that suppression of ABCG2 and CXCR4 decreased the rate of apoptosis in caba-DU145 cells as expected. However, there was no influence of NCT-501 (ALDH1A1 inhibitor) on caba-DU145 cells, and A37 (another ALDH1A1 inhibitor) slightly enhanced the apoptosis rate of caba-DU145 cells (**Figure 34** and **Figure 47**). Therefore, we only considered ABCG2 and CXCR4 in the following experiments. Our results suggested that berbamine could reverse the cabazitaxel resistance via downregulating the expression of ABCG2 and CXCR4.

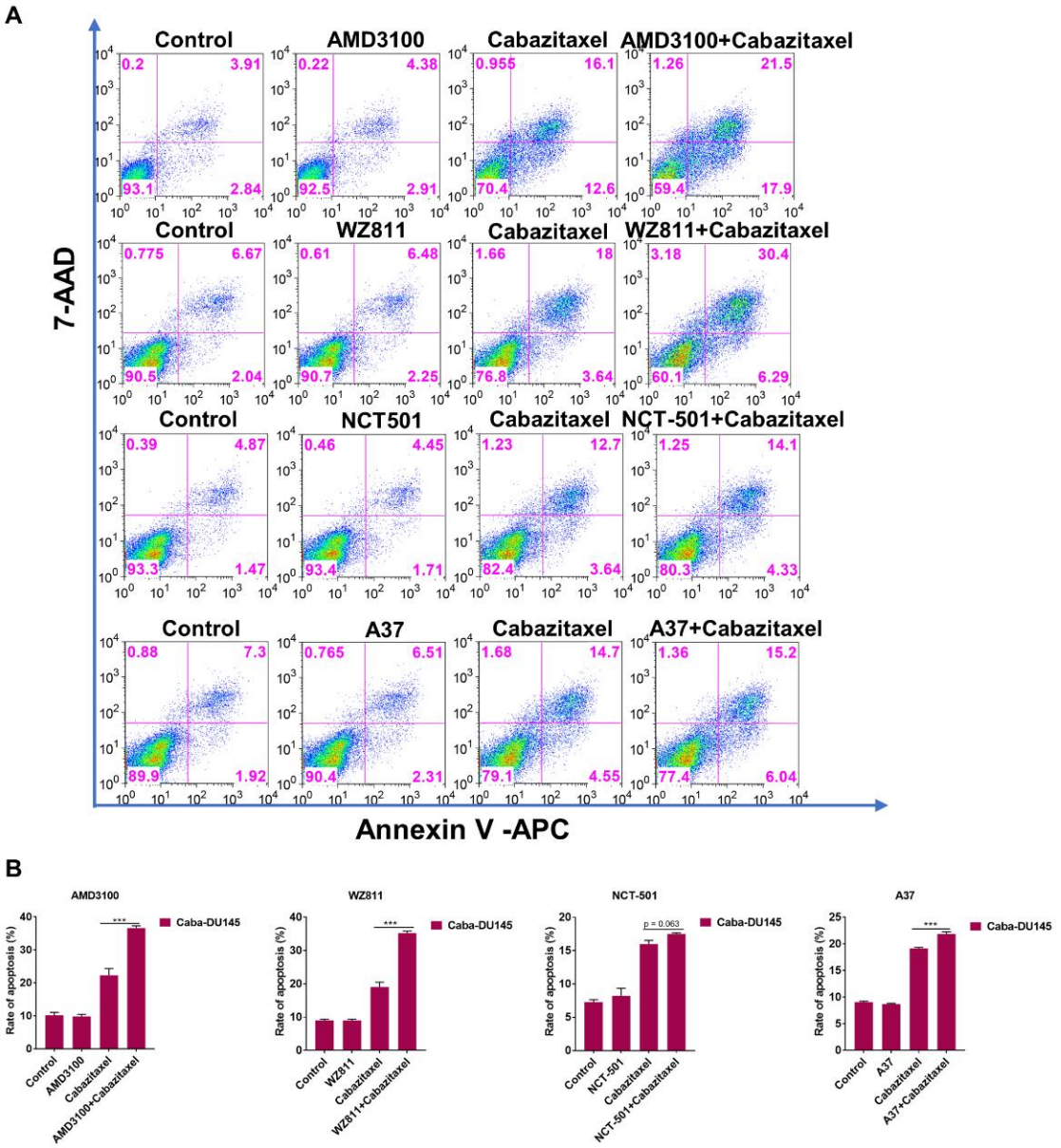

Figure 47. Inhibition of ABCG2 and CXCR4 sensitizes caba-DU145 cells to cabazitaxel. **A**. The flow cytometry results showed that an enhanced rate of apoptosis was observed following treatment with cabazitaxel and AMD3100 (CXCR4 inhibitor, 10 µM) or WZ811 (CXCR4 inhibitor, 5 µM) compared to cabazitaxel (3 nM) alone. NCT-501 (ALDH1A1 inhibitor, 5 µM) did not influence the apoptosis rate in caba-DU145. Another ALDH1A1 inhibitor (A37, 10 µM) slightly enhanced the apoptosis rate in caba-DU145. **B**. The bar charts summarize the results. Annexin V positivity was considered as the percentage of apoptotic cells. The data were acquired from three separate experiments and calculated as means ± SEM. *p < 0.05; **p < 0.01; ***p < 0.001.

3.2.4 Berbamine enhances the expression of the let-7 family and miR-26

To investigate the microRNAs involved in berbamine targeting the PCSCs, small RNA-

sequencing was performed. Venn diagrams were generated to visualize the overlap of differentially expressed small RNAs between different comparisons. Each Venn diagram showed the overlaps between small RNAs that were called differential in any of the cell line comparisons **Figure 48A** shows the overlap of significantly differentially expressed small RNAs for berbamine versus control treatment between the replicates for DU145, caba-DU145, and DU145 CSCs. **Figure 48B** shows the overlap of significantly differentially expressed small RNAs for berbamine plus cabazitaxel versus cabazitaxel treatment between the replicates for DU145, caba-DU145, and DU145 CSCs. **Figure 48C** shows the overlap of significantly differentially expressed small RNAs for cabazitaxel versus control treatment between the replicates for DU145, caba-DU145, and DU145 CSCs.

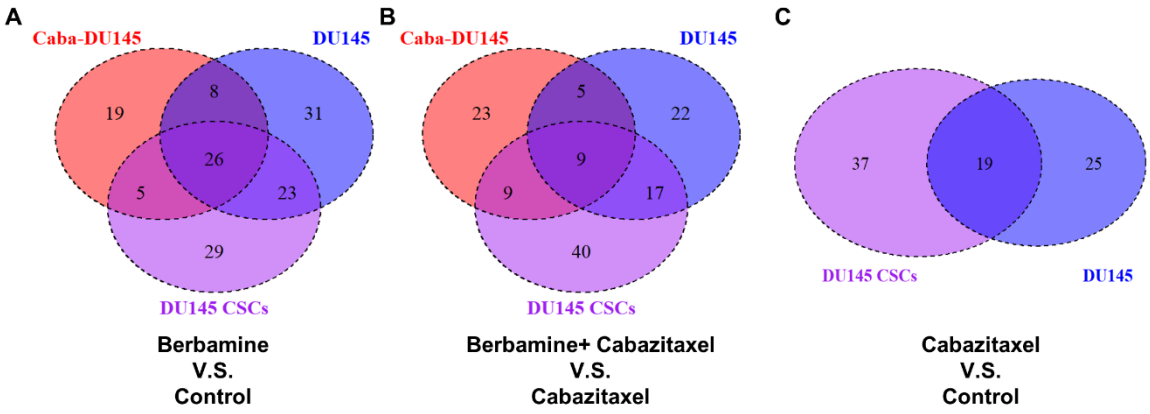

Figure 48. Venn diagrams visualize the overlap of differentially expressed small RNAs between different cell lines. A. Venn diagram showing the overlap of small RNAs differentially expressed between biological replicates of three different cell lines for berbamine versus control treatment. All small RNAs with an FDR < 0.01 and a fold change ≥ 2 in any of the comparisons were included. **B.** Venn diagram showing the overlap of small RNAs differentially expressed between biological replicates of three different cell lines for berbamine plus cabazitaxel versus cabazitaxel treatment. All small RNAs with an FDR < 0.01 and a fold change ≥ 2 in any of the comparisons were included. **C.** Venn diagram showing the overlap of small RNAs differentially expressed between biological replicates of three different cell lines for cabazitaxel versus control treatment. All small RNAs with an FDR < 0.01 and a fold change ≥ 2 in any of the comparisons were included. V.S. means versus.

Based on the RNA-sequencing results, we found that berbamine enhanced the expression of the let-7 miRNA family members, miR-26a, and miR-26b (**Figure 49**) both in caba-DU145 cells and DU145 CSCs.

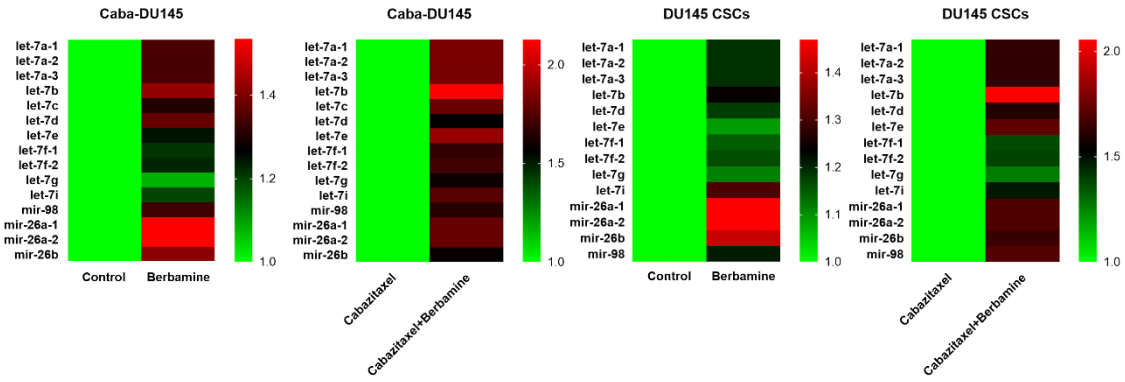

Figure 49. Berbamine enhances the expression of the let-7 family members, miR-26a and miR-26b. Heatmap of small RNA-sequencing results: berbamine enhanced the expression of the let-7 family members, miR-26a, and miR-26b in caba-DU145 cells and DU145 CSCs. Green represented 1, and red represented fold change of levels of miRNAs compared to 1.

Individual miRCURY LNA miRNA PCR assays further verified that berbamine upregulated the expression of the let-7 family members, miR-26a-5p, and miR-26b-5p in caba-DU145 cells (**Figure 50**) and in DU145 CSCs (**Figure 51**). Furthermore, berbamine plus cabazitaxel enhanced dramatically the expression level of the let-7 family members, miR-26a-5p, and miR-26b-5p in DU145 CSCs (**Figure 51**).

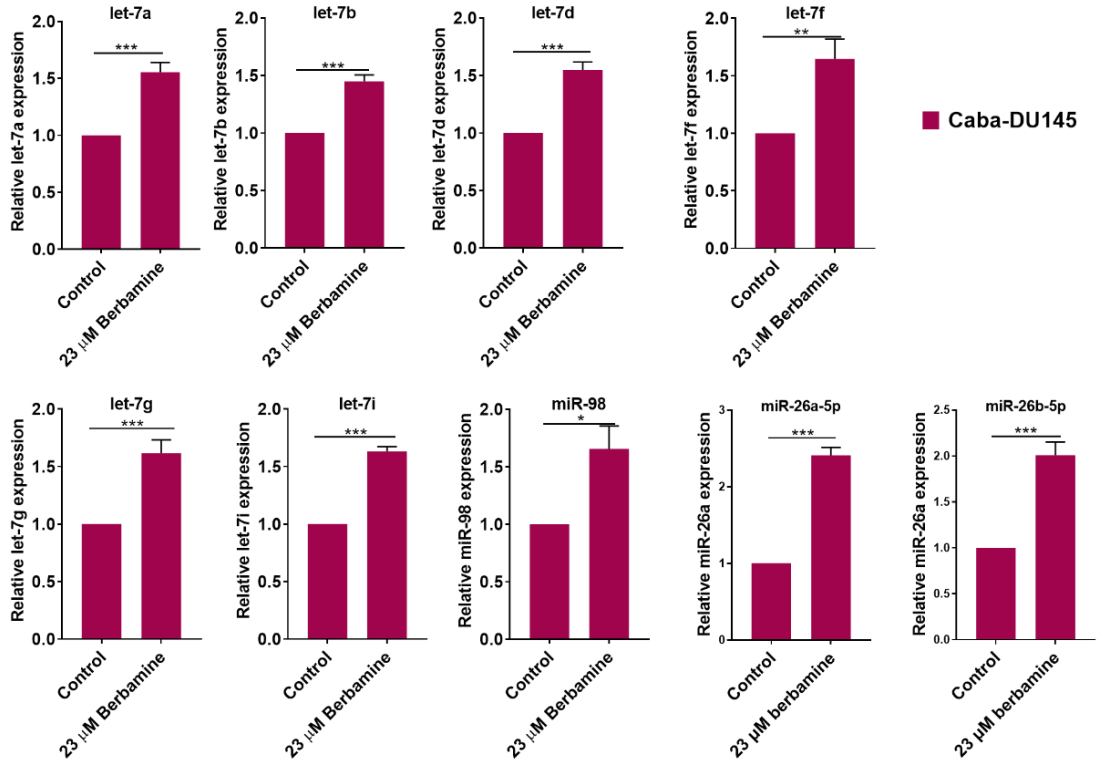

Figure 50. Berbamine enhances the expression level of let-7 family members, miR-26a and miR-26b in caba-DU145 cells. Individual miRCURY LNA miRNA PCR assays: berbamine

enhanced the expression of let-7 family members, miR-26a, and miR-26b in caba-DU145 cells. The data were acquired from three separate experiments and calculated as means ± SEM. *p < 0.05; **p < 0.01; ***p < 0.001.

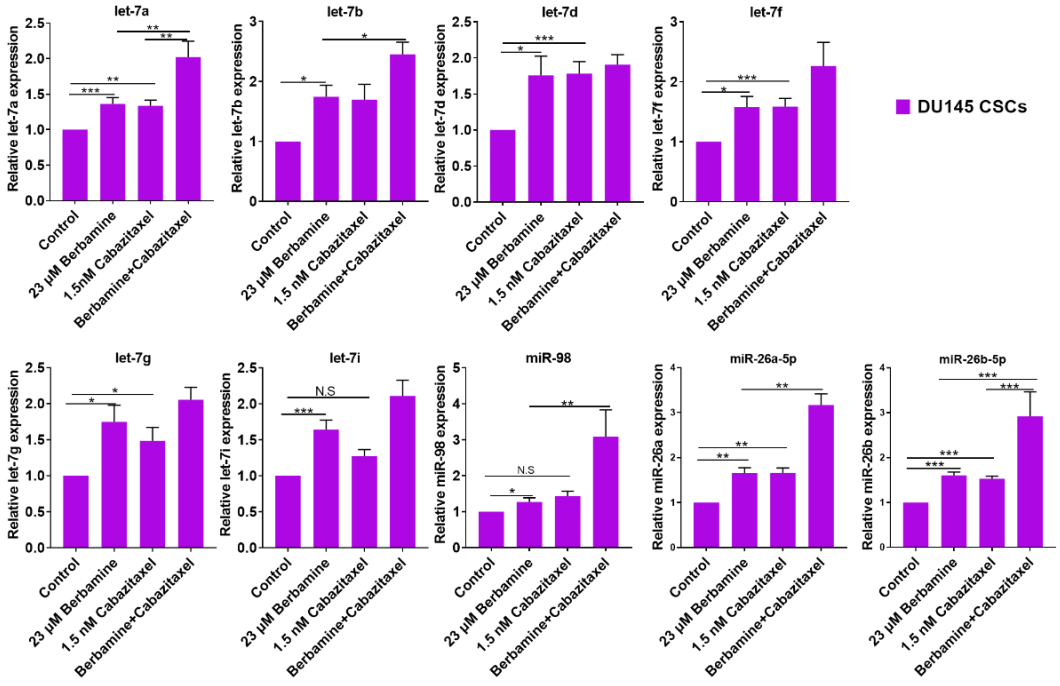

Figure 51. Berbamine enhances the expression of let-7 family members, miR-26a and miR-26b in DU145 CSCs. Individual miRCURY LNA miRNA PCR assays: berbamine enhanced the expression of let-7 family members, miR-26a, and miR-26b in caba-DU145 cells. The combination of berbamine and cabazitaxel significantly upregulated the expression of let-7, and miR-26. The data were acquired from three separate experiments and calculated as means ± SEM. *p < 0.05; **p < 0.01; ***p < 0.001. NS: not significant.

3.2.5 Berbamine targets CXCR4/ let-7/ IGF2BP1 axis and ABCG2/ miR-26b/ p-STAT3 axis

To investigate the downstream pathways that berbamine is involved in, the online database of miRDB (http://mirdb.org/mirdb/index.html) was used. The results showed that the let-7 family can target the genes of *STARD13, IGF2BP1*, *LIN28*, and so forth (**Table 8**).

Table 8. The targets of let-7 miRNA family

Gene Symbol	Target Score	Gene Description
STARD13	100	StAR related lipid transfer domain containing 13
HMGA2	100	high mobility group AT-hook 2
IGDCC3	100	immunoglobulin superfamily DCC subclass member 3

IGF2BP1	100	insulin like growth factor 2 mRNA binding protein 1
FIGNL2	100	fidgetin like 2
PRTG	100	protogenin
NR6A1	100	nuclear receptor subfamily 6 group A member 1
LIN28B	100	lin-28 homolog B
ARID3B	100	AT-rich interaction domain 3B
C14orf28	100	chromosome 14 open reading frame 28
TRIM71	100	tripartite motif containing 71

Note: table was adapted from the miRDB database.

Furthermore, we were also interested in PTEN, a target of miR-26, which is important for miR-26b-induced CSCs properties, migration, and invasion [98]. Quantitative RT-PCR experiments showed that berbamine could not influence the expression of *PTEN* and *STARD13* (**Figure 52A**). However, berbamine could decrease the expression of *IGF2BP1*, and *STAT3* (**Figure 52B**), which were relevant to maintaining the CSCs' properties [99, 100] and drug resistance [101, 102].

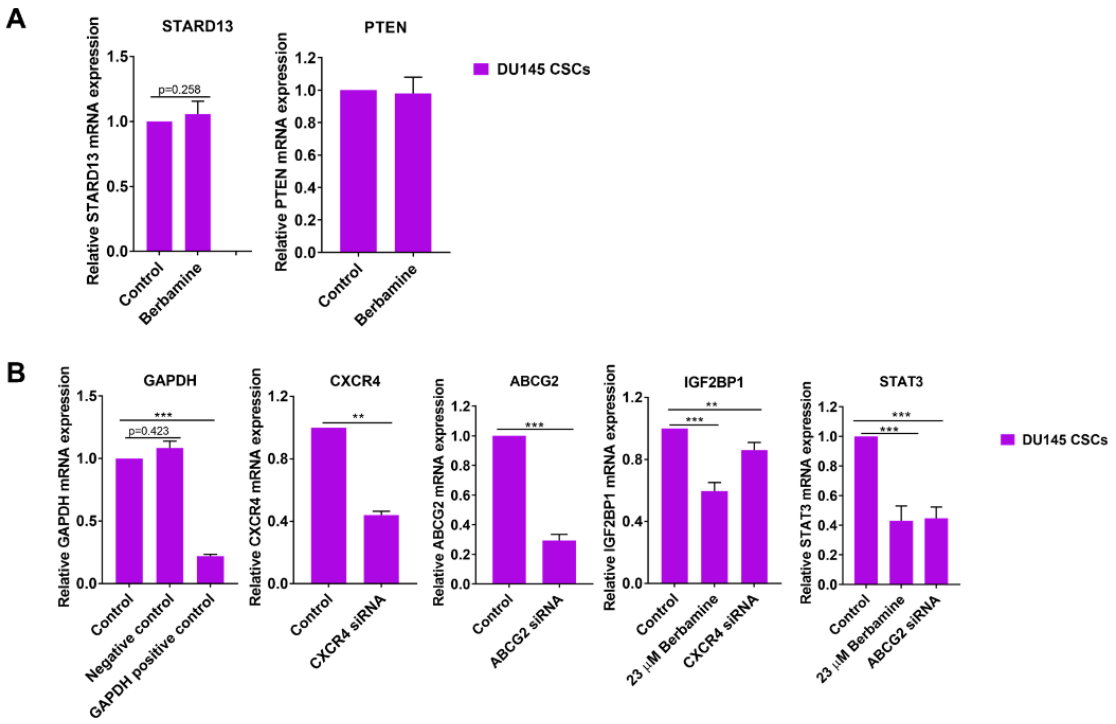

Figure 52. Berbamine downregulates ABCG2, CXCR4, IGF2BP1, and STAT3. A. qRT-PCR: berbamine could not influence the expression of *PTEN* and *STARD13.* **B**. qRT-PCR: berbamine downregulated the expression of *IGF2BP1* and *STAT3*. Silencing *ABCG2* using siRNAs also decreased the expression of *STAT3*, and downregulating *CXCR4* also repressed the *IGF2BP1*. The Silencer® Select negative and *GAPDH* positive control were utilized as controls. The qRT-PCR showed that CXCR4 siRNA and ABCG2 siRNA dramatically silence *CXCR4* and *ABCG2* respectively. The data were acquired from three separate experiments and calculated as means ± SEM. *p < 0.05; **p < 0.01; ***p < 0.001.

Flow cytometry showed that berbamine inhibited the expression of LIN28B in caba-DU145 cells (**Figure 53**), which is a microRNA regulator and stem cell reprogramming factor. Overexpression of LIN28B enhances tumorigenicity and associates with cancer progression and CSCs [103].

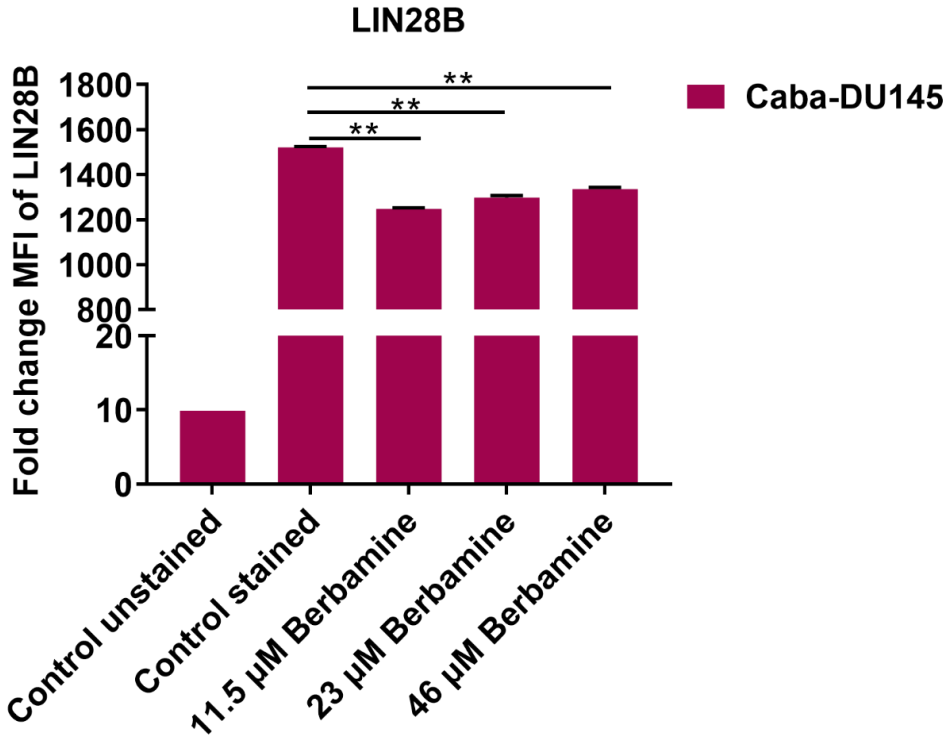

Figure 53. Berbamine slightly downregulates the expression of LIN28B. Flow cytometry: berbamine slightly inhibited the expression of LIN28B in caba-DU145 cells. The data were acquired from three separate experiments and calculated as means ± SEM. **p < 0.01.

Likewise, silencing of *CXCR*4 downregulated *IGF2BP1* and silencing of *ABCG2* downregulated *STAT3* (**Figure 52B**). Berbamine and ABCG2 inhibitor, Ko143, decreased phosphorylated-STAT3 (p-STAT3) and upregulated STAT3 expression as shown by the results of flow cytometry (**Figure 54**). The results suggested that berbamine targeted PCSCs through CXCR4/IGF2BP1 and ABCG2/p-STAT3 pathways.

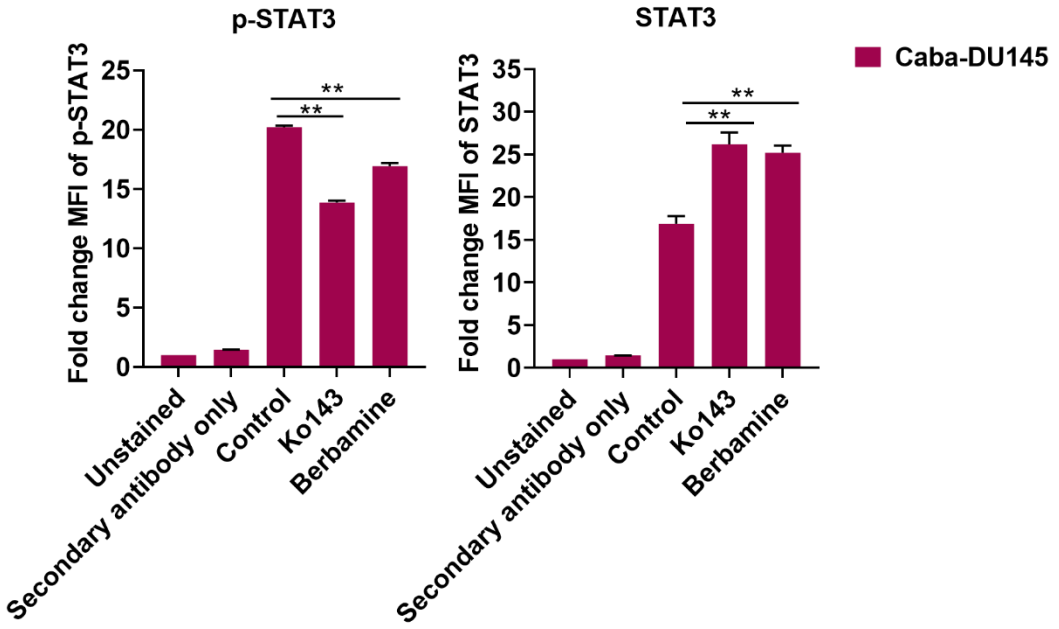

Figure 54. Inhibition of ABCG2 targets p-STAT3. Flow cytometry: berbamine and Ko143, an inhibitor of ABCG2, inhibited the p-STAT3 expression and enhanced the STAT3 expression. The data were acquired from three separate experiments and calculated as means ± SEM. **p < 0.01.

Afterwards, qRT-PCR indicated that mimics of let-7a, let-7b, let-7i repressed the expression of *IGF2BP1* both in caba-DU145 cells and DU145 CSCs (**Figure 55**). The inhibitors of let-7 reversed the repression of *IGF2BP1* (**Figure 55**).

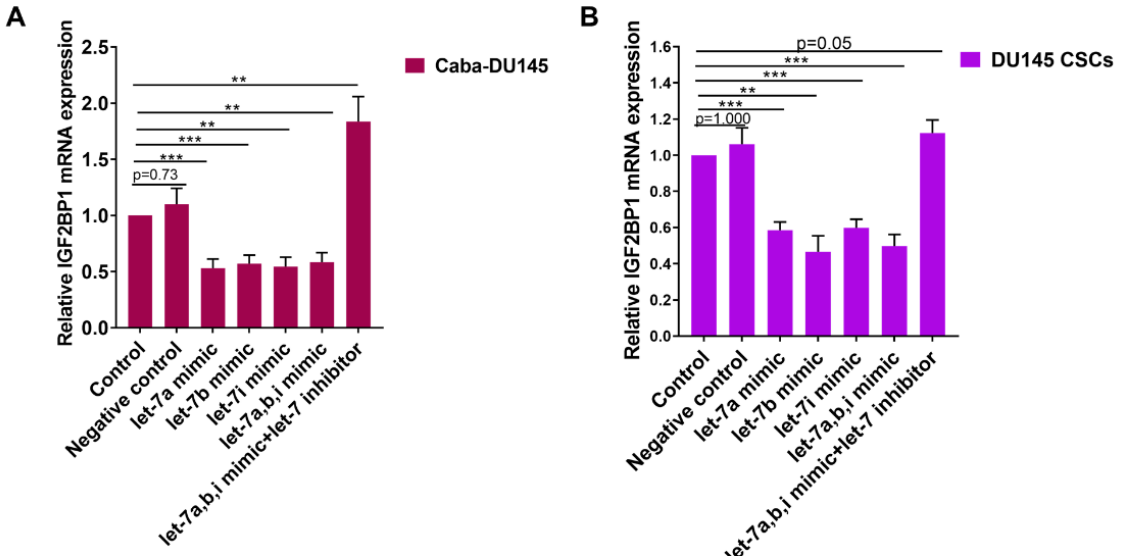

Figure 55. Enhancement of let-7 family decreases the expression of IGF2BP1. A. qRT-PCR: upregulation of let-7 family by mimics significantly repressed *IGF2BP1* expression in caba-DU145 cells. **B**. qRT-PCR: upregulation of let-7 family by mimics significantly repressed *IGF2BP1* expression in DU145 CSCs. The let-7 inhibitor reversed the effect of the miRNA mim-

ics. The data were acquired from three separate experiments and calculated as means ± SEM. **p < 0.01; ***p < 0.001.

The fact that the let-7 family targeted IGF2BP1 was consistent with the results of TargetScan (http://www.targetscan.org/vert_72/), which indicated that all members of the let-7 family targeted the 3'UTR of IGF2BP1 (**Table 9**).

Table 9. Let-7 miRNA family targeted the 3'UTR of IGF2BP1

miRNAs	Position in the 3'UTR	Seed match	Context++ score	Context++ score percentile	Weighted context++ score	Conserved branch length	Pct
hsa-let-7d-5p	1632-1639	8mer	-0.43	96	-0.35	7.14	0.96
hsa-let-7i-5p	1632-1639	8mer	-0.4	95	-0.33	7.14	0.96
hsa-let-7b-5p	1632-1639	8mer	-0.4	95	-0.33	7.14	0.96
hsa-let-7e-5p	1632-1639	8mer	-0.4	95	-0.33	7.14	0.96
hsa-miR-98-5p	1632-1639	8mer	-0.4	95	-0.33	7.14	0.96
hsa-let-7f-5p	1632-1639	8mer	-0.4	95	-0.33	7.14	0.96
hsa-let-7g-5p	1632-1639	8mer	-0.4	95	-0.33	7.14	0.96
hsa-let-7a-5p	1632-1639	8mer	-0.4	95	-0.33	7.14	0.96
hsa-let-7c-5p	1632-1639	8mer	-0.4	95	-0.33	7.14	0.96
hsa-let-7g-5p	1651-1657	7mer-1A	-0.17	69	-0.14	7.14	0.95
hsa-let-7d-5p	1651-1657	7mer-1A	-0.18	69	-0.15	7.14	0.95
hsa-let-7e-5p	1651-1657	7mer-1A	-0.16	67	-0.13	7.14	0.95
hsa-miR-98-5p	1651-1657	7mer-1A	-0.16	67	-0.13	7.14	0.95
hsa-let-7a-5p	1651-1657	7mer-1A	-0.16	67	-0.13	7.14	0.95
hsa-let-7c-5p	1651-1657	7mer-1A	-0.16	67	-0.13	7.14	0.95
hsa-let-7b-5p	1651-1657	7mer-1A	-0.16	67	-0.13	7.14	0.95
hsa-let-7i-5p	1651-1657	7mer-1A	-0.16	67	-0.13	7.14	0.95
hsa-let-7f-5p	1651-1657	7mer-1A	-0.16	66	-0.13	7.14	0.95
hsa-let-7d-5p	4269-4276	8mer	-0.23	78	-0.14	4.934	0.95
hsa-let-7i-5p	4269-4276	8mer	-0.21	77	-0.13	4.934	0.95
hsa-let-7b-5p	4269-4276	8mer	-0.19	73	-0.12	4.934	0.95
hsa-let-7e-5p	4269-4276	8mer	-0.19	72	-0.12	4.934	0.95
hsa-let-7a-5p	4269-4276	8mer	-0.19	72	-0.12	4.934	0.95
hsa-let-7f-5p	4269-4276	8mer	-0.19	72	-0.12	4.934	0.95
hsa-let-7c-5p	4269-4276	8mer	-0.19	72	-0.12	4.934	0.95
hsa-let-7g-5p	4269-4276	8mer	-0.19	72	-0.12	4.934	0.95
hsa-miR-98-5p	4269-4276	8mer	-0.19	72	-0.12	4.934	0.95
hsa-let-7d-5p	4923-4930	8mer	-0.33	91	-0.21	6.346	0.96
hsa-let-7e-5p	4923-4930	8mer	-0.31	90	-0.2	6.346	0.96
hsa-miR-4500	4923-4930	8mer	-0.31	90	-0.2	6.346	0.96
hsa-let-7f-5p	4923-4930	8mer	-0.31	90	-0.2	6.346	0.96
hsa-let-7a-5p	4923-4930	8mer	-0.31	90	-0.2	6.346	0.96
hsa-let-7i-5p	4923-4930	8mer	-0.3	89	-0.19	6.346	0.96

hsa-miR-98-5p	4923-4930	8mer	-0.31	89	-0.19	6.346	0.96
hsa-let-7b-5p	4923-4930	8mer	-0.3	89	-0.19	6.346	0.96
hsa-let-7c-5p	4923-4930	8mer	-0.31	89	-0.19	6.346	0.96
hsa-let-7g-5p	4923-4930	8mer	-0.3	88	-0.19	6.346	0.96
hsa-let-7f-5p	5568-5574	7mer-m8	-0.32	90	-0.2	6.486	> 0.99
hsa-miR-98-5p	5568-5574	7mer-m8	-0.32	90	-0.2	6.486	> 0.99
hsa-let-7a-5p	5568-5574	7mer-m8	-0.32	90	-0.2	6.486	> 0.99
hsa-let-7g-5p	5568-5574	7mer-m8	-0.32	90	-0.2	6.486	> 0.99
hsa-let-7e-5p	5568-5574	7mer-m8	-0.32	90	-0.2	6.486	> 0.99
hsa-let-7d-5p	5568-5574	7mer-m8	-0.31	89	-0.19	6.486	> 0.99
hsa-let-7i-5p	5568-5574	7mer-m8	-0.31	89	-0.19	6.486	> 0.99
hsa-let-7b-5p	5568-5574	7mer-m8	-0.31	89	-0.19	6.486	> 0.99
hsa-let-7c-5p	5568-5574	7mer-m8	-0.31	89	-0.19	6.486	> 0.99

Note: table was adapted from the TargetScan database.

Mimics of miR-26b inhibited the expression of *p-STAT3* (**Figure 56A**), not *STAT3* (**Figure 56B**). Inhibitor of miR-26 counteracted the downregulation of *p-STAT3* (**Figure 56A**). It seems that miR-26a mimics could not decrease the expression of *p-STAT3*. However, the combination of miR-26a mimics and miR-26b mimics also downregulated *p-STAT3* (**Figure 56A**). The results suggested that berbamine targets caba-DU145 cells through CXCR4/let-7/IGF2BP1 axis and ABCG2/miR-26b/p-STAT3 axis.

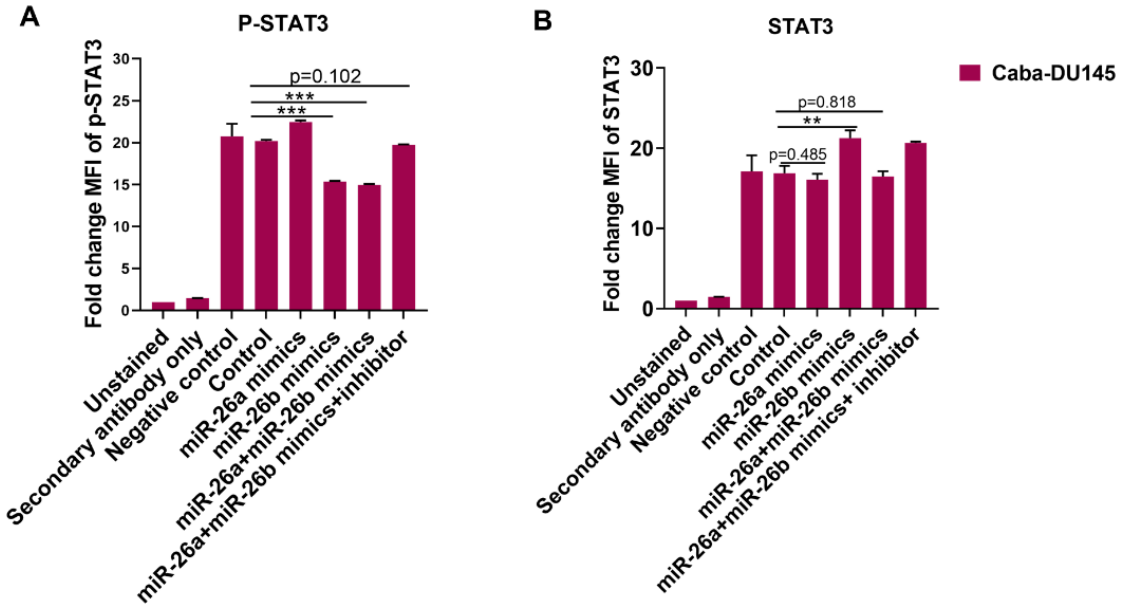

Figure 56. Enhancement of miR-26b decreases the expression of p-STAT3. Flow cytometry: upregulation of miR-26b by mimics significantly repressed the p-STAT3 expression (**A**) and enhanced the STAT3 expression (**B**). The combination of miR-26a mimics and miR-26b mimics also inhibited p-STAT3. The miR-26 inhibitor reversed the effect of mimics. The data were acquired from three separate experiments and calculated as means ± SEM. **p < 0.01; *** <

0.001.

Next, to see whether inhibition of IGF2BP1 and p-STAT3 could reverse the cabazitaxel-resistant state, the inhibitors of IGF2BP1 (BTYNB IMP1 inhibitor at 2.5 µM, BTYNB) and p-STAT3 (Cryptotanshinone, CPT, at 4.6 µM) were used. The apoptosis assay showed that both the IGF2BP1 inhibitor and the p-STAT3 inhibitor enhanced the apoptosis rates compared to the cabazitaxel alone group (**Figure 57**), which indicates that the suppression of IGF2BP1 and p-STAT3 surely reversed the cabazitaxel resistant state as we expected. Taken together, berbamine reversed the cabazitaxel-resistant state through CXCR4/let-7/IGF2BP1 axis and ABCG2/miR-26b/p-STAT3 axis.

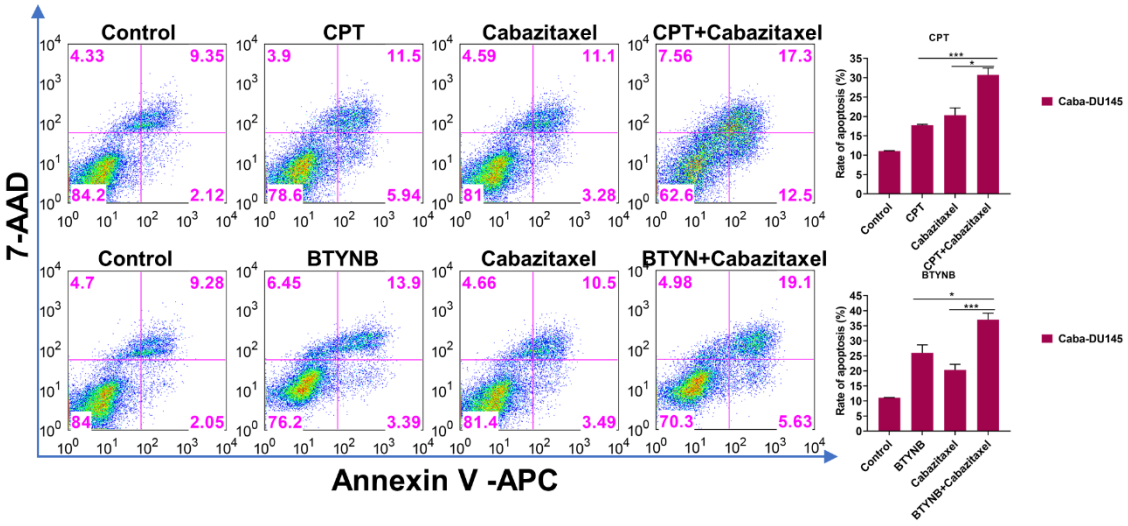

Figure 57. Suppression of p-STAT3 and IGF2BP1 sensitizes caba-DU145 cells to cabazitaxel. Apoptosis assay: inhibition of p-STAT3 and IGF2BP1 using the inhibitors Cryptotanshinone (CPT) and BTYNB IMP1 inhibitor (BTYNB), respectively combined with cabazitaxel enhanced the apoptosis rates compared to cabazitaxel alone. The data were acquired from three separate experiments and calculated as means ± SEM. *p < 0.05; **p < 0.01; *** < 0.001.

In summary, our results reveal for the first time that berbamine has an anti-tumor effect on PCSCs. Berbamine reverses the cabazitaxel-resistant state by CXCR4/let-7/IGF2BP1 axis and ABCG2/miR-26b/p-STAT3 axis. Berbamine is a potential promising phytochemical which augments the anti-cancer effect of cabazitaxel in PCa cells and PCSCs.

3.2.6 Berbamine enhanced the expression of exosomal let-7 and miR-26b

To investigate the exosomes' function in the process that berbamine regulated let-7 family and miR-26b, several exosome related experiments were conducted. Exosomes

were isolated using the ExoQuick-TC kit from the cell culture supernatant. The existence of exosomes was confirmed by the validation of exosomal markers (CD9, TSG101, HSP70) in the western blot (**Figure 58A**). Calnexin was used as a negative control marker, which is expressed in cell samples, not in exosomes (**Figure 58B**).

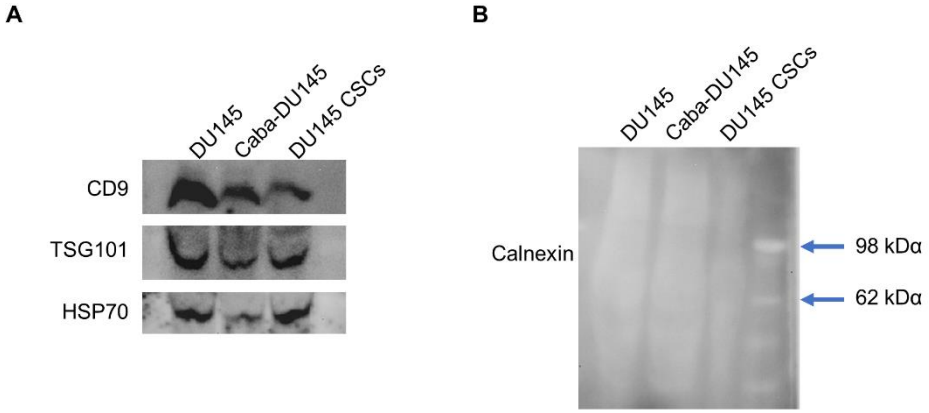

Figure 58. PCSCs and PCa cells secret exosomes. A. Western blot: exosomes which were extracted from the supernatant of DU145, caba-DU145 cells, and DU145 CSCs, expressed the exosomal markers CD9, TSG101, and HSP70. **B.** Western blot: the exosomal negative control marker, calnexin (90 kDα), was not detected. The experiments were repeated independently three times.

Furthermore, to investigate the expression level of let-7 and miR-26b influenced by berbamine in exosomes, the miRCURY LNA miRNA PCR assay was performed. **Figure 59** showed that berbamine enhanced the levels of let-7, miR-26b in the exosomes, which suggested that berbamine might also influence the expression of let-7 and miR-26b through exosome delivery.

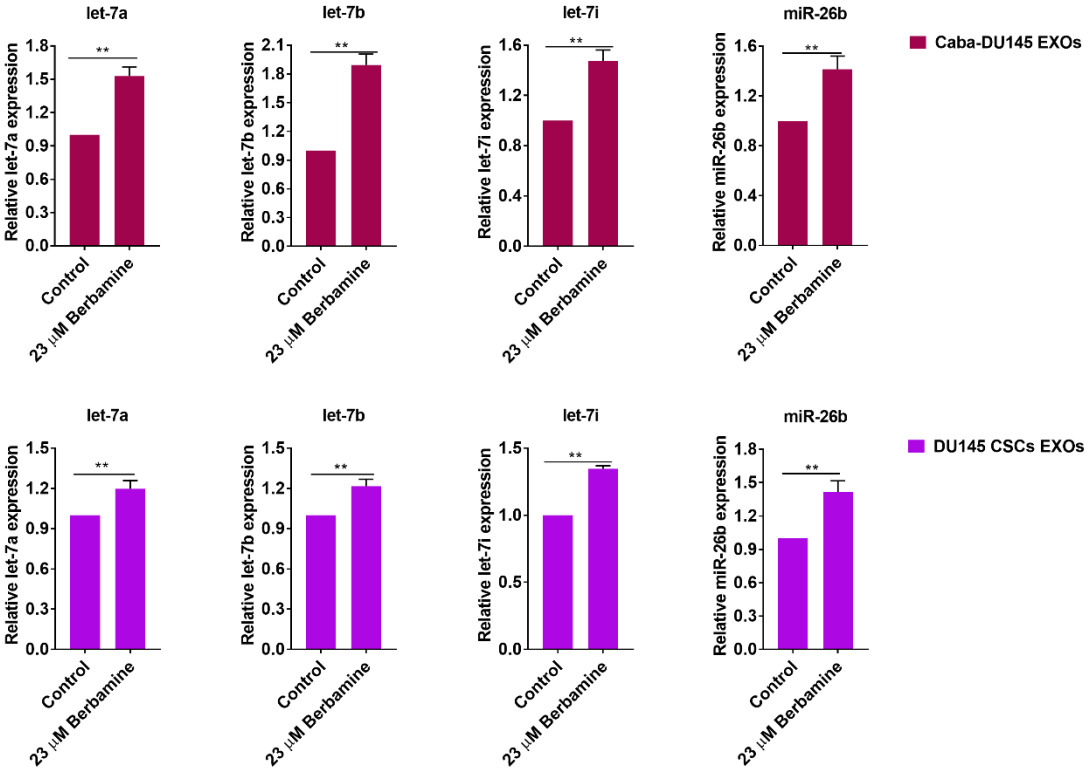

Figure 59. Berbamine enhances the expression of exosomal let-7 miRNA family and miR-26b. Exosomes were extracted from the cell culture supernatant of DU145 CSCs and caba-DU145 cells with or without treatment of berbamine at 23 μM for 4 days. After extracting the total RNAs from exosomes using miRNeasy Micro kit, cDNA synthesis, and miRCURY LNA miRNA PCR assay was conducted: berbamine augmented the levels of exosomal let-7a, let-7b, let-7i, and miR-26b. The data were acquired from three separate experiments and calculated as means ± SEM. *$p < 0.05$; **$p < 0.01$; ***$p < 0.001$. (Caba-DU145 EXOs: exosomes isolated from the cell culture supernatant of caba-DU145 cells; DU145 CSCs EXOs: exosomes isolated from the cell culture supernatant of DU145 CSCs).

4. Discussion

4.1 The influence of shikonin on PCSCs

Note: This part was already published in the American Journal of Cancer Research [90]: Wang L, Stadlbauer B, Lyu C, Buchner A, Pohla H: Shikonin enhances the anti-tumor effect of cabazitaxel in prostate cancer stem cells and reverses cabazitaxel resistance by inhibiting ABCG2 and ALDH3A1. Am J Cancer Res 2020, 10:3784-3800.

Our results implied that shikonin re-sensitizes the cabazitaxel resistance by downregulating the expression of ABCG2 and ALDH3A1. In addition, shikonin induces apoptosis through ROS/mitochondria dysfunction apoptosis pathway in PCSCs and PCa cells.

Initially, we found that shikonin repressed the viability, proliferation, migration, and invasion of PCSCs and PCa cells. Furthermore, shikonin augmented the anti-cancer effects of cabazitaxel both in PCSCs and PCa cells. Then, shikonin induced apoptosis through the ROS/mitochondria dysfunction pathway. What's more, shikonin downregulated the expression levels of the CSC marker ABCG2 and ALDH3A1 measured using qRT-PCR, flow cytometry, confocal microscopy, and siRNA technology. Last but not least, shikonin resensitized the cabazitaxel-resistant PCa cells to cabazitaxel by downregulating ABCG2 and ALDH3A1, and ALDH3A1 was targeted by inhibiting ABCG2.

4.1.1 The roles of ABCG2 and ALDH3A1 in cancer progression and drug resistance

It was demonstrated that shikonin targets glioblastoma cells [81] and PCa cells [78, 80, 104]. We found that shikonin has anti-cancer effects on PCa cells and PCSCs. Those CSCs can drive chemotherapeutic resistance [7] as we introduced in 1.2. We found that shikonin downregulated the levels of ABCG2 and ALDH3A1, which are two PCSCs markers [23]. In addition, blocking of ABCG2 reduced ALDH3A1 expression and can regulate those pathways reversing the resistant state as the literature reported that ABCG2 [105, 106] and ALDH3A1 [107, 108] are in charge of drug resistance. Suppression of ABCG2 enhanced drug sensitivity in breast cancer [109], and ovarian cancer [110]. ALDH is also considered as a CSC marker, that enhances tumor progression, and maintains stemness properties like self-renewal and other features [111]. ALDH3A1 belongs to the ALDH family and is related to prostate cancer progression [112]. A high level of ALDH3A1 was observed in DU145-derived metastases in a xenograft tumor model [112]. Furthermore, inhibition of ALDH3A1 re-sensitizes different

types of cancer cells to drugs, such as glioblastoma cells [113] and head and neck squamous cell carcinoma cells [114]. We found that shikonin re-sensitized the PCa cells to cabazitaxel via blocking the expression of ABCG2 and ALDH3A1.

4.1.2 The potential pathways shikonin influences

In our studies, shikonin attacks PCa cells and PCSCs by suppressing proliferation, migration, and invasion, and also by enhancing the rate of apoptosis. It was further demonstrated that apoptosis was activated through the ROS/ mitochondria dysfunction pathway.

Furthermore, there are reports suggesting that the anti-cancer effect of shikonin was activated via blocking the PI3K/AKT pathway [115]. Furthermore, suppressing the activity of the PI3K/AKT pathway re-sensitizes cancer cells to anti-cancer drugs [29, 116]. Probably shikonin re-sensitizes the cabazitaxel-resistant PCa cells to cabazitaxel via modulating the PI3K/AKT pathways as well.

4.1.3 Our new insight

This is the first time to demonstrate that shikonin targeted PCSCs. Furthermore, shikonin can re-sensitize cabazitaxel-resistant PCa cells to cabazitaxel through targeting ABCG2 and ALDH3A1. The mechanism of shikonin on the induction of apoptosis and reversing cabazitaxel-related resistance is shown in **Figure 60**.

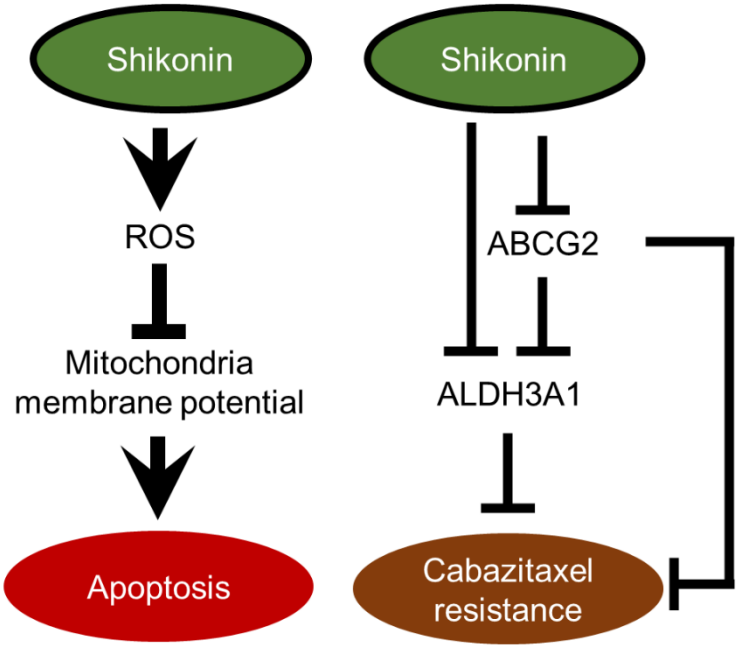

Figure 60. The potential mechanism of shikonin on anti-cancer effect and drug-resistance

rescue. On one hand, shikonin induces apoptosis through ROS/mitochondria dysregulation apoptotic pathway. On the other hand, shikonin rescues cabazitaxel resistance by downregulating ABCG2 and ALDH3A1. Meanwhile, inhibition of ABCG2 decreases the level of ALDH3A1 (Figure adapted from Wang et al. [90]).

4.1.4 Limitations

In our studies, several limitations exist. First, only in vitro experiments were performed, in other words, the function and side effects of shikonin in vivo are unclear. Second, much more preclinical studies or clinical trials should be done to evaluate other promising inhibitors of ALDH3A1 and ABCG2 for the treatment of those patients who suffer from drug resistance.

4.2 The influence of berbamine on PCSCs

Our results indicated that berbamine reverses the cabazitaxel-resistant state via targeting the CXCR4/let-7/IGF2BP1 axis, and the ABCG2/miR-26/p-STAT3 axis.

First of all, the results showed that berbamine attacks PCSCs and adherent prostate cancer cells by blocking viability, proliferation, migration, invasion, and enhancing apoptosis. Second, berbamine enhanced the toxicity of cabazitaxel on prostate cancer cells and PCSCs. Then, we found that berbamine inhibited the expression of the cancer stem cell markers ABCG2, CXCR4, and ALDH1A1 using flow cytometry and qRT-PCR. More importantly, downregulation of ABCG2 and CXCR4 using the inhibitors sensitized the cabazitaxel effect, except ALDH1A1. Furthermore, small RNA-sequencing revealed that berbamine enhanced the expression of let-7 family members, miR-26a and miR-26b. Mimics of let-7 decreased the expression of IGF2BP1, and mimics of miR26b decreased the expression of p-STAT3. Berbamine suppressed the expression of IGF2BP1 by inhibiting CXCR4, and berbamine also suppressed p-STAT3 by inhibiting ABCG2. Last but not least, suppression of IGF2BP1 and p-STAT3 sensitized the cabazitaxel-resistant DU145 cells to cabazitaxel verified by the apoptosis assay.

4.2.1 ABCG2 and CXCR4, two important cancer stem cell markers are related to drug resistance

ABCG2 is a cancer stem cell marker, belonging to the ABC transporters, which promotes cell resistance through drug efflux [27]. ABCG2 is one of the prostate cancer stem cell markers, which is related to drug resistance and prostate relapse [23]. Inhibi-

tion of ABCG2 reverses the multidrug resistance in breast cancer [117], hepatocellular carcinoma [118], lung cancer [119-121], and colorectal cancer [106, 122, 123]. It was consistent with our results that as described for shikonin berbamine also reverses the cabazitaxel resistance by inhibiting ABCG2.

CXCR4 is another prostate cancer stem cell marker, which is associated with an increased risk of distant metastases and local recurrence in PCa [36]. Reports show that inhibition of CXCR4 resensitizes prostate cancer cells to docetaxel [37], colon cancer cells against paclitaxel therapy [124], chronic myelogenous leukemia cells to imatinib [125], hepatocellular carcinoma cells to sorafenib [126], neuroblastoma cells to cisplatin [127], non-small cell lung cancer cells to cisplatin [128]. Our results showed that berbamine resensitizes the prostate cancer cells to cabazitaxel through downregulating CXCR4 as we expected.

4.2.2 The role of IGF2BP1 in carcinogenesis and drug-resistance

Insulin-like growth factor 2 mRNA-binding protein 1 (IGF2BP1) plays an important role in carcinogenesis and drug-resistance in cancer therapy [101]. The stemness properties are highly correlated to drug resistance or cancer recurrence [11]. IGF2BP1 is reported to maintain the mesenchymal cell properties or stem cell properties [99, 129, 130]. IGF2BP1 maintains the stemness of breast cancer stem cells by influencing downstream regulators of the c-Myc axis [131, 132]. Additionally, IGF2BP1 maintains leukemia stem cell properties through targeting the expression of HOXB4, MYB, and ALDH1A1 [99]. Suppression of IGF2BP1 negatively influences cancer cell viability and migration ability, and stemness properties like self-renewal [133].

Our results showed that berbamine targeted PCSCs by downregulating IGF2BP1 and then PCSCs lose the stem cell properties. Furthermore, our results showed that inhibition of IGF2BP1 resensitized cabazitaxel-resistant prostate cancer cells to cabazitaxel.

4.2.3 Functions of let-7 miRNA family in cancer stem cells and drug-resistance

Recently, it has been reported that multiple microRNAs play vital roles in regulating CSCs. MicroRNAs are defined as small non-coding RNAs containing 21-25 nucleotides, which can regulate the specific target genes by mRNA degradation or inhibition of translation by binding to the 3'-untranslated regions (3'UTR) of mRNAs [13]. Increasing pieces of evidence show that let-7 microRNA decreases the stemness of CSCs [134]. Let-7b inhibits the self-renewal of non-small cell lung cancer stem cells and resensitiz-

es 5-FU resistance through downregulating CCND1 [135]. Let-7 miRNA/PD-L1 axis mediates drug resistance, cell growth, mobility, and stemness properties in non-small cell lung cancer cells [136]. Let-7 promotes self-renewal and drives the gefitinib resistance in non-small cell lung cancer [137]. The loss of let-7 being an important component of the cancer stem cell phenotype in ovarian carcinoma [134]. Also, the let-7 miRNA family decreases the self-renewal and migration of neuroblastoma cells [138]. Regulation of the LIN28A/let-7 pathway [139], the LIN28B/let-7/HMGA2 axis, or the LIN28B/let-7/Wnt pathway [140, 141] suppresses the self-renewal in breast cancer stem cells. Let-7c reduces the ratio of CSCs, decreases the capability of tumor formation, enhances the effect of tamoxifen, and inhibits Wnt signaling in breast cancer cells [142]. Let-7b sensitizes the stem cells to agents through inhibiting the Wnt pathway in esophageal cancer [143]. Let-7 also suppresses the stemness properties like self-renewal in hepatocellular cancer stem cells via EMT and Wnt/β-catenin pathway [144]. Importantly, one report verifies that activation of LIN28/let-7 axis promotes the CSCs properties in prostate cancer [145], which indicates that let-7 miRNA perhaps plays a critical role in PCSCs.

The let-7 family is a vital expression modulator for IGF2BP1 in tumor cells through 3' UTR regulation, and IGF2BP1 mRNA is a major target of the let-7 family [133]. Furthermore, low expression of let‑7 miRNA increases the level of MYC, then contributes to maintaining the undifferentiated status, which is a stem cell-like characteristic and resulted in gefitinib resistance [137]. Lack of let-7 family expression also contributed to gemcitabine resistance in pancreatic cancer [146]. Elevated expression of let-7 eases the cisplatin resistance in gastric cancer [147], sensitizes epithelial ovarian cancer cells to cisplatin [148], and sensitizes hepatocellular carcinoma cells to cetuximab [149].

4.2.4 The role of STAT3 in CSCs and drug-resistance

As mentioned in 4.2.2, the stemness properties are highly correlated to drug resistance or cancer recurrence [11]. Signal transducer and activator of transcription 3 (STAT3) is reported to be related to stem cell properties. Blocking the Wnt/β-catenin/STAT3 axis inhibits the stem cell-like properties in oral squamous cell carcinoma [100]. Also, regulation of the JAK/ STAT3 signaling pathway suppresses the stem cell-like properties in glioblastoma [150], breast cancer [151], myxoid liposarcoma [152], non-small cell lung cancer stem cells [153], oral cancer [154], anaplastic thyroid cancer [155], and in prostate cancer [156]. Inhibition of IL-6/STAT3 signaling pathway suppresses cancer stemness properties in oral carcinomas [157], and gastric cancer [158]. The target of the

CXCR4/STAT3 axis inhibits the stemness of esophageal squamous cell carcinoma cells [159].

Previous research has focused on p-STAT3, which is a transcription factor and signaling molecule, related to drug resistance [102]. Blocking p-STAT3 overcomes tamoxifen resistance in breast cancer [160], docetaxel resistance in triple-negative breast cancer cells [102], castration resistance in prostate cancer cells [161], radioresistance in nasopharyngeal carcinoma [162], adriamycin resistance in nasal NK/T-cell lymphoma [163], sorafenib resistance in hepatocellular carcinoma [164], EGFR inhibitor resistance in colorectal cancer cells [165], temozolomide resistance in glioblastoma cells [166], cisplatin resistance in cervical cancer cells [167], BRAF inhibitor resistance in melanoma [168], taxol resistance in nasopharyngeal carcinoma cells [169], cisplatin resistance in esophageal squamous cell carcinoma cells [170], gefitinib resistance in non-small cell lung cancer [171], and adriamycin resistance in breast cancer cells [172]. Diminishing or inactivating the level of p-STAT3 reversed the resistance to different chemotherapeutic drugs in a variety of cancers similar to our results. In our study, we found that inhibiting the expression of p-STAT3 resensitized resistant prostate cancer cells to cabazitaxel.

4.2.5 The role of miR-26b in cancer progression

It has been verified that miR-26b takes part in the cancer progression of different cancer types [173, 174] through targeting its downstream genes [175]. Elevated expression of miR-26b represses cell proliferation and induces the apoptosis of CSCs by downregulating PTEN through the means of 3’ UTR binding [176]. MiR-26b elevates the sensitivity to doxorubicin through USP9X-dependent p53 degradation and autophagy regulation [175], enhances the doxorubicin sensitivity through targeting TAK1 and TAB3 in hepatocellular carcinoma cells [177], reverses the cisplatin resistance by targeting Tafazzin in non-small cell lung cancer [178] and reverses temozolomide resistance through targeting Wee1 in glioma cells [179]. Also, miR-26b-5p maintains the CSCs properties in hepatocellular carcinoma [180].

Our results showed that mimics of miR-26b suppress the expression of p-STAT3, and the inhibition of p-STAT3 could reverse the cabazitaxel resistance in prostate cancer cells.

4.2.6 Berbamine shows anti-tumor effects in different types of cancer

Mounting research has also focused on berbamine, which is a natural herb derived

from the root of Berberis amurensis. The combination of berbamine and aspirin significantly inhibited the viability of hepatocellular carcinoma cells in vitro and in vivo [181]. The combination of detoxified pneumolysin derivative ΔA146Ply with berbamine significantly inhibited breast cancer cells verified in the aspects of proliferation, apoptosis, cell-cycle arrest, migration, and invasion [182]. Berbamine also enhanced the efficacy of gefitinib in pancreatic cancer cells via suppressing the STAT3 signaling pathway [183]. Berbamine contributes to cancer progression in different types of cancer. It suppressed the cancer progression in bladder cancer through ROS/NF-kappaB axis [184], in osteosarcoma through targeting NF- kappaB, ERK, and AKT pathway [185], in colorectal cancer via the p53-dependent apoptotic pathway [186], in prostate cancer via triggering intrinsic apoptosis pathway [187], in melanoma cells through inhibiting Jak2/STAT3 signaling pathway [87], and in breast cancer [86]. In our study, the results suggest that berbamine might suppress cancer progression through the IGF2BP1axis and the p-STAT3 axis.

4.2.7 Exosomal microRNAs in CSCs

Exosomes are small vesicles with 40-100 nm, which are delivered by many cells and are also secreted by tumor cells [188]. Exosomes constitute a lipid bilayer containing transmembrane proteins. They can cargo proteins, mRNA, non-coding RNA, and DNA [189]. Mechanistically, exosomes are secreted from cells and facilitate intercellular communication by straight cellular internalization through receptors in the receiver cell [190]. CSCs derived exosomes (CSC-EXO) are considered to be powerful tumor microenvironment mediators, maintain tumor heterogeneity, and change the tumor progression. The CSC-EXO can increase angiogenesis in glioblastoma, renal, and liver cancer stem cells [190]. The microRNAs can be delivered by exosomes and influence the downstream signaling pathways [190]. Our results showed that berbamine enhances the expression of exosomal let-7 miRNA family members, and miR-26b, which suggested that the let-7 miRNA family members and miR-26b could be delivered via exosomes to facilitate intercellular communication, and further influence the downstream targets IGF2BP1 and p-STAT3.

4.2.8 Our new insight

It is the first time we report that berbamine attacks both PCSCs and PCa cells. Also, berbamine enhances the anti-tumor effect of cabazitaxel in both PCSCs and PCa cells. Furthermore, berbamine reverses the cabazitaxel resistance through CXCR4/let-7 family/IGF2BP1 axis, and ABCG2/miR-26b/ p-STAT3 axis. The potential mechanism of

berbamine in inducing anti-tumor activity and reversing cabazitaxel resistance is shown in **Figure 61**.

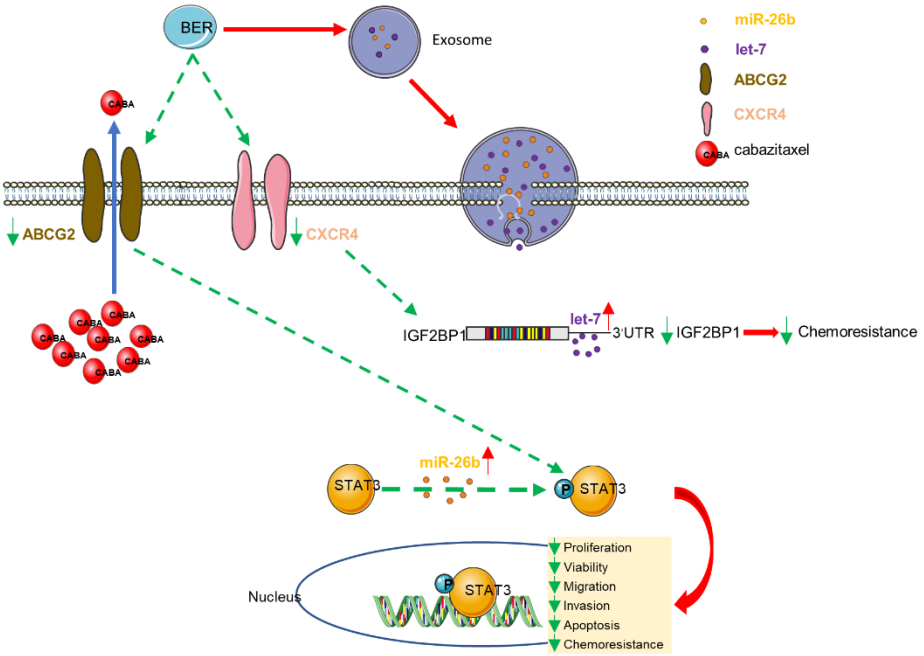

Figure 61. **The potential mechanisms of berbamine involved in the process of anti-tumor activity and reversing cabazitaxel resistance.** On one hand, berbamine suppresses the function of ABCG2 to decrease the efflux of cabazitaxel. On the other hand, berbamine plays a role in the anti-tumor activity and drug resistance through CXCR4/let-7 miRNA/IGF2BP1 axis and ABCG2/miR-26b/p-STAT3 axis. First, berbamine enhances the expression of the let-7 miRNA family members, and miR-26b, which decrease the activation or expression of IGF2BP1 and p-STAT3 respectively, as we verified that downregulation of IGF2BP1 and p-STAT3 could reverse the cabazitaxel resistance. The let-7 and miR-26b could be delivered by exosomes as we found that berbamine enhanced the expression of the exosomal let-7 family and miR-26b. Furthermore, inhibition of ABCG2 downregulates the p-STAT3 expression, and inhibition of CXCR4 could downregulate the IGF2BP1 expression. (BER: berbamine, red line: increasing effects, green and dotted line: decreasing effects.)

4.2.9 Limitations

As discussed for shikonin more studies related to berbamine in vivo should be conducted to prove our results. Besides, further work is needed to find out whether berbamine and other promising inhibitors of ABCG2, CXCR4, IGF2BP1, and p-STAT3 can be utilized for those patients who are resistant to chemotherapeutic drugs.

5. Summary

We found that shikonin targeted PCSCs and PCa cells verified by the viability, proliferation, migration, invasion, and apoptosis assays. Furthermore, the combination of shikonin and cabazitaxel enhanced the anti-tumor effect much more than cabazitaxel alone verified again by the viability, proliferation, invasion, and apoptosis assays. Importantly, shikonin downregulated the two cancer stem cell markers ABCG2 and ALDH3A1, which were in charge of drug resistance. Inhibitors of ABCG2 and ALDH3A1 reversed the cabazitaxel-resistant state. Last but not least, shikonin induced apoptosis mainly through the ROS-mitochondria membrane potential apoptosis pathway. In summary, shikonin targets PCSCs and PCa cells, enhances the anti-cancer effect of cabazitaxel, and reverses cabazitaxel-related resistance.

As shikonin also berbamine targeted PCSCs and PCa cells, enhanced the cabazitaxel effect when combined with cabazitaxel. Compared to shikonin, berbamine inhibited the expression of the three cancer stem cell markers ABCG2, CXCR4, and ALDH1A1, instead of ALDH3A1. Inhibitors of ABCG2 and CXCR4 resensitized resistant PCa cells to cabazitaxel. One of the ALDH1A1 inhibitors slightly reversed the cabazitaxel resistance, while the other showed no effect on caba-DU145 cells. Therefore, we focused on the two cancer stem cell markers ABCG2 and CXCR4 as targets of berbamine in the following experiments. Afterwards, we found that berbamine significantly enhanced the let-7 miRNA family members, miR-26a, and miR-26b by small RNA-sequencing technique. For further verification, individual miRCURY LNA miRNA PCR assays were conducted and showed that berbamine upregulated the let-7 family members, miR-26a, and miR-26b. Next, we found that berbamine downregulated IGF2BP1 through silencing CXCR4. Likewise, enhancement of the let-7 family members using mimics also decreased the expression of IGF2BP1. Another downstream regulator of berbamine and ABCG2 was p-STAT3. We found that berbamine downregulated p-STAT3 through silencing ABCG2. Upregulating miR-26b using mimics also repressed p-STAT3. Taken together, we conclude that berbamine targets PCSC, PCa cells, and reverses the cabazitaxel resistance through berbamine/CXCR4/let-7 family/IGF2BP1 axis, and berbamine/ABCG2/miR-26b/p-STAT3 axis.

In addition to shikonin and berbamine there are many other phytochemicals, like berberine, curcumin, quercetin, resveratrol and so forth, showing an anti-tumor effect on CSCs [13] and they are also worth to be tested in clinical studies.

6. References

1. Sung H, Ferlay J, Siegel RL, Laversanne M, Soerjomataram I, Jemal A, Bray F: Global cancer statistics 2020: GLOBOCAN estimates of incidence and mortality worldwide for 36 cancers in 185 countries. CA Cancer J Clin 2021.
2. Kahn B, Collazo J, Kyprianou N: Androgen receptor as a driver of therapeutic resistance in advanced prostate cancer. Int J Biol Sci 2014, 10**:**588-595.
3. Tucci M, Caffo O, Buttigliero C, Cavaliere C, D'Aniello C, Di Maio M, Kinspergher S, Maines F, Rizzo M, Rossetti S, et al: Therapeutic options for first-line metastatic castration-resistant prostate cancer: Suggestions for clinical practise in the CHAARTED and LATITUDE era. Cancer Treat Rev 2019, 74**:**35-42.
4. Moreira DM, Howard LE, Sourbeer KN, Amarasekara HS, Chow LC, Cockrell DC, Hanyok BT, Aronson WJ, Kane CJ, Terris MK, et al: Predictors of Time to Metastasis in Castration-resistant Prostate Cancer. Urology 2016, 96**:**171-176.
5. Al-Mansouri L, Gurney H: Clinical concepts for cabazitaxel in the management of metastatic castration-resistant prostate cancer. Asia Pac J Clin Oncol 2019, 15**:**288-295.
6. Shiota M, Nakamura M, Yokomizo A, Tomoda T, Sakamoto N, Seki N, Hasegawa S, Yunoki T, Harano M, Kuroiwa K, Eto M: Efficacy and safety of cabazitaxel for castration-resistant prostate cancer in patients with > 10 cycles of docetaxel chemotherapy: a multi-institutional study. Med Oncol 2019, 36**:**32.
7. Kreso A, Dick JE: Evolution of the cancer stem cell model. Cell Stem Cell 2014, 14**:**275-291.
8. Lobo NA, Shimono Y, Qian D, Clarke MF: The biology of cancer stem cells. Annu Rev Cell Dev Biol 2007, 23**:**675-699.
9. Zhou HM, Zhang JG, Zhang X, Li Q: Targeting cancer stem cells for reversing therapy resistance: mechanism, signaling, and prospective agents. Signal Transduct Target Ther 2021, 6**:**62.
10. Reya T, Morrison SJ, Clarke MF, Weissman IL: Stem cells, cancer, and cancer stem cells. Nature 2001, 414**:**105-111.
11. Keyvani-Ghamsari S, Khorsandi K, Rasul A, Zaman MK: Current understanding of epigenetics mechanism as a novel target in reducing cancer stem cells resistance. Clin Epigenetics 2021, 13**:**120.
12. Borst P: Cancer drug pan-resistance: pumps, cancer stem cells, quiescence, epithelial to mesenchymal transition, blocked cell death pathways, persisters or what? Open Biol 2012, 2**:**120066.
13. Hong M, Tan HY, Li S, Cheung F, Wang N, Nagamatsu T, Feng Y: Cancer Stem Cells: The Potential Targets of Chinese Medicines and Their Active Compounds. Int J Mol Sci 2016, 17.
14. Steinbichler TB, Dudas J, Skvortsov S, Ganswindt U, Riechelmann H, Skvortsova, II: Therapy resistance mediated by cancer stem cells. Semin Cancer Biol 2018, 53**:**156-167.
15. Begicevic RR, Falasca M: ABC Transporters in Cancer Stem Cells: Beyond Chemoresistance. Int J Mol Sci 2017, 18.
16. Bunting KD: ABC transporters as phenotypic markers and functional regulators of stem cells. Stem Cells 2002, 20**:**11-20.
17. Sugano T, Seike M, Noro R, Soeno C, Chiba M, Zou F, Nakamichi S, Nishijima N, Matsumoto M, Miyanaga A, et al: Inhibition of ABCB1 Overcomes Cancer Stem Cell-like Properties and Acquired Resistance to MET Inhibitors in Non-Small Cell Lung Cancer. Mol Cancer Ther 2015, 14**:**2433-2440.

18. Safa AR: Resistance to Cell Death and Its Modulation in Cancer Stem Cells. Crit Rev Oncog 2016, 21:203-219.

19. Vassalli G: Aldehyde Dehydrogenases: Not Just Markers, but Functional Regulators of Stem Cells. Stem Cells Int 2019, 2019:3904645.

20. Wang R, Sun Q, Wang P, Liu M, Xiong S, Luo J, Huang H, Du Q, Geller DA, Cheng B: Notch and Wnt/beta-catenin signaling pathway play important roles in activating liver cancer stem cells. Oncotarget 2016, 7:5754-5768.

21. Safa AR, Saadatzadeh MR, Cohen-Gadol AA, Pollok KE, Bijangi-Vishehsaraei K: Emerging targets for glioblastoma stem cell therapy. J Biomed Res 2016, 30:19-31.

22. Yuan ZX, Mo J, Zhao G, Shu G, Fu HL, Zhao W: Targeting Strategies for Renal Cell Carcinoma: From Renal Cancer Cells to Renal Cancer Stem Cells. Front Pharmacol 2016, 7:423.

23. Harris KS, Kerr BA: Prostate Cancer Stem Cell Markers Drive Progression, Therapeutic Resistance, and Bone Metastasis. Stem Cells Int 2017, 2017:8629234.

24. Stavrovskaya AA: Cellular mechanisms of multidrug resistance of tumor cells. Biochemistry (Mosc) 2000, 65:95-106.

25. Leonard GD, Fojo T, Bates SE: The role of ABC transporters in clinical practice. Oncologist 2003, 8:411-424.

26. An Y, Ongkeko WM: ABCG2: the key to chemoresistance in cancer stem cells? Expert Opin Drug Metab Toxicol 2009, 5:1529-1542.

27. Patrawala L, Calhoun T, Schneider-Broussard R, Zhou J, Claypool K, Tang DG: Side population is enriched in tumorigenic, stem-like cancer cells, whereas ABCG2+ and ABCG2- cancer cells are similarly tumorigenic. Cancer Res 2005, 65:6207-6219.

28. Stacy AE, Jansson PJ, Richardson DR: Molecular pharmacology of ABCG2 and its role in chemoresistance. Mol Pharmacol 2013, 84:655-669.

29. Wang L, Lin N, Li Y: The PI3K/AKT signaling pathway regulates ABCG2 expression and confers resistance to chemotherapy in human multiple myeloma. Oncol Rep 2019, 41:1678-1690.

30. Erdogan S, Turkekul K, Dibirdik I, Doganlar O, Doganlar ZB, Bilir A, Oktem G: Midkine downregulation increases the efficacy of quercetin on prostate cancer stem cell survival and migration through PI3K/AKT and MAPK/ERK pathway. Biomed Pharmacother 2018, 107:793-805.

31. Zhang L, Guo X, Zhang D, Fan Y, Qin L, Dong S, Zhang L: Upregulated miR-132 in Lgr5(+) gastric cancer stem cell-like cells contributes to cisplatin-resistance via SIRT1/CREB/ABCG2 signaling pathway. Mol Carcinog 2017, 56:2022-2034.

32. Moreb JS: Aldehyde dehydrogenase as a marker for stem cells. Curr Stem Cell Res Ther 2008, 3:237-246.

33. Vasiliou V, Pappa A, Petersen DR: Role of aldehyde dehydrogenases in endogenous and xenobiotic metabolism. Chem Biol Interact 2000, 129:1-19.

34. Li T, Su Y, Mei Y, Leng Q, Leng B, Liu Z, Stass SA, Jiang F: ALDH1A1 is a marker for malignant prostate stem cells and predictor of prostate cancer patients' outcome. Lab Invest 2010, 90:234-244.

35. Germann M, Wetterwald A, Guzman-Ramirez N, van der Pluijm G, Culig Z, Cecchini MG, Williams ED, Thalmann GN: Stem-like cells with luminal progenitor phenotype survive castration in human prostate cancer. Stem Cells 2012, 30:1076-1086.

36. Mochizuki H, Matsubara A, Teishima J, Mutaguchi K, Yasumoto H, Dahiya R, Usui T, Kamiya K: Interaction of ligand-receptor system between stromal-cell-derived factor-1 and CXC chemokine receptor 4 in human prostate cancer: a possible predictor of metastasis. Biochem Biophys Res Commun 2004, 320:656-663.

37. Domanska UM, Timmer-Bosscha H, Nagengast WB, Oude Munnink TH, Kruizinga RC, Ananias HJ, Kliphuis NM, Huls G, De Vries EG, de Jong IJ, Walenkamp AM: CXCR4 inhibition with AMD3100 sensitizes prostate cancer to docetaxel chemotherapy. Neoplasia 2012, 14:709-718.

38. Clevers H: The cancer stem cell: premises, promises and challenges. Nat Med 2011, 17:313-319.

39. Toh TB, Lim JJ, Chow EK: Epigenetics in cancer stem cells. Mol Cancer 2017, 16:29.

40. Beachy PA, Hymowitz SG, Lazarus RA, Leahy DJ, Siebold C: Interactions between Hedgehog proteins and their binding partners come into view. Genes Dev 2010, 24:2001-2012.

41. Agliano A, Calvo A, Box C: The challenge of targeting cancer stem cells to halt metastasis. Semin Cancer Biol 2017, 44:25-42.

42. Matsui WH: Cancer stem cell signaling pathways. Medicine (Baltimore) 2016, 95:S8-S19.

43. Merchant AA, Matsui W: Targeting Hedgehog--a cancer stem cell pathway. Clin Cancer Res 2010, 16:3130-3140.

44. Yang L, Shi P, Zhao G, Xu J, Peng W, Zhang J, Zhang G, Wang X, Dong Z, Chen F, Cui H: Targeting cancer stem cell pathways for cancer therapy. Signal Transduct Target Ther 2020, 5:8.

45. Saygin C, Matei D, Majeti R, Reizes O, Lathia JD: Targeting Cancer Stemness in the Clinic: From Hype to Hope. Cell Stem Cell 2019, 24:25-40.

46. Habib JG, O'Shaughnessy JA: The hedgehog pathway in triple-negative breast cancer. Cancer Med 2016, 5:2989-3006.

47. Cochrane CR, Szczepny A, Watkins DN, Cain JE: Hedgehog Signaling in the Maintenance of Cancer Stem Cells. Cancers (Basel) 2015, 7:1554-1585.

48. Po A, Ferretti E, Miele E, De Smaele E, Paganelli A, Canettieri G, Coni S, Di Marcotullio L, Biffoni M, Massimi L, et al: Hedgehog controls neural stem cells through p53-independent regulation of Nanog. EMBO J 2010, 29:2646-2658.

49. Wu J, Zhu P, Lu T, Du Y, Wang Y, He L, Ye B, Liu B, Yang L, Wang J, et al: The long non-coding RNA LncHDAC2 drives the self-renewal of liver cancer stem cells via activation of Hedgehog signaling. J Hepatol 2019, 70:918-929.

50. Mondal S, Bhattacharya K, Mandal C: Nutritional stress reprograms dedifferention in glioblastoma multiforme driven by PTEN/Wnt/Hedgehog axis: a stochastic model of cancer stem cells. Cell Death Discov 2018, 4:110.

51. Nanta R, Shrivastava A, Sharma J, Shankar S, Srivastava RK: Inhibition of sonic hedgehog and PI3K/Akt/mTOR pathways cooperate in suppressing survival, self-renewal and tumorigenic potential of glioblastoma-initiating cells. Mol Cell Biochem 2019, 454:11-23.

52. Butti R, Gunasekaran VP, Kumar TVS, Banerjee P, Kundu GC: Breast cancer stem cells: Biology and therapeutic implications. Int J Biochem Cell Biol 2019, 107:38-52.

53. Qin T, Li B, Feng X, Fan S, Liu L, Liu D, Mao J, Lu Y, Yang J, Yu X, et al: Abnormally elevated USP37 expression in breast cancer stem cells regulates stemness, epithelial-mesenchymal transition and cisplatin sensitivity. J Exp Clin Cancer Res 2018, 37:287.

54. Yang Z, Zhang C, Qi W, Cui Y, Xuan Y: GLI1 promotes cancer stemness through intracellular signaling pathway PI3K/Akt/NFkappaB in colorectal adenocarcinoma. Exp Cell Res 2018, 373:145-154.

55. Zhang Y, Xue X, Zhao X, Qin L, Shen Y, Dou H, Sun J, Wang T, Yang DQ: Vasohibin 2 promotes malignant behaviors of pancreatic cancer cells by inducing epithelial-mesenchymal transition via Hedgehog signaling pathway. Cancer Med 2018, 7:5567-5576.

56. Giroux-Leprieur E, Costantini A, Ding VW, He B: Hedgehog Signaling in Lung Cancer: From Oncogenesis to Cancer Treatment Resistance. Int J Mol Sci 2018, 19.

57. de Sousa EMF, Vermeulen L: Wnt Signaling in Cancer Stem Cell Biology. Cancers (Basel) 2016, 8.

58. Martin-Orozco E, Sanchez-Fernandez A, Ortiz-Parra I, Ayala-San Nicolas M: WNT Signaling in Tumors: The Way to Evade Drugs and Immunity. Front Immunol 2019, 10:2854.

59. Yang K, Wang X, Zhang H, Wang Z, Nan G, Li Y, Zhang F, Mohammed MK, Haydon RC, Luu HH, et al: The evolving roles of canonical WNT signaling in stem cells and tumorigenesis: implications in targeted cancer therapies. Lab Invest 2016, 96:116-136.

60. Onyido EK, Sweeney E, Nateri AS: Wnt-signalling pathways and microRNAs network in carcinogenesis: experimental and bioinformatics approaches. Mol Cancer 2016, 15:56.

61. Najafi M, Mortezaee K, Majidpoor J: Cancer stem cell (CSC) resistance drivers. Life Sci 2019, 234:116781.

62. Xu H, Zhao G, Zhang Y, Jiang H, Wang W, Zhao D, Hong J, Yu H, Qi L: Mesenchymal stem cell-derived exosomal microRNA-133b suppresses glioma progression via Wnt/beta-catenin signaling pathway by targeting EZH2. Stem Cell Res Ther 2019, 10:381.

63. Xiao W, Gao Z, Duan Y, Yuan W, Ke Y: Notch signaling plays a crucial role in cancer stem-like cells maintaining stemness and mediating chemotaxis in renal cell carcinoma. J Exp Clin Cancer Res 2017, 36:41.

64. Takebe N, Miele L, Harris PJ, Jeong W, Bando H, Kahn M, Yang SX, Ivy SP: Targeting Notch, Hedgehog, and Wnt pathways in cancer stem cells: clinical update. Nat Rev Clin Oncol 2015, 12:445-464.

65. Yan B, Liu L, Zhao Y, Xiu LJ, Sun DZ, Liu X, Lu Y, Shi J, Zhang YC, Li YJ, et al: Xiaotan Sanjie decoction attenuates tumor angiogenesis by manipulating Notch-1-regulated proliferation of gastric cancer stem-like cells. World J Gastroenterol 2014, 20:13105-13118.

66. McAuliffe SM, Morgan SL, Wyant GA, Tran LT, Muto KW, Chen YS, Chin KT, Partridge JC, Poole BB, Cheng KH, et al: Targeting Notch, a key pathway for ovarian cancer stem cells, sensitizes tumors to platinum therapy. Proc Natl Acad Sci U S A 2012, 109:E2939-2948.

67. Massague J: TGFbeta signalling in context. Nat Rev Mol Cell Biol 2012, 13:616-630.

68. Liu S, Chen S, Zeng J: TGFbeta signaling: A complex role in tumorigenesis (Review). Mol Med Rep 2018, 17:699-704.

69. You H, Ding W, Rountree CB: Epigenetic regulation of cancer stem cell marker CD133 by transforming growth factor-beta. Hepatology 2010, 51:1635-1644.

70. Kim BN, Ahn DH, Kang N, Yeo CD, Kim YK, Lee KY, Kim TJ, Lee SH, Park MS, Yim HW, et al: TGF-beta induced EMT and stemness characteristics are associated with epigenetic regulation in lung cancer. Sci Rep 2020, 10:10597.

71. Asadzadeh Z, Mansoori B, Mohammadi A, Aghajani M, Haji-Asgarzadeh K, Safarzadeh E, Mokhtarzadeh A, Duijf PHG, Baradaran B: microRNAs in cancer stem cells: Biology, pathways, and therapeutic opportunities. J Cell Physiol 2019, 234:10002-10017.

72. Sohel MMH: Circulating microRNAs as biomarkers in cancer diagnosis. Life Sci 2020, 248:117473.

73. Tomei S, Ibnaof O, Ravindran S, Ferrone S, Maccalli C: Cancer Stem Cells Are Possible Key Players in Regulating Anti-Tumor Immune Responses: The Role of Immunomodulating Molecules and MicroRNAs. Cancers (Basel) 2021, 13.

74. Tatsumi K, Yano M, Kaminade K, Sugiyama A, Sato M, Toyooka K, Aoyama T, Sato F, Yazaki K: Characterization of Shikonin Derivative Secretion in Lithospermum

erythrorhizon Hairy Roots as a Model of Lipid-Soluble Metabolite Secretion from Plants. Front Plant Sci 2016, 7:1066.

75. Chen X, Yang L, Oppenheim JJ, Howard MZ: Cellular pharmacology studies of shikonin derivatives. Phytother Res 2002, 16:199-209.

76. Wei PL, Tu CC, Chen CH, Ho YS, Wu CT, Su HY, Chen WY, Liu JJ, Chang YJ: Shikonin suppresses the migratory ability of hepatocellular carcinoma cells. J Agric Food Chem 2013, 61:8191-8197.

77. Wang Y, Zhou Y, Jia G, Han B, Liu J, Teng Y, Lv J, Song Z, Li Y, Ji L, et al: Shikonin suppresses tumor growth and synergizes with gemcitabine in a pancreatic cancer xenograft model: Involvement of NF-kappaB signaling pathway. Biochem Pharmacol 2014, 88:322-333.

78. Chen Y, Zheng L, Liu J, Zhou Z, Cao X, Lv X, Chen F: Shikonin inhibits prostate cancer cells metastasis by reducing matrix metalloproteinase-2/-9 expression via AKT/mTOR and ROS/ERK1/2 pathways. Int Immunopharmacol 2014, 21:447-455.

79. Lee MJ, Kao SH, Hunag JE, Sheu GT, Yeh CW, Hseu YC, Wang CJ, Hsu LS: Shikonin time-dependently induced necrosis or apoptosis in gastric cancer cells via generation of reactive oxygen species. Chem Biol Interact 2014, 211:44-53.

80. Jang SY, Jang EH, Jeong SY, Kim JH: Shikonin inhibits the growth of human prostate cancer cells via modulation of the androgen receptor. Int J Oncol 2014, 44:1455-1460.

81. Liu J, Qu CB, Xue YX, Li Z, Wang P, Liu YH: MiR-143 enhances the antitumor activity of shikonin by targeting BAG3 expression in human glioblastoma stem cells. Biochem Biophys Res Commun 2015, 468:105-112.

82. Zhang FL, Wang P, Liu YH, Liu LB, Liu XB, Li Z, Xue YX: Topoisomerase I inhibitors, shikonin and topotecan, inhibit growth and induce apoptosis of glioma cells and glioma stem cells. PLoS One 2013, 8:e81815.

83. Wu H, Xie J, Pan Q, Wang B, Hu D, Hu X: Anticancer agent shikonin is an incompetent inducer of cancer drug resistance. PLoS One 2013, 8:e52706.

84. Zarei A, Changizi-Ashtiyani S, Taheri S, Ramezani M: A quick overview on some aspects of endocrinological and therapeutic effects of Berberis vulgaris L. Avicenna J Phytomed 2015, 5:485-497.

85. Zhao Y, Tan Y, Wu G, Liu L, Wang Y, Luo Y, Shi J, Huang H: Berbamine overcomes imatinib-induced neutropenia and permits cytogenetic responses in Chinese patients with chronic-phase chronic myeloid leukemia. Int J Hematol 2011, 94:156-162.

86. Wang S, Liu Q, Zhang Y, Liu K, Yu P, Liu K, Luan J, Duan H, Lu Z, Wang F, et al: Suppression of growth, migration and invasion of highly-metastatic human breast cancer cells by berbamine and its molecular mechanisms of action. Mol Cancer 2009, 8:81.

87. Nam S, Xie J, Perkins A, Ma Y, Yang F, Wu J, Wang Y, Xu RZ, Huang W, Horne DA, Jove R: Novel synthetic derivatives of the natural product berbamine inhibit Jak2/Stat3 signaling and induce apoptosis of human melanoma cells. Mol Oncol 2012, 6:484-493.

88. Yang F, Nam S, Brown CE, Zhao R, Starr R, Ma Y, Xie J, Horne DA, Malkas LH, Jove R, Hickey RJ: A novel berbamine derivative inhibits cell viability and induces apoptosis in cancer stem-like cells of human glioblastoma, via up-regulation of miRNA-4284 and JNK/AP-1 signaling. PLoS One 2014, 9:e94443.

89. Gu Y, Chen T, Meng Z, Gan Y, Xu X, Lou G, Li H, Gan X, Zhou H, Tang J, et al: CaMKII gamma, a critical regulator of CML stem/progenitor cells, is a target of the natural product berbamine. Blood 2012, 120:4829-4839.

90.* Wang L, Stadlbauer B, Lyu C, Buchner A, Pohla H: Shikonin enhances the antitumor effect of cabazitaxel in prostate cancer stem cells and reverses cabazitaxel resistance by inhibiting ABCG2 and ALDH3A1. Am J Cancer Res 2020, 10:3784-3800.

91. Schindelin J, Arganda-Carreras I, Frise E, Kaynig V, Longair M, Pietzsch T, Preibisch S, Rueden C, Saalfeld S, Schmid B, et al: Fiji: an open-source platform for biological-image analysis. Nat Methods 2012, 9**:**676-682.

92. Hum C, Loiselle J, Ahmed N, Shaw TA, Toudic C, Pezacki JP: MicroRNA Mimics or Inhibitors as Antiviral Therapeutic Approaches Against COVID-19. Drugs 2021, 81**:**517-531.

93. Abbaszadegan MR, Bagheri V, Razavi MS, Momtazi AA, Sahebkar A, Gholamin M: Isolation, identification, and characterization of cancer stem cells: A review. J Cell Physiol 2017, 232**:**2008-2018.

94. Chang IC, Huang YJ, Chiang TI, Yeh CW, Hsu LS: Shikonin induces apoptosis through reactive oxygen species/extracellular signal-regulated kinase pathway in osteosarcoma cells. Biol Pharm Bull 2010, 33**:**816-824.

95. Singh F, Gao D, Lebwohl MG, Wei H: Shikonin modulates cell proliferation by inhibiting epidermal growth factor receptor signaling in human epidermoid carcinoma cells. Cancer Lett 2003, 200**:**115-121.

96. Gong K, Li W: Shikonin, a Chinese plant-derived naphthoquinone, induces apoptosis in hepatocellular carcinoma cells through reactive oxygen species: A potential new treatment for hepatocellular carcinoma. Free Radic Biol Med 2011, 51**:**2259-2271.

97. Liu Y, Kang X, Niu G, He S, Zhang T, Bai Y, Li Y, Hao H, Chen C, Shou Z, Li B: Shikonin induces apoptosis and prosurvival autophagy in human melanoma A375 cells via ROS-mediated ER stress and p38 pathways. Artif Cells Nanomed Biotechnol 2019, 47**:**626-635.

98. Fan D, Lin X, Zhang F, Zhong W, Hu J, Chen Y, Cai Z, Zou Y, He X, Chen X, et al: MicroRNA 26b promotes colorectal cancer metastasis by downregulating phosphatase and tensin homolog and wingless-type MMTV integration site family member 5A. Cancer Sci 2018, 109**:**354-362.

99. Elcheva IA, Wood T, Chiarolanzio K, Chim B, Wong M, Singh V, Gowda CP, Lu Q, Hafner M, Dovat S, et al: RNA-binding protein IGF2BP1 maintains leukemia stem cell properties by regulating HOXB4, MYB, and ALDH1A1. Leukemia 2020, 34**:**1354-1363.

100. Liu SC, Huang CS, Huang CM, Hsieh MS, Huang MS, Fong IH, Yeh CT, Lin CC: Isoorientin inhibits epithelial-to-mesenchymal properties and cancer stem-cell-like features in oral squamous cell carcinoma by blocking Wnt/beta-catenin/STAT3 axis. Toxicol Appl Pharmacol 2021, 424**:**115581.

101. Huang X, Zhang H, Guo X, Zhu Z, Cai H, Kong X: Insulin-like growth factor 2 mRNA-binding protein 1 (IGF2BP1) in cancer. J Hematol Oncol 2018, 11**:**88.

102. Byun WS, Bae ES, Cui J, Park HJ, Oh DC, Lee SK: Antitumor Activity of Pulvomycin via Targeting Activated-STAT3 Signaling in Docetaxel-Resistant Triple-Negative Breast Cancer Cells. Biomedicines 2021, 9.

103. Zhou J, Bi C, Ching YQ, Chooi JY, Lu X, Quah JY, Toh SH, Chan ZL, Tan TZ, Chong PS, Chng WJ: Inhibition of LIN28B impairs leukemia cell growth and metabolism in acute myeloid leukemia. J Hematol Oncol 2017, 10**:**138.

104. Kuo LJ, Huang CY, Cheng WL, Hung CS, Wu CT, Lin FY, Chang YJ, Huang MT: Glucose-regulated protein 78 mediates the anticancer efficacy of shikonin in hormone-refractory prostate cancer cells. Tumour Biol 2015, 36**:**5063-5070.

105. Xiao H, Zheng Y, Ma L, Tian L, Sun Q: Clinically-Relevant ABC Transporter for Anti-Cancer Drug Resistance. Front Pharmacol 2021, 12**:**648407.

106. Narayanan S, Gujarati NA, Wang JQ, Wu ZX, Koya J, Cui Q, Korlipara VL, Ashby CR, Jr., Chen ZS: The Novel Benzamide Derivative, VKNG-2, Restores the Efficacy of Chemotherapeutic Drugs in Colon Cancer Cell Lines by Inhibiting the ABCG2 Transporter. Int J Mol Sci 2021, 22.

107. Katamune C, Koyanagi S, Hashikawa KI, Kusunose N, Akamine T, Matsunaga N, Ohdo S: Mutation of the gene encoding the circadian clock component PERIOD2 in oncogenic cells confers chemoresistance by up-regulating the Aldh3a1 gene. J Biol Chem 2019, 294**:**547-558.

108. Duong HQ, You KS, Oh S, Kwak SJ, Seong YS: Silencing of NRF2 Reduces the Expression of ALDH1A1 and ALDH3A1 and Sensitizes to 5-FU in Pancreatic Cancer Cells. Antioxidants (Basel) 2017, 6.

109. Rabindran SK, Ross DD, Doyle LA, Yang W, Greenberger LM: Fumitremorgin C reverses multidrug resistance in cells transfected with the breast cancer resistance protein. Cancer Res 2000, 60**:**47-50.

110. Ricci JW, Lovato DM, Severns V, Sklar LA, Larson RS: Novel ABCG2 Antagonists Reverse Topotecan-Mediated Chemotherapeutic Resistance in Ovarian Carcinoma Xenografts. Mol Cancer Ther 2016, 15**:**2853-2862.

111. Chen Y, Koppaka V, Thompson DC, Vasiliou V: Focus on molecules: ALDH1A1: from lens and corneal crystallin to stem cell marker. Exp Eye Res 2012, 102**:**105-106.

112. Yan J, De Melo J, Cutz JC, Aziz T, Tang D: Aldehyde dehydrogenase 3A1 associates with prostate tumorigenesis. Br J Cancer 2014, 110**:**2593-2603.

113. Parajuli B, Fishel ML, Hurley TD: Selective ALDH3A1 inhibition by benzimidazole analogues increase mafosfamide sensitivity in cancer cells. J Med Chem 2014, 57**:**449-461.

114. Okazaki S, Shintani S, Hirata Y, Suina K, Semba T, Yamasaki J, Umene K, Ishikawa M, Saya H, Nagano O: Synthetic lethality of the ALDH3A1 inhibitor dyclonine and xCT inhibitors in glutathione deficiency-resistant cancer cells. Oncotarget 2018, 9**:**33832-33843.

115. Li B, Yuan Z, Jiang J, Rao Y: Anti-tumor activity of Shikonin against afatinib resistant non-small cell lung cancer via negative regulation of PI3K/Akt signaling pathway. Biosci Rep 2018, 38.

116. Hu CF, Huang YY, Wang YJ, Gao FG: Upregulation of ABCG2 via the PI3K-Akt pathway contributes to acidic microenvironment-induced cisplatin resistance in A549 and LTEP-a-2 lung cancer cells. Oncol Rep 2016, 36**:**455-461.

117. Ni W, Fan H, Zheng X, Xu F, Wu Y, Li X, Wang A, Huang S, Chen W, Wang S, Lu Y: Cryptotanshinone Inhibits ERalpha-Dependent and -Independent BCRP Oligomer Formation to Reverse Multidrug Resistance in Breast Cancer. Front Oncol 2021, 11**:**624811.

118. Liang X, Wang Y, Shi H, Dong M, Han H, Li Q: Nucleolin-Targeting AS1411 Aptamer-Modified Micelle for the Co-Delivery of Doxorubicin and miR-519c to Improve the Therapeutic Efficacy in Hepatocellular Carcinoma Treatment. Int J Nanomedicine 2021, 16**:**2569-2584.

119. Lei ZN, Teng QX, Gupta P, Zhang W, Narayanan S, Yang DH, Wurpel JND, Fan YF, Chen ZS: Cabozantinib Reverses Topotecan Resistance in Human Non-Small Cell Lung Cancer NCI-H460/TPT10 Cell Line and Tumor Xenograft Model. Front Cell Dev Biol 2021, 9**:**640957.

120. Wu ZX, Yang Y, Wang G, Wang JQ, Teng QX, Sun L, Lei ZN, Lin L, Chen ZS, Zou C: Dual TTK/CLK2 inhibitor, CC-671, selectively antagonizes ABCG2-mediated multidrug resistance in lung cancer cells. Cancer Sci 2020, 111**:**2872-2882.

121. Ke B, Wei T, Huang Y, Gong Y, Wu G, Liu J, Chen X, Shi L: Interleukin-7 Resensitizes Non-Small-Cell Lung Cancer to Cisplatin via Inhibition of ABCG2. Mediators Inflamm 2019, 2019**:**7241418.

122. Wang Z, Zhan Y, Xu J, Wang Y, Sun M, Chen J, Liang T, Wu L, Xu K: beta-Sitosterol Reverses Multidrug Resistance via BCRP Suppression by Inhibiting the p53-MDM2 Interaction in Colorectal Cancer. J Agric Food Chem 2020, 68**:**3850-3858.

123. Gao Q, Li XX, Xu YM, Zhang JZ, Rong SD, Qin YQ, Fang J: IRE1alpha-targeting downregulates ABC transporters and overcomes drug resistance of colon cancer cells. Cancer Lett 2020, 476**:**67-74.

124. Nengroo MA, Maheshwari S, Singh A, Verma A, Arya RK, Chaturvedi P, Saini KK, Singh AK, Sinha A, Meena S, et al: CXCR4 intracellular protein promotes drug resistance and tumorigenic potential by inversely regulating the expression of Death Receptor 5. Cell Death Dis 2021, 12**:**464.

125. Cao H, Gao Y, Wang R, Guo Q, Hui H: Wogonin reverses the drug resistance of chronic myelogenous leukemia cells to imatinib through CXCL12-CXCR4/7 axis in bone marrow microenvironment. Ann Transl Med 2020, 8**:**1046.

126. Zheng N, Liu W, Li B, Nie H, Liu J, Cheng Y, Wang J, Dong H, Jia L: Co-delivery of sorafenib and metapristone encapsulated by CXCR4-targeted PLGA-PEG nanoparticles overcomes hepatocellular carcinoma resistance to sorafenib. J Exp Clin Cancer Res 2019, 38**:**232.

127. Li C, Yang C, Wei G: Vandetanib inhibits cisplatinresistant neuroblastoma tumor growth and invasion. Oncol Rep 2018, 39**:**1757-1764.

128. Xie S, Tu Z, Xiong J, Kang G, Zhao L, Hu W, Tan H, Tembo KM, Ding Q, Deng X, et al: CXCR4 promotes cisplatin-resistance of non-small cell lung cancer in a CYP1B1-dependent manner. Oncol Rep 2017, 37**:**921-928.

129. Mahaira LG, Katsara O, Pappou E, Iliopoulou EG, Fortis S, Antsaklis A, Fotinopoulos P, Baxevanis CN, Papamichail M, Perez SA: IGF2BP1 expression in human mesenchymal stem cells significantly affects their proliferation and is under the epigenetic control of TET1/2 demethylases. Stem Cells Dev 2014, 23**:**2501-2512.

130. Zirkel A, Lederer M, Stohr N, Pazaitis N, Huttelmaier S: IGF2BP1 promotes mesenchymal cell properties and migration of tumor-derived cells by enhancing the expression of LEF1 and SNAI2 (SLUG). Nucleic Acids Res 2013, 41**:**6618-6636.

131. Zhu P, He F, Hou Y, Tu G, Li Q, Jin T, Zeng H, Qin Y, Wan X, Qiao Y, et al: A novel hypoxic long noncoding RNA KB-1980E6.3 maintains breast cancer stem cell stemness via interacting with IGF2BP1 to facilitate c-Myc mRNA stability. Oncogene 2021, 40**:**1609-1627.

132. Ma F, Liu X, Zhou S, Li W, Liu C, Chadwick M, Qian C: Long non-coding RNA FGF13-AS1 inhibits glycolysis and stemness properties of breast cancer cells through FGF13-AS1/IGF2BPs/Myc feedback loop. Cancer Lett 2019, 450**:**63-75.

133. Busch B, Bley N, Muller S, Glass M, Misiak D, Lederer M, Vetter M, Strauss HG, Thomssen C, Huttelmaier S: The oncogenic triangle of HMGA2, LIN28B and IGF2BP1 antagonizes tumor-suppressive actions of the let-7 family. Nucleic Acids Res 2016, 44**:**3845-3864.

134. Chirshev E, Hojo N, Bertucci A, Sanderman L, Nguyen A, Wang H, Suzuki T, Brito E, Martinez SR, Castanon C, et al: Epithelial/mesenchymal heterogeneity of high-grade serous ovarian carcinoma samples correlates with miRNA let-7 levels and predicts tumor growth and metastasis. Mol Oncol 2020, 14**:**2796-2813.

135. Li X, Wang M, Du N, Liang T, Xiao GD, Li K, Wang JC, Xu CW, Peng ZY, Tang SC, Sun X: Matrine Inhibitory Effect on Self-renewal and Re-sensitization of 5-FU Resistant NSCLC Stem Cells were through Let-7b dependent Downregulation of CCND1. Cell Cycle 2020, 19**:**3249-3259.

136. Hong W, Xue M, Jiang J, Zhang Y, Gao X: Circular RNA circ-CPA4/ let-7 miRNA/PD-L1 axis regulates cell growth, stemness, drug resistance and immune evasion in non-small cell lung cancer (NSCLC). J Exp Clin Cancer Res 2020, 39**:**149.

137. Yin J, Hu W, Pan L, Fu W, Dai L, Jiang Z, Zhang F, Zhao J: let7 and miR17 promote selfrenewal and drive gefitinib resistance in nonsmall cell lung cancer. Oncol Rep 2019, 42**:**495-508.

138. Chen D, Cox J, Annam J, Weingart M, Essien G, Rathi KS, Rokita JL, Khurana P, Cuya SM, Bosse KR, et al: LIN28B promotes neuroblastoma metastasis and regulates PDZ binding kinase. Neoplasia 2020, 22:231-241.

139. Li X, Liang T, Chen SS, Wang M, Wang R, Li K, Wang JC, Xu CW, Du N, Qin S, Ren H: Matrine suppression of self-renewal was dependent on regulation of LIN28A/Let-7 pathway in breast cancer stem cells. J Cell Biochem 2020, 121:2139-2149.

140. Guo L, Cheng X, Chen H, Chen C, Xie S, Zhao M, Liu D, Deng Q, Liu Y, Wang X, et al: Induction of breast cancer stem cells by M1 macrophages through Lin-28B-let-7-HMGA2 axis. Cancer Lett 2019, 452:213-225.

141. Liang R, Li Y, Wang M, Tang SC, Xiao G, Sun X, Li G, Du N, Liu D, Ren H: MiR-146a promotes the asymmetric division and inhibits the self-renewal ability of breast cancer stem-like cells via indirect upregulation of Let-7. Cell Cycle 2018, 17:1445-1456.

142. Sun X, Xu C, Xiao G, Meng J, Wang J, Tang SC, Qin S, Du N, Li G, Ren H, Liu D: Breast cancer stem-like cells are sensitized to tamoxifen induction of self-renewal inhibition with enforced Let-7c dependent on Wnt blocking. Int J Mol Med 2018, 41:1967-1975.

143. Pang Y, Liu J, Li X, Zhang Y, Zhang B, Zhang J, Du N, Xu C, Liang R, Ren H, et al: Nano Let7b sensitization of eliminating esophageal cancer stemlike cells is dependent on blockade of Wnt activation of symmetric division. Int J Oncol 2017, 51:1077-1088.

144. Jin B, Wang W, Meng XX, Du G, Li J, Zhang SZ, Zhou BH, Fu ZH: Let-7 inhibits self-renewal of hepatocellular cancer stem-like cells through regulating the epithelial-mesenchymal transition and the Wnt signaling pathway. BMC Cancer 2016, 16:863.

145. Albino D, Civenni G, Dallavalle C, Roos M, Jahns H, Curti L, Rossi S, Pinton S, D'Ambrosio G, Sessa F, et al: Activation of the Lin28/let-7 Axis by Loss of ESE3/EHF Promotes a Tumorigenic and Stem-like Phenotype in Prostate Cancer. Cancer Res 2016, 76:3629-3643.

146. Xiong G, Liu C, Yang G, Feng M, Xu J, Zhao F, You L, Zhou L, Zheng L, Hu Y, et al: Long noncoding RNA GSTM3TV2 upregulates LAT2 and OLR1 by competitively sponging let-7 to promote gemcitabine resistance in pancreatic cancer. J Hematol Oncol 2019, 12:97.

147. Han X, Zhang JJ, Han ZQ, Zhang HB, Wang ZA: Let-7b attenuates cisplatin resistance and tumor growth in gastric cancer by targeting AURKB. Cancer Gene Ther 2018, 25:300-308.

148. Xiao M, Cai J, Cai L, Jia J, Xie L, Zhu Y, Huang B, Jin D, Wang Z: Let-7e sensitizes epithelial ovarian cancer to cisplatin through repressing DNA double strand break repair. J Ovarian Res 2017, 10:24.

149. Xue F, Liu Y, Zhang H, Wen Y, Yan L, Tang Q, Xiao E, Zhang D: Let-7a enhances the sensitivity of hepatocellular carcinoma cells to cetuximab by regulating STAT3 expression. Onco Targets Ther 2016, 9:7253-7261.

150. Jia M, Wang Y, Guo Y, Yu P, Sun Y, Song Y, Zhao L: Nitidine chloride suppresses epithelial-mesenchymal transition and stem cell-like properties in glioblastoma by regulating JAK2/STAT3 signaling. Cancer Med 2021, 10:3113-3128.

151. To NB, Nguyen YT, Moon JY, Ediriweera MK, Cho SK: Pentadecanoic Acid, an Odd-Chain Fatty Acid, Suppresses the Stemness of MCF-7/SC Human Breast Cancer Stem-Like Cells through JAK2/STAT3 Signaling. Nutrients 2020, 12.

152. Dolatabadi S, Jonasson E, Linden M, Fereydouni B, Backsten K, Nilsson M, Martner A, Forootan A, Fagman H, Landberg G, et al: JAK-STAT signalling controls cancer stem cell properties including chemotherapy resistance in myxoid liposarcoma. Int J Cancer 2019, 145:435-449.

153. Xiong J, Zhang X, Zhang Y, Wu B, Fang L, Wang N, Yi H, Chang N, Chen L, Zhang J: Aryl hydrocarbon receptor mediates Jak2/STAT3 signaling for non-small cell lung cancer stem cell maintenance. Exp Cell Res 2020, 396:112288.

154. Lin CS, Bamodu OA, Kuo KT, Huang CM, Liu SC, Wang CH, Tzeng YM, Chao TY, Yeh CT: Investigation of ovatodiolide, a macrocyclic diterpenoid, as a potential inhibitor of oral cancer stem-like cells properties via the inhibition of the JAK2/STAT3/JARID1B signal circuit. Phytomedicine 2018, 46:93-103.

155. Shiraiwa K, Matsuse M, Nakazawa Y, Ogi T, Suzuki K, Saenko V, Xu S, Umezawa K, Yamashita S, Tsukamoto K, Mitsutake N: JAK/STAT3 and NF-kappaB Signaling Pathways Regulate Cancer Stem-Cell Properties in Anaplastic Thyroid Cancer Cells. Thyroid 2019, 29:674-682.

156. Liu YQ, Wang SK, Xu QQ, Yuan HQ, Guo YX, Wang Q, Kong F, Lin ZM, Sun DQ, Wang RM, Lou HX: Acetyl-11-keto-beta-boswellic acid suppresses docetaxel-resistant prostate cancer cells in vitro and in vivo by blocking Akt and Stat3 signaling, thus suppressing chemoresistant stem cell-like properties. Acta Pharmacol Sin 2019, 40:689-698.

157. Peng CY, Yu CC, Huang CC, Liao YW, Hsieh PL, Chu PM, Yu CH, Lin SS: Magnolol inhibits cancer stemness and IL-6/Stat3 signaling in oral carcinomas. J Formos Med Assoc 2021.

158. Sun B, Han Y, Cai H, Huang H, Xuan Y: Long non-coding RNA SNHG3, induced by IL-6/STAT3 transactivation, promotes stem cell-like properties of gastric cancer cells by regulating the miR-3619-5p/ARL2 axis. Cell Oncol (Dordr) 2021, 44:179-192.

159. Yue D, Zhang D, Shi X, Liu S, Li A, Wang D, Qin G, Ping Y, Qiao Y, Chen X, et al: Chloroquine Inhibits Stemness of Esophageal Squamous Cell Carcinoma Cells Through Targeting CXCR4-STAT3 Pathway. Front Oncol 2020, 10:311.

160. Zhu N, Zhang J, Du Y, Qin X, Miao R, Nan J, Chen X, Sun J, Zhao R, Zhang X, et al: Loss of ZIP facilitates JAK2-STAT3 activation in tamoxifen-resistant breast cancer. Proc Natl Acad Sci U S A 2020, 117:15047-15054.

161. Tan B, Chen X, Fan Y, Yang Y, Yang J, Tan L: STAT3 phosphorylation is required for the HepaCAM-mediated inhibition of castration-resistant prostate cancer cell viability and metastasis. Prostate 2021, 81:603-611.

162. Lin Y, Zhou X, Yang K, Chen Y, Wang L, Luo W, Li Y, Liao J, Zhou Y, Lei Y, et al: Protein tyrosine phosphatase receptor type D gene promotes radiosensitivity via STAT3 dephosphorylation in nasopharyngeal carcinoma. Oncogene 2021, 40:3101-3117.

163. Gao M, Liu L, Zhang X, Li Z, Zhang M: Interleukin-6 reverses Adriamycin resistance in nasal NK/T-cell lymphoma via downregulation of ABCC4 and inactivation of the JAK2/STAT3/NF-kappaB/P65 pathway. Environ Toxicol Pharmacol 2021, 85:103639.

164. Saraswati S, Alhaider A, Abdelgadir AM, Tanwer P, Korashy HM: Phloretin attenuates STAT-3 activity and overcomes sorafenib resistance targeting SHP-1-mediated inhibition of STAT3 and Akt/VEGFR2 pathway in hepatocellular carcinoma. Cell Commun Signal 2019, 17:127.

165. Zhuang Y, Bai Y, Hu Y, Guo Y, Xu L, Hu W, Yang L, Zhao C, Li X, Zhao H: Rhein sensitizes human colorectal cancer cells to EGFR inhibitors by inhibiting STAT3 pathway. Onco Targets Ther 2019, 12:5281-5291.

166. Liu T, Li A, Xu Y, Xin Y: Momelotinib sensitizes glioblastoma cells to temozolomide by enhancement of autophagy via JAK2/STAT3 inhibition. Oncol Rep 2019, 41:1883-1892.

167. Huang LL, Rao W: SiRNA interfering STAT3 enhances DDP sensitivity in cervical cancer cells. Eur Rev Med Pharmacol Sci 2018, 22:4098-4106.

168. Wang X, Qu H, Dong Y, Wang G, Zhen Y, Zhang L: Targeting signal-transducer-and-activator-of-transcription 3 sensitizes human cutaneous melanoma cells to BRAF inhibitor. Cancer Biomark 2018, 23:67-77.

169. Gao J, Shao Z, Yan M, Fu T, Zhang L, Yan Y: Targeted regulationof STAT3 by miR-29a in mediating Taxol resistance of nasopharyngeal carcinoma cell line CNE-1. Cancer Biomark 2018, 22:641-648.

170. Zhao Y, Ma K, Yang S, Zhang X, Wang F, Zhang X, Liu H, Fan Q: MicroRNA-125a-5p enhances the sensitivity of esophageal squamous cell carcinoma cells to cisplatin by suppressing the activation of the STAT3 signaling pathway. Int J Oncol 2018, 53**:**644-658.

171. Tang JC, Ren YG, Zhao J, Long F, Chen JY, Jiang Z: Shikonin enhances sensitization of gefitinib against wild-type EGFR non-small cell lung cancer via inhibition PKM2/stat3/cyclinD1 signal pathway. Life Sci 2018, 204**:**71-77.

172. Seo HS, Ku JM, Choi HS, Woo JK, Lee BH, Kim DS, Song HJ, Jang BH, Shin YC, Ko SG: Apigenin overcomes drug resistance by blocking the signal transducer and activator of transcription 3 signaling in breast cancer cells. Oncol Rep 2017, 38**:**715-724.

173. Zhang C, Tong J, Huang G: Nicotinamide phosphoribosyl transferase (Nampt) is a target of microRNA-26b in colorectal cancer cells. PLoS One 2013, 8**:**e69963.

174. Xia M, Duan ML, Tong JH, Xu JG: MiR-26b suppresses tumor cell proliferation, migration and invasion by directly targeting COX-2 in lung cancer. Eur Rev Med Pharmacol Sci 2015, 19**:**4728-4737.

175. Chen E, Li E, Liu H, Zhou Y, Wen L, Wang J, Wang Y, Ye L, Liang T: miR-26b enhances the sensitivity of hepatocellular carcinoma to Doxorubicin via USP9X-dependent degradation of p53 and regulation of autophagy. Int J Biol Sci 2021, 17**:**781-795.

176. Gao Z, Ye X, Bordeaux A, Hettich S, Lin S, Han F, Jia Y: miR-26b regulates cell proliferation and apoptosis of CD117+CD44+ ovarian cancer stem cells by targeting PTEN. Eur J Histochem 2021, 65.

177. Zhao N, Wang R, Zhou L, Zhu Y, Gong J, Zhuang SM: MicroRNA-26b suppresses the NF-kappaB signaling and enhances the chemosensitivity of hepatocellular carcinoma cells by targeting TAK1 and TAB3. Mol Cancer 2014, 13**:**35.

178. Zang S, Zhao S, Gao X, Li Y, Zhong C, Gao J: Restoration of miR-26b expression partially reverses the cisplatin resistance of NSCLC by targeting tafazzin. Onco Targets Ther 2019, 12**:**7551-7560.

179. Wang L, Su J, Zhao Z, Hou Y, Yin X, Zheng N, Zhou X, Yan J, Xia J, Wang Z: MiR-26b reverses temozolomide resistance via targeting Wee1 in glioma cells. Cell Cycle 2017, 16**:**1954-1964.

180. Khosla R, Hemati H, Rastogi A, Ramakrishna G, Sarin SK, Trehanpati N: miR-26b-5p helps in EpCAM+cancer stem cells maintenance via HSC71/HSPA8 and augments malignant features in HCC. Liver Int 2019, 39**:**1692-1703.

181. Zhang H, Yang S, Wang J, Jiang Y: Blockade of AMPK-Mediated cAMP-PKA-CREB/ATF1 Signaling Synergizes with Aspirin to Inhibit Hepatocellular Carcinoma. Cancers (Basel) 2021, 13.

182. Zhang H, Zhu T, Fu R, Peng Y, Jing P, Xu W, Wang H, Li S, Shu Z, Yin Y, Zhang X: Combination of Detoxified Pneumolysin Derivative DeltaA146Ply and Berbamine as a Treatment Approach for Breast Cancer. Mol Ther Oncolytics 2020, 18**:**247-261.

183. Hu B, Cai H, Yang S, Tu J, Huang X, Chen G: Berbamine Enhances the Efficacy of Gefitinib by Suppressing STAT3 Signaling in Pancreatic Cancer Cells. Onco Targets Ther 2019, 12**:**11437-11451.

184. Han C, Wang Z, Chen S, Li L, Xu Y, Kang W, Wei C, Ma H, Wang M, Jin X: Berbamine Suppresses the Progression of Bladder Cancer by Modulating the ROS/NF-kappaB Axis. Oxid Med Cell Longev 2021, 2021**:**8851763.

185. Li W, Li Y, Tian W, Han X, Zhao J, Xin Z, Hu H, Li J, Hang K, Xu R: 2-methylbenzoyl berbamine, a multi-targeted inhibitor, suppresses the growth of human osteosarcoma through disabling NF-kappaB, ERK and AKT signaling networks. Aging (Albany NY) 2020, 12**:**15037-15049.

186. Zhang H, Jiao Y, Shi C, Song X, Chang Y, Ren Y, Shi X: Berbamine suppresses cell viability and induces apoptosis in colorectal cancer via activating p53-dependent apoptotic signaling pathway. Cytotechnology 2018, 70**:**321-329.

187. Zhao Y, Lv JJ, Chen J, Jin XB, Wang MW, Su ZH, Wang LY, Zhang HY: Berbamine inhibited the growth of prostate cancer cells in vivo and in vitro via triggering intrinsic pathway of apoptosis. Prostate Cancer Prostatic Dis 2016, 19**:**358-366.

188. Heiler S, Wang Z, Zoller M: Pancreatic cancer stem cell markers and exosomes - the incentive push. World J Gastroenterol 2016, 22**:**5971-6007.

189. Vlassov AV, Magdaleno S, Setterquist R, Conrad R: Exosomes: current knowledge of their composition, biological functions, and diagnostic and therapeutic potentials. Biochim Biophys Acta 2012, 1820**:**940-948.

190. Sharma A: Role of stem cell derived exosomes in tumor biology. Int J Cancer 2018, 142**:**1086-1092.

*own publication

Acknowledgements

First of all, I would like to deeply express my sincere gratitude to PD Dr. Heike Pohla, my supervisor, for offering me the opportunity to work in her lab to finish my doctoral thesis. She helps me a lot to establish my academic thinking, enrich my scientific research experience, and support me mentally and in daily life. I cannot make it without her supervision and it is such a wonderful life experience in her lab. Thanks to the friendly atmosphere she creates in our group, and I feel comfortable and happy all the time in the lab. Thanks for her patience and carefulness in revising my paper manuscript, reports, or other documents. I have to say that it is my honor to know her and work with her.

Second, I would like to thank Prof. Dr. Alexander Buchner, my co-supervisor, for his excellent support and guide for my research work, especially in the field of statistics during my project, and for his patience with my struggle and problem in daily life. He is so nice and patient all the time. I would like to go to him whenever my computer strikes in somehow. I admire and respect him for his profession in statistics and computer skills.

Third, I also would like to thank Prof. Dr. Elfriede Nössner, one of my TAC members, for her kindness to give me the chance to complete my doctoral degree. I would like to thank her for her patience and profession in revising the thesis and target meeting reports for me.

Also, I would like to thank Birgit Stadlbauer for her kindness and help during my work. She has taught me a lot about my research. She sets up a good example for me in aspects of life and work. I respect her attitude to the work. Impressively, her experiment records are perfect.

Furthermore, I would like to thank our team members, Chen Lyu, Sarah Hubschneider, Isabel Schrader, and Maxim Werner. I will miss you guys, and we are one family united to help each other.

I am also sincerely grateful to Linglin Zhang, Lei Shi, Yuhan Liu, Bingsheng Li, Ru Huang, Xiaolong Wang, Ruixiao Wang, Maximilian Christian Aumiller, Christian Heckl, Max Eisel, and all people for their help, support, and care during the period I lived in Munich.

Especially I would like to thank Chen Lyu, and Yuhan Liu. I really appreciate that Chen provides me the information concerning academic conferences, workshops, and cours-

es. It is also inspiring, efficient, and enjoyable to learn with her regardless of the content. The parties she organized were lively, full of laughter, and always made me linger. Meanwhile, I thank Yuhan Liu for teaching me the evidence-based research method of meta-analysis. I think it will help me solve certain problems I will encounter in the clinic. Also, I would like to thank Yuhan for his spirit of optimism and full of positive energy, which influences all the members of our association.

In addition, I would like to thank my husband, parents, all my families, and friends for their support and understanding towards my study. I am very grateful to my husband for his belief in the success of long-distance relationships over the last four years.

Finally, I would like to thank the scholarship from China Scholarship Council (CSC) for financial support for my study and work in the Laboratory of Tumor Immunology, LIFE Center, LMU Klinikum, University Munich, Germany. Without CSC, I would not have the opportunity to study in Munich. I love Munich, not only the lifestyle and way of working but the scenery and environment, while especially love the people I have met.

Affidavit

Affidavit

Wang, Lili
Surname, first name

Fraunhoferstr. 20
Street

82152 Planegg/ Martinsried, Germany
Zip code, town, country

I hereby declare, that the submitted thesis entitled:

The influence of phytochemicals on cancer stem cells in prostate cancer

is my own work. I have only used the sources indicated and have not made unauthorised use of services of a third party. Where the work of others has been quoted or reproduced, the source is always given.

I further declare that the submitted thesis or parts thereof have not been presented as part of an examination degree to any other university.

Hangzhou, 16.11.2021
place, date

Lili Wang
Signature doctoral candidate

Confirmation of congruency

Confirmation of congruency between printed and electronic version of the doctoral thesis

Wang, Lili

Surname, first name

Fraunhoferstr. 20

Street

82152 Planegg/ Martinsried, Germany

Zip code, town, country

I hereby declare, that the submitted thesis entitled:

The influence of phytochemicals on cancer stem cells in prostate cancer

is congruent with the printed version both in content and format.

Hangzhou, 16.11.2021

place, date

Lili Wang

Signature doctoral candidate

List of publications

Publications related to the thesis:

1. Wang L, Stadlbauer B, Lyu C, Buchner A, Pohla H: Shikonin enhances the antitumor effect of cabazitaxel in prostate cancer stem cells and reverses cabazitaxel resistance by inhibiting ABCG2 and ALDH3A1. Am J Cancer Res 2020, 10:3784-3800

2. Wang L et al. Berbamine targets cancer stem cells and reverses cabazitaxel resistance via CXCR4/let-7/IGF2BP1 axis and ABCG2/miR-26b/p-STAT3 axis in prostate cancer (writing)

Other publication:

1. Wang L, Liu Y, Lyu C, Buchner A, Pohla H: Diagnostic and Prognostic Role of miR-192 in Different Cancers: A Systematic Review and Meta-Analysis. Biomed Res Int 2021, 2021:8851035.